Corrosion Resistant Alloys for Reinforced Concrete

PUBLICATION NO. FHWA-HRT-09-020

APRIL 2009

U.S. Department of Transportation
Federal Highway Administration

Research, Development, and Technology
Turner-Fairbank Highway Research Center
6300 Georgetown Pike
McLean, VA 22101-2296

FOREWORD

Initial cost considerations have historically precluded widespread utilization of high performance (corrosion resistant) reinforcements, such as stainless steel in bridge construction. However, because of concerns regarding long-term serviceability of epoxy-coated reinforcing steel in northern and coastal bridge decks and substructures, advent of life cycle cost analysis as a project planning tool, and requirements that major bridge structures have a 75–100-year design life, the competitiveness of such steels has increased that enhanced attention has focused in recent years upon these materials.

This investigation was initiated to evaluate the corrosion resistance of various types of corrosion resistant reinforcement, including new products that are becoming available in bridge structures that are exposed to chlorides. Both long-term (4+ years) test yard exposures and accelerated laboratory experiments in simulated concrete pore waters are being performed. The ultimate objective was to, first, evaluate the corrosion properties and service life of the different candidate materials and, second, develop tools whereby long-term performance in actual structures can be projected from a short-term accelerated test. An interim report provided results from the initial three years of this overall 6-year program, and this report serves as a second interim report.

Cheryl Richter
Acting Director, Office of Infrastructure
Research and Development

TECHNICAL REPORT DOCUMENTATION PAGE

1. Report No. HRT-09-020	2. Government Accession No.	3. Recipient's Catalog No.
4. Title and Subtitle Corrosion Resistant Alloys for Reinforced Concrete		5. Report Date April 2009
		6. Performing Organization Code FAU-OE-CMM-0901
7. Author(s) William H. Hartt,* Rodney G. Powers,** Francisco Presuel Marino,* Mario Paredes,** Ronald Simmons,** Hui Yu,* Rodrigo Himiob,* Y. Paul Virmani*** (See boxes 9 and 12)		8. Performing Organization Report No.
9. Performing Organization Name and Address *Florida Atlantic University–Sea Tech Campus, 101 North Beach Road, Dania Beach, FL 33004 **Florida Department of Transportation–State Materials Office, 5007 NE 39th Street, Gainesville, FL 32609 ***Office of Infrastructure Research and Development Federal Highway Administration 6300 Georgetown Pike McLean, VA 22012		10. Work Unit No. (TRAIS) 11. Contract or Grant No.
12. Sponsoring Agency Name and Address Office of Infrastructure Research and Development Federal Highway Administration 6300 Georgetown Pike McLean, VA 22012		13. Type of Report and Period Covered Interim Report 14. Sponsoring Agency Code
15. Supplementary Notes Contracting Officer's Technical Representative (COTR): Y.P. Virmani, HRDI-10		

16. Abstract

Deterioration of concrete bridges because of reinforcing steel corrosion has been recognized for 4-plus decades as a major technical and economic challenge for the United States. As an option for addressing this problem, renewed interest has focused on corrosion resistant reinforcements, stainless steels in particular. The present research study was performed jointly by Florida Atlantic University and the Florida Department of Transportation to evaluate reinforcements of this type. These included solid stainless steels 3Cr12 (UNS-S41003), 2101LDX (ASTM A955-98), 2304 (UNS-S31803), 2205 (UNS 31803), two 316L (UNS S31603) alloys, two 316 stainless steel clad black bar products, and ASTM A1035 commonly known as MMFX 2. Black bar (ASTM A615) reinforcement provided a baseline for comparison purposes. Results from short-term tests and preliminary results from long-term exposure of reinforced concrete slabs were presented in the first interim report for this project. This second interim report provides longer-term data and analyses of chloride exposures that involved four different types of reinforced concrete specimens, two of which were intended to simulate northern bridge decks exposed to deicing salts and the remaining two to marine substructure elements. Three different concrete mix designs were employed, and specimen types included combinations with a (1) simulated concrete crack, (2) bent top bar, (3) corrosion resistant upper bar(s) and black steel lower bars, and (4) intentional clad defects such that the carbon steel substrate was exposed. Cyclic wet-dry ponding with a sodium chloride (NaCl) solution was employed in the case of specimens intended to simulate northern bridge decks, and continuous partial submergence in either a NaCl solution or at a coastal marine site in Florida was used for specimens intended to represent a coastal bridge substructure. The exposures were for periods in excess of 4 years. The candidate alloys were ranked according to performance, and an analysis is reported that projects performance in actual concrete structures.

17. Key Word Reinforced Concrete, Bridges, Corrosion Resistance, Corrosion Testing, High Performance Reinforcement, Stainless Steel, MMFX-2		18. Distribution Statement No restrictions. This document is available to the public through NTIS, Springfield, VA 22161	
19. Security Classif. (of this report) Unclassified	20. Security Classif. (of this page) Unclassified	21. No. of Pages 146	22. Price

Form DOT F 1700.7 (8-72) Reproduction of completed page authorized

SI* (MODERN METRIC) CONVERSION FACTORS

APPROXIMATE CONVERSIONS TO SI UNITS

Symbol	When You Know	Multiply By	To Find	Symbol
		LENGTH		
in	inches	25.4	millimeters	mm
ft	feet	0.305	meters	m
yd	yards	0.914	meters	m
mi	miles	1.61	kilometers	km
		AREA		
in^2	square inches	645.2	square millimeters	mm^2
ft^2	square feet	0.093	square meters	m^2
yd^2	square yard	0.836	square meters	m^2
ac	acres	0.405	hectares	ha
mi^2	square miles	2.59	square kilometers	km^2
		VOLUME		
fl oz	fluid ounces	29.57	milliliters	mL
gal	gallons	3.785	liters	L
ft^3	cubic feet	0.028	cubic meters	m^3
yd^3	cubic yards	0.765	cubic meters	m^3
		NOTE: volumes greater than 1000 L shall be shown in m^3		
		MASS		
oz	ounces	28.35	grams	g
lb	pounds	0.454	kilograms	kg
T	short tons (2000 lb)	0.907	megagrams (or "metric ton")	Mg (or "t")
		TEMPERATURE (exact degrees)		
°F	Fahrenheit	5 (F-32)/9 or (F-32)/1.8	Celsius	°C
		ILLUMINATION		
fc	foot-candles	10.76	lux	lx
fl	foot-Lamberts	3.426	candela/m^2	cd/m^2
		FORCE and PRESSURE or STRESS		
lbf	poundforce	4.45	newtons	N
lbf/in^2	poundforce per square inch	6.89	kilopascals	kPa

APPROXIMATE CONVERSIONS FROM SI UNITS

Symbol	When You Know	Multiply By	To Find	Symbol
		LENGTH		
mm	millimeters	0.039	inches	in
m	meters	3.28	feet	ft
m	meters	1.09	yards	yd
km	kilometers	0.621	miles	mi
		AREA		
mm^2	square millimeters	0.0016	square inches	in^2
m^2	square meters	10.764	square feet	ft^2
m^2	square meters	1.195	square yards	yd^2
ha	hectares	2.47	acres	ac
km^2	square kilometers	0.386	square miles	mi^2
		VOLUME		
mL	milliliters	0.034	fluid ounces	fl oz
L	liters	0.264	gallons	gal
m^3	cubic meters	35.314	cubic feet	ft^3
m^3	cubic meters	1.307	cubic yards	yd^3
		MASS		
g	grams	0.035	ounces	oz
kg	kilograms	2.202	pounds	lb
Mg (or "t")	megagrams (or "metric ton")	1.103	short tons (2000 lb)	T
		TEMPERATURE (exact degrees)		
°C	Celsius	1.8C+32	Fahrenheit	°F
		ILLUMINATION		
lx	lux	0.0929	foot-candles	fc
cd/m^2	candela/m^2	0.2919	foot-Lamberts	fl
		FORCE and PRESSURE or STRESS		
N	newtons	0.225	poundforce	lbf
kPa	kilopascals	0.145	poundforce per square inch	lbf/in^2

*SI is the symbol for the International System of Units. Appropriate rounding should be made to comply with Section 4 of ASTM E380.
(Revised March 2003)

TABLE OF CONTENTS

LIST OF FIGURES

LIST OF TABLES

LIST OF ABBREVIATIONS AND SYMBOLS

Acronym

3BTC	3-Bar tombstone columns
BB	Black bar
CDF	Cumulative distribution function
CRR	Corrosion resistant reinforcements
DOT	Department of transportation
ECR	Epoxy-coated reinforcing steel
ERF	Gaussian error function
FAU	Florida Atlantic University
FC	Field columns
FDOT-SMO	Florida Department of Transportation State Materials Office
LCCA	Life-cycle cost analysis
MS	Macrocell slabs
SDS	Simulated deck slabs
w/c	Water-to-cement ratio

Symbol

∂	Mathematical symbol indicating a partial derivative
Ω	Ohm, unit of electrical resistance
μA	Microampere, unit of current

1.0 INTRODUCTION

1.1 BACKGROUND

The United States has a major investment in its highway system, whose operational performance, in conjunction with that of other transportation modes, is critical to economic strength and societal well-being. While deterioration of structures with time is a normal and expected occurrence, the rate at which this deterioration has occurred for highway bridges since the advent in the 1960s of a clear roads policy and application during wintertime of deicing salts in northern locations has been abnormally advanced and posed significant maintenance challenges. Also important is similar advanced deterioration of reinforced concrete bridges in coastal locations, both northern and southern, as a consequence of sea water and spray exposure. In either case (deicing salt or marine exposure), the deterioration is a consequence of the aggressive nature of the chloride ion in combination with moisture and oxygen.[1] Over half of the total bridge inventory in the United States is of the reinforced concrete type, and these structures have been particularly affected. A recent study indicated that the annual direct cost of corrosion to bridges is $5.9 billion to $9.7 billion.[2] If indirect factors are also included, this cost can be as much as 10 times higher.[3]

As this problem has manifested itself during the past 40+ years, technical efforts have been directed towards understanding the deterioration mechanism and developing prevention and intervention strategies. With regard to the former, steel and concrete are in most aspects mutually compatible, as exemplified by the fact that in the absence of chlorides, the relatively high pH of concrete pore solution (pH ≈ 13.0–13.8) promotes formation of a protective oxide (passive) film such that corrosion rate is negligible, and decades of relatively low maintenance result. However, in the presence of chlorides, even at concentrations at the steel depth as low as 0.6 kg/m^3 (1.0 pcy) on a concrete weight basis, the passive film may become locally disrupted, and active corrosion will commence.[4] Once this occurs, solid corrosion products form progressively near the steel-concrete interface and lead ultimately to concrete cracking and spalling. Figure 1 shows a photograph illustrating such damage for the case of a coastal bridge piling. Because corrosion-induced deterioration is progressive, inspections for damage assessment must be routinely performed. Present Federal guidelines require a visual inspection every 2 years.[5] If indicators of deterioration are not addressed, public safety is at risk. For example, corrosion-induced concrete spalls occur as potholes in a bridge deck and contribute to unsafe driving conditions. In the extreme, structural failure and collapse result.

Figure 1. Photo. A cracked and spalled marine bridge piling.

1.2 MODELING OF REINFORCED CONCRETE STRUCTURE DETERIORATION AND SERVICE LIFE PROJECTION

Corrosion-induced deterioration of reinforced concrete can be modeled in terms of three sequential component steps or periods, which include the following:

1. Time for corrosion initiation (T_i).

2. Time, subsequent to corrosion initiation, for appearance of cracking on the external concrete surface (crack propagation) (T_c).

3. Time for surface cracks to evolve into spalls, which progress to the point where maintenance beyond what is routine is required (T_s).

The sum $T_c + T_s$ is termed the corrosion propagation period, T_p. Maintenance-free service life, T_{mf}, is then $T_i + T_p$. As defined, maintenance-free service life is not intended to include occasional minor or routine repairs, as are likely to be required for any structure of significant size prior to T_{mf} or even T_i being reached. Figure 2 illustrates these parameters schematically in conjunction with a plot of cumulative damage versus time (adapted from Tutti).[6]

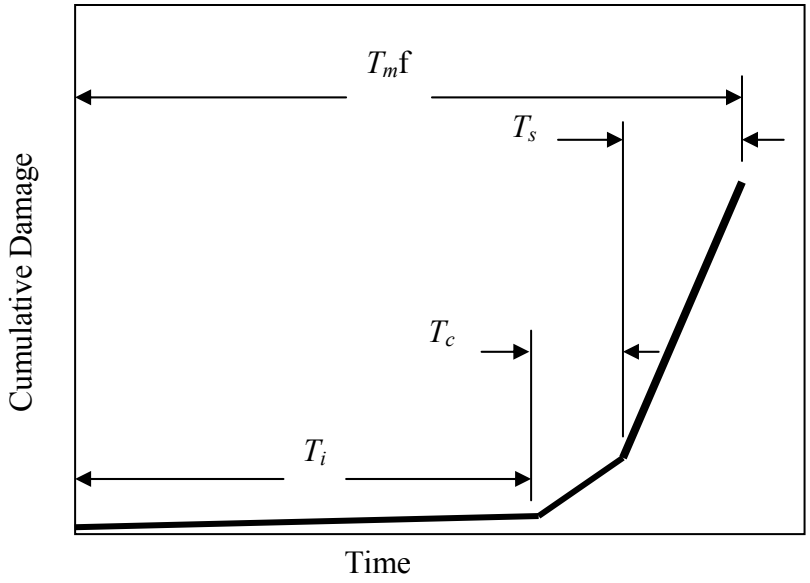

Figure 2. Graph. Schematic illustration of the various steps in deterioration of reinforced concrete due to chloride-induced corrosion.

Thus, the critical challenge for T_{mf} determinations is to develop data from laboratory and test yard experiments, service experience, or both that facilitate projection of T_i and T_p. Of course, T_i for actual structures cannot be determined directly from laboratory experimentation, since T_i for laboratory specimens is necessarily more brief than for structures. However, it is generally recognized that passive film breakdown and initiation of active corrosion for reinforcing steel in concrete commence once a critical chloride concentration, C_T, is achieved at the reinforcement depth.[7] Consequently, if C_T is known from test yard exposures and the same value applies to actual structures, then T_i for the latter can be calculated using the solution to Fick's second law of diffusion, assuming that diffusion is the predominant Cl^- transport mechanism in both cases (test yard specimens and structure). Fick's second law for one-dimensional diffusion is as follows:

$$\frac{\partial^2 C(x,T)}{\partial T^2} = D_e \frac{\partial^2 C(x,T)}{\partial x^2} \tag{1}$$

where ∂ indicates the partial derivative, $C(x,T)$ is chloride concentration, $[Cl^-]$, after time T at distance x into the concrete in the direction of diffusion measured from the exposed surface, and D_e is the effective diffusion coefficient. As equation 1 is written, if D_e is assumed to be independent of x and T, then its solution is as follows:

$$C(x,T) = C_s \cdot ERF\left(\frac{x}{2 \cdot (D_e \cdot T)^{0.5}}\right) \tag{2}$$

where, C_s is [Cl^-] at the concrete surface, also assumed constant with time, and ERF is the Gaussian error function. Further, at corrosion initiation $C(x,T)$ is C_T, x is the rebar cover, and $T = T_i$. Thus,

$$C_T = C_s \cdot ERF\left(\frac{x}{2 \cdot (D_e \cdot T_i)^{0.5}}\right) \tag{3}$$

This solution assumes that C_T, C_s, x, and D_e are spatially and chronologically constant, whereas they are, in fact, distributed parameters with the range for C_T varying by more than an order of magnitude.[8, 9] In addition, C_s and D_e may vary with exposure time and concrete age. Equation 3, as written, considers that initial [Cl^-] in the concrete is 0. Also, implicit in this expression is that the diffusion media (concrete) is homogeneous and without cracks. Nonetheless, analyses based on equation 3 are generally accepted as a viable engineering tool for projection of T_i.

Less focus has been placed upon T_c; however, some authors have developed sophisticated models that consider the tendency for solid corrosion products and corroding reinforcement to develop tensile hoop stresses and ultimately concrete cracking.[10] Influential variables that influence T_c include corrosion rate, specific volume of solid corrosion products and rate at which these form, concrete microstructure and strength, and ratio of concrete cover to rebar diameter. Alternatively, T_c can be assumed as a specific time, such as 5 years, for surface cracks to appear in the case of black bar (BB).[9] Less attention has focused upon T_s and any subsequent period that might lapse before maintenance intervention commences.

Based upon the corrosion deterioration model represented in figure 2, methods of life-cycle cost analysis (LCCA) are now commonly employed to evaluate and compare different material selection and design alternatives. This approach considers both initial cost and the projected life history of maintenance, repair, and rehabilitation expenses that are required to achieve the design life (synonymous with T_{mf}). These are evaluated in terms of the time value of money from which present worth is determined. Comparisons between different options can then be made on a cost normalized basis. Thus, materials selection choices define C_T which, in combination with design parameters, allows calculation of T_i. With estimation of T_c and T_s, T_{mf} can be projected. Iterations may be required depending upon cost and design life considerations. Figure 3 schematically illustrates this progression.

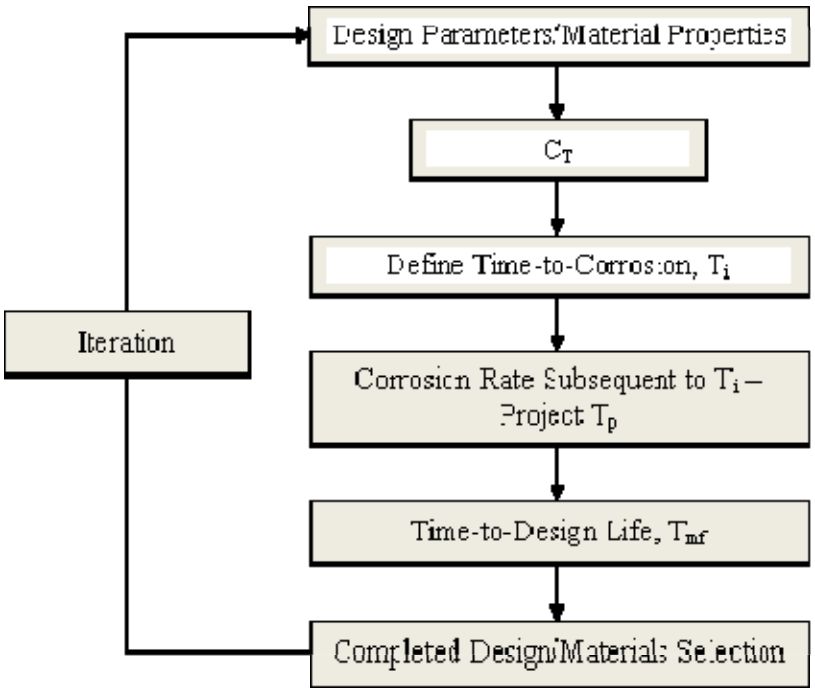

Figure 3. Chart. Representation of the sequential steps involved in the design process.

1.3 EPOXY-COATED REINFORCING (ECR) STEEL

In the early 1970s, research studies were performed that qualified epoxy-coated reinforcing (ECR) steel as an alternative to BB for reinforced concrete bridge construction.[11, 12] For the past 30 years, ECR has been specified by most State departments of transportation (DOTs) for bridges, decks, and substructures exposed to chlorides. At the same time, concrete mix designs were improved by specification of low water-to-cement ratio (w/c), possibly admixed with pozzolans or corrosion inhibitors (or both), and covered over reinforcement of 65 mm or more.[13] However, premature corrosion-induced cracking of marine bridge substructures in Florida indicate that ECR is of little benefit for this type of exposure. (See references 14, 15, 16, and 17.) While performance of ECR in northern bridge decks has been generally good to date (30+ years), the degree of corrosion resistance afforded in the long term for major structures with design lives of 75 years to 100 years is still uncertain.

2.0 PROJECT OBJECTIVE

In response to the above concerns regarding ECR, interest has focused on additional corrosion-resistant alternatives to ECR, stainless steels in particular, over the past 15 years. Such alloys may become competitive on a life-cycle cost basis since the higher initial expense of the steel per se may be recovered over the life of the structure via reduced maintenance expenses arising from corrosion-induced damage.

Corrosion resistant reinforcements (CRR) may be advantageous beyond the considerations discussed above. This is illustrated by the flow diagram in figure 4, where the obvious explicit benefit of reduced corrosion rate and extended service life is indicated to the left. However, CRR can also impact design by possibly allowing concrete cover to be reduced which, in turn, should result in lower superstructure weight and potentially smaller substructure size and weight. Furthermore, lower cover can lead to the reduced width of concrete cracks and, hence, less corrosion at these cracks, which translates to lower maintenance costs.

This research was performed jointly by Florida Atlantic University (FAU) and the Florida Department of Transportation (FDOT) as a 6-year effort to evaluate the suitability of various CRR for concrete bridges exposed to chlorides. An initial phase of the study provided a critical literature review of CRR and an initial interim report, as subsequently published.[18,19] The present report updates results from this interim report and provides findings for the subsequent 3 years of the project.

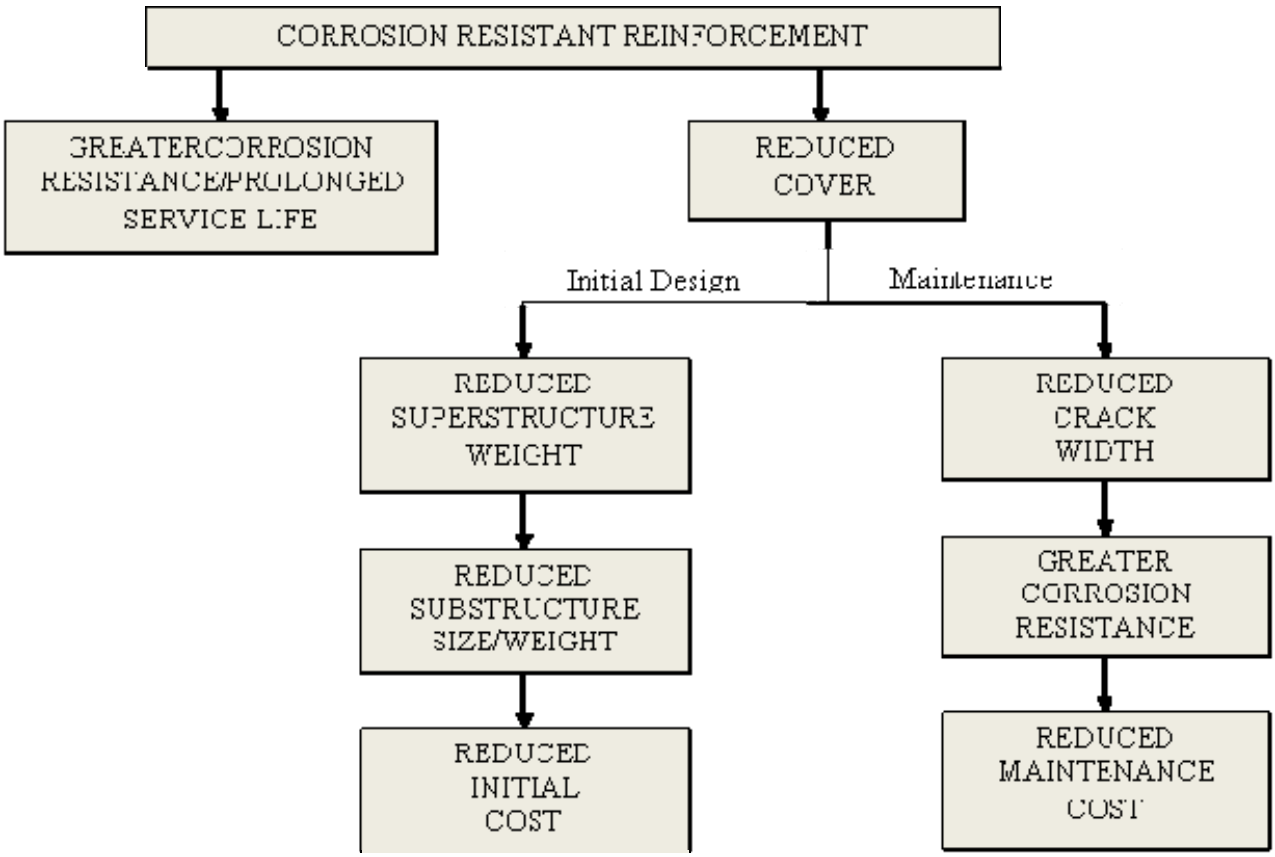

Figure 4. Chart. Schematic representation of benefits that can be derived from CRR.

3.0 MATERIALS AND EXPERIMENTAL PROCEDURES

3.1 REINFORCING STEELS

Table 1 lists the various steels that were employed in this study. These steels are the same as those addressed in the initial interim report for this project, except that Type 304 and Type 2304SS were acquired in the meantime and added to the test matrix. [19]

Table 1. Listing of reinforcements that were investigated.

Designation/Spec	Common Design	As-Rec'd Cond	Microstructure	PREN[1]	Supplier
UNS-S31603	Type 316LSS	Pickled[2]	Austenite	26.4[3]	Slater Steels Corporation
				25.1[4]	Dunkirk Specialty Steel
UNS-S30400	Type 304SS	Pickled[2]	Austenite	19.6	Dunkirk Specialty Steel
UNS-S32304	Type 2304SS	Pickled	Duplex (Austenite plus Ferrite)	24.9	UGITECH
ASTM A955-98	Type 2101LDXSS	As-Rolled	Lean Duplex (Austenite plus Ferrite)	25.1	Gerdau AmeriSteel Corporation
ASTM A1035	MMFX 2	As-Rolled	Microcomposite austenite-martensite	9.4	MMFX Corporation
AASHTO MP 13M/MP 13-04	Nouvinox	Pickled	316 Clad/Carbon Steel Core	—	Stelax Industries, Ltd.
	SMI	Pickled	316 Clad/Carbon Steel Core	—	CMC Steel Group
UNS-S41003	Type 3Cr12SS	Pickled	Ferritic	12	American Utility Metals
ASTM A615	Black Bar	As-Rolled	Ferrite/Pearlite	0.3	Gerdau AmeriSteel Corporation

— indicates that the calculation is not applicable.
[1] PREN (Pitting Resistance Equivalent Number) where PREN = %Cr + 3.3·%Mo + 16·%N
[2] Pickled with HF and nitric acid per ASTM A380.
[3] Subsequently designated as 316.16.
[4] Subsequently designated as 316.18.

Composition for all of the bars is shown in table 2. Bar size in all cases was #5 (nominally 16 mm diameter) except for Type 304 SS, which was #4 (12.7 mm diameter). The two types of clad bars (designated as STAX and SMI) were fabricated by two distinct processes. The former were created by packing a stainless steel tube with steel scrap followed by rolling. The latter was created by applying a plasma spray of stainless steel to a carbon steel billet and then rolling it. Unless noted otherwise, bars were tested in the as-received surface condition.

Table 2. Composition of the reinforcements.

Alloy	C	Mn	P	S	Si	Cr	Ni	Mo	Cu	N	Fe
Type 316.16	0.03	1.55	0.025	0.001	0.59	18.43	10.06	2.08	0.42	0.068	Bal
Type 316.18	0.03	1.66	0.026	0.005	0.42	16.97	10.07	2.15	0.85	0.065	Bal
Type 304SS	0.07	0.94	0.020	0.001	0.58	18.25	8.12	0.40	0.30	—	Bal
Type 2205SS	0.029	1.68	0.028	0.004	0.63	21.58	4.80	2.64	—	0.15	Bal
Type 2304SS	0.03	1.16	0.026	0.002	0.45	22.33	4.16	0.25	0.30	0.11	Bal
Type 2101SS	0.04	4.70	0.019	0.001	0.80	22.47	1.68	0.24	0.38	0.117	Bal
A 1035	0.05	0.45	0.012	0.015	0.23	9.30	0.10	0.03	0.12	—	Bal
Type 3Crl2SS	0.04	0.38	0.018	0.024	0.71	11.69	0.50	0.09	0.02	—	Bal
A 615	0.30	1.22	0.013	0.032	0.26	0.21	0.19	0.04	—	—	Bal

— indicates element not reported.

3.2 CONCRETE MIX DESIGNS

Three concrete test designs designated STD1 (five bags cement and 0.50 water-to-cement ratio (w/c)), which yields a high permeability concrete; STD2 (seven bags of cement and 0.41 w/c), which results in moderate permeability; and STD3 (seven bags of cement and 0.50 w/c), which is of improved permeability between that of STD1 and STD2, were employed. Target mix designs for each of these are listed in table 3. The various corrosion resistant alloy types, in addition to BB (table 1), were used as reinforcements.

Table 3. Concrete batch mix design.

Material	STD1	STD2	STD3
Cement (bags)	5	7	7
Cement, kg	213	300	300
Water, kg	107	122	149
Water/Cement	0.50	0.41	0.50
Fine aggregate (silica sand), kg	652	540	489
Coarse aggregate (limestone), kg	753	753	747

3.3 SPECIMEN TYPES, DESIGN, AND FABRICATION

3.3.1 General

Four different types of reinforced concrete specimens were fabricated by the Florida Department of Transportation State Materials Office (FDOT-SMO) in Gainesville, FL. The specimens include the following:

- Simulated deck slabs (SDS).
- Macrocell slabs (MS).
- 3-Bar tombstone columns (3BTC).
- Field columns (FC).

The first two specimen designs were intended to simulate a northern bridge deck or slab exposed to chlorides from either deicing salts or sea water, whereas the latter two specimens represent a marine substructure element. The SDS specimens underwent exposure at FAU, the MS and 3BTC specimen underwent exposure at the FDOT-SMO Corrosion Laboratory, and the FC underwent exposure at the Intracoastal Waterway site at Crescent Beach, FL. The STD consisted of all straight bars in the as-received condition in concrete compacted according to ASTM C192.[20] However, other specimens employed variations of this according to the description and nomenclature listed in table 4.

Table 4. Listing of the various specimen types, variables, and the nomenclature for each.

Specimen Designation	Description	Specimen Type
STD1	STD1 concrete mix.	SDS, FC
STD2	STD2 concrete mix.	SDS, 3BTC
STD3	STD3 concrete mix.	3BTC
BCAT	STD1 concrete, bottom mat black steel.	SDS, MS
CCON	STD1 concrete mix, simulated concrete crack.	SDS, MS
CCNB	STD1 concrete mix, bottom mat (cathode) black bars, simulated concrete crack.	SDS, MS
CREV	STD1 concrete mix, top bar crevice.	SDS
CRV	STD1 concrete mix, simulated concrete crack, top bar crevice.	SDS
BENT	STD1 concrete mix, top bar bent.	MS
	STD3 concrete mix, top bar bent.	3BTC
BNTB	STD1 concrete mix, top bar bent, bottom bars black steel.	MS
CBNT	STD1 concrete mix, simulated concrete crack, top bar bent.	MS
CBNB	STD1 concrete mix, simulated concrete crack, bottom bars black steel, top bar bent.	MS
ELEV	STD3 concrete mix, one bar elevated.	3BTC
WB	STD1 concrete mix, top bars wire brushed.	SDS
ARWB	STD1 concrete mix, top bars as received.	MS
USDB	STD1 concrete mix, 3 mm diameter clad holes 25 mm apart on top bars.	SDS, MS
UBDB	STD1 concrete mix, 3 mm diameter clad holes 25 mm apart on top bars, top bar bent.	MS
CSDB	STD1 concrete mix, simulated concrete crack, 3 mm diameter clad holes 25 mm apart.	SDS, MS
CBDB	STD1 concrete, cracked concrete, 3 mm diameter clad holes 25 mm apart on top bars, top bar bent.	MS
BCCD	STD1 concrete mix, 3 mm diameter clad holes 25 mm apart on top bars, bottom bars black steel.	SDS. MS
ACID	STD1 concrete mix, top bars lab pickled, cathode as received.	SDS
ABRD	STD1 concrete mix, blasted/abraded top bars, bottom bars as received.	SDS
CVNC	STD1 concrete mix, top bar crevice, no end caps.	SDS

Prior to casting, the reinforcement was degreased by cleaning it with hexane. Next, heat shrink tubing was applied at the bar ends to provide an electrical barrier at the concrete-reinforcement interface. This process left only the center portion of the reinforcement to within approximately 25 mm of the concrete surface exposed. The casting procedure was similar for all specimen types. This process involved placing freshly mixed concrete in the specimen molds in two lifts, followed by consolidating each lift for 20 s to 30 s on a vibration table. The first lift filled the specimen mold approximately half full, and the second lift filled the mold completely. The surface of the specimens was troweled smooth using a wooden or metal float. After 24 hours, the molds were dissembled. The specimens were removed, placed in sealed plastic bags, and stored for 6 months. The design of the four specimen types is provided below.

3.3.2 Design and Fabrication of Simulated Deck Slab (SDS) Specimens

SDS specimens were fabricated with six bars, three of which comprised a top layer and three a bottom layer, as illustrated schematically in figure 5. The heat shrink tubing at the bar ends is not depicted in the figure.

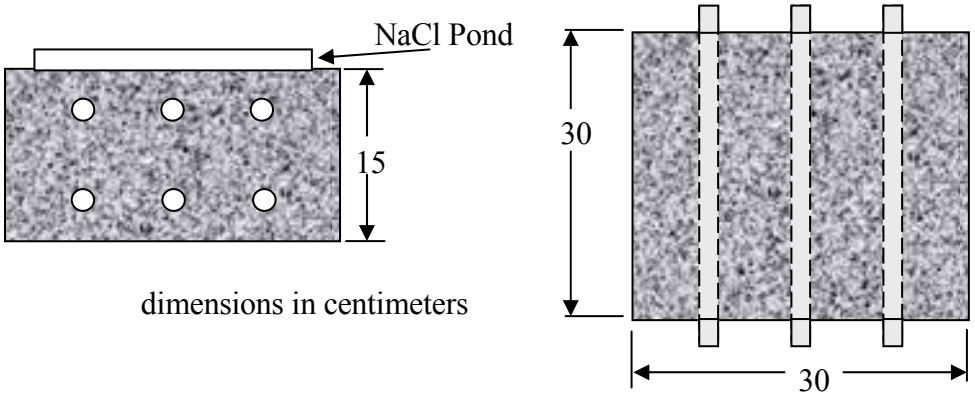

Figure 5. Chart. Standard SDS specimens.

Concrete cover for all of the bars was 25 mm, and triplicate specimens were prepared for each bar type and specimen variable (described subsequently). Because of the large inventory of specimens, fabrication and delivery to FAU occurred at six different times. The interim report provides results for the exposure of the initial three specimen lots (lots 1–3), and data for these have been updated in this report.[19] In addition, data acquired from the final three lots (lots 4–6) are presented and discussed. Specimens in lots 4–6 are listed in table 5.

Table 5. Listing of SDS specimens in lots 4–6.

Lot 4 Specimens	Lot 5 Specimens	Lot 6 Specimens
4-STD2-SMI-1	5-STD1-2304-1	6-CCRV-304-1
4-STD2-SMI-2	5-STD1-2304-2	6-CCRV-304-2
4-STD2-SMI-3	5-STD1-2304-3	6-CCRV-304-3
4-STD1-SMI-1	5-STD1-MMFX-1	6-CCON-304-1
4-STD1-SMI-2	5-STD1-MMFX-2	6-CCON-304-2
4-STD1-SMI-3	5-STD1-MMFX-3	6-CCON-304-3
4-CCON-SMI-1	5-STD1-BB-1	6-WB-304-1
4-CCON-SMI-2	5-STD1-BB-2	6-WB-304-2
4-CCON-SMI-3	5-STD1-BB-3	6-WB-304-3
4-CREV-SMI-1	5-STD1-2101-1	6-CVNC-SMI-1
4-CREV-SMI-2	5-STD1-2101-2	6-CVNC-SMI-2
4-CREV-SMI-3	5-STD1-2101-3	6-CVNC-SMI-3
4-BCCD-SMI-1	5-STD1-3Cr12-1	6-CCNB-304-1
4-BCCD-SMI-2	5-STD1-3Cr12-2	6-CCNB-304-2
4-BCCD-SMI-3	5-STD1-3Cr12-3	6-CCNB-304-3
4-CCRV-SMI-1	5-USDB-MMFX-1	6-CREV-304-1
4-CCRV-SMI-2	5-USDB-MMFX-2	6-CREV-304-2
4-CCRV-SMI-3	5-USDB-MMFX-3	6-CREV-304-3
4-USDB-SMI-1	—	6-STD1-304-1
4-USDB-SMI-2	—	6-STD1-304-2
4-USDB-SMI-3	—	6-STD1-304-3
4-CCRV-3Cr12-1	—	6-STD2-304-1
4-CCRV-3Cr12-2	—	6-STD2-304-2
4-CCRV-3Cr12-3	—	6-STD2-304-3
4-CSDB-SMI-1	—	6-BCAT-304-1
4-CSDB-SMI-2	—	6-BCAT-304-2
4-CSDB-SMI-3	—	6-BCAT-304-3

— indicates that no specimen was fabricated.

A distinction between the initial and final three lots is that heat shrink end sleeves were not installed on bar ends of the specimens in lots 1–3. Because of the concern that the absence of sleeves on bars of the initial three lots may have resulted in premature corrosion initiation where rebars exited the concrete, replicates of BB, 3Cr12, MMFX-2, and 2101 reinforced specimens (these were the only STD type specimens that initiated corrosion) were included in lot 5. Otherwise, specimens in lots 4–6 consisted of reinforcement types/specimen configurations that were not present in lots 1–3. Figure 6 illustrates the nomenclature that was adapted to identify a standard specimen.

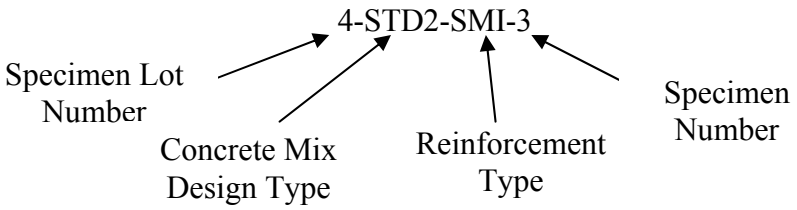

Figure 6. Chart. Example nomenclature for standard specimens.

There were six specimen lots, and these correspond to the order in which they were fabricated and delivered to FAU by FDOT. Likewise, designation of specimens that were non-standard (BCAT, CCON; see table 4) is illustrated in figure 7.

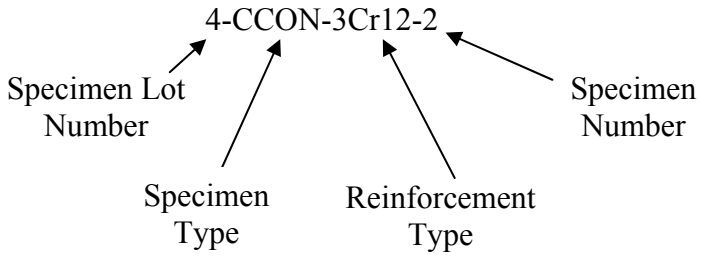

Figure 7. Chart. Example nomenclature for non-standard specimens.

Thus, the last digit identifies the above example as SDS specimen 2. The reinforcement is 3Cr12 with a simulated crack from lot 4. The default mix design (no indication) is STD1. Concrete mix designs STD1 and STD2 were employed for Type 304SS and SMI bars but with most specimens being prepared using the former. Eight different modifications to the above standard SDS specimen configuration were prepared and exposed, as listed and described below.

1. Slabs with a corrosion resistant bar type for the top layer and BB in the bottom layer are designated BCAT. All specimens of this type, except for those reinforced with Type 304SS, were included in the first three lots, and results were provided in the interim report.[19] Results for Type 304SS BCAT specimens are presented in this report.

2. Slabs with a simulated concrete crack are designated CCON. In fabrication of these specimens, a 1.6-mm-thick stainless steel shim was placed vertically in the form on top of and perpendicular to the upper bars at the mid-span. The shim was removed subsequent

to initial concrete set. Reinforcement types in lots 4–6 SDS specimens that employed this configuration were Type 304SS and SMI.

3. Slabs with a bar splice that formed a crevice are designated CREV. In this case, two bars that overlapped for a portion of their embedded length replaced each of the three single top bars in the standard specimen. Hence, the top reinforcement layer consisted of six rebars instead of three, as was the case for the other specimen types. Cover for each of the bar pairs was maintained at 25 mm.

4. Slabs with a bar crevice (splice) per the above configuration but also with a simulated concrete crack are designated CCRV. Reinforcement types in lots 4–6 SDS specimens that employed this configuration were 3Cr12, Type 304SS, and SMI.

5. Slabs with a simulated concrete crack and BB cathode are designated CCNB. The only reinforcement type in lots 4–6 SDS specimens that employed this configuration was Type 304SS.

6. Slabs with wire brushed bars are designated WB. The only specimen that employed this condition was Type 304SS.

7. Slabs with a simulated concrete crack and 3-mm holes drilled through the cladding on the top of upper bars at 25-mm spacing are designated CSDB. The only specimen that employed this condition was SMI.

8. Slabs with 3-mm holes drilled through the cladding or surface layer on the top of upper bars at 25-mm spacing are designated USDB. Reinforcement types in lots 4–6 SDS specimens that employed this configuration were SMI and MMFX-2.

Figure 8 illustrates this specimen type schematically. Reinforcement types in lots 4–6 SDS specimens that employed this configuration were Type 304SS and SMI.

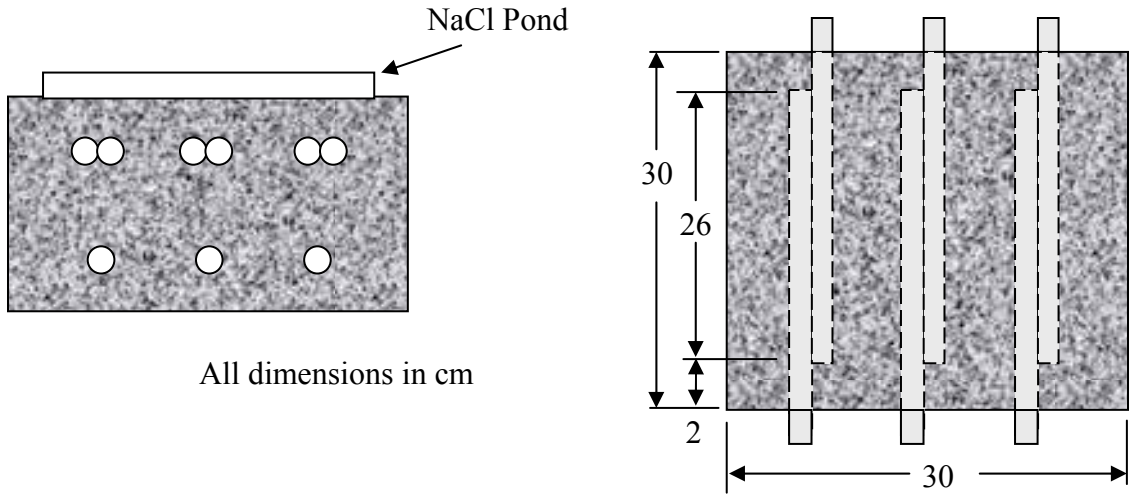

Figure 8. Chart. Schematic illustration of the CREV type simulated deck slab specimens.

Upon delivery to FAU, an electrical connection was established between bars in both layers of each slab using a stainless steel wire in conjunction with a drilled hole and connection screw at one end of each bar. Periodically, a 10 Ω resistor, where Ω designates the units for resistance, was temporarily inserted in the circuit between the two bar layers. Voltage drop across the resistor was then measured, and the macrocell current was calculated. The specimen sides were coated with an ultraviolet-resistant paint and inverted relative to their orientation at casting. A plastic bath with a vented lid was mounted on what was the bottom-formed face. Prior to ponding, the specimens were stored outdoors in a covered location for 2 months at the FAU Sea Tech Campus, which is approximately 300 m inland from the Atlantic Ocean southeast of Ft. Lauderdale, FL. The initial week of ponding occurred with potable water to promote saturation or a high humidity pore structure so that upon ponding, diffusion, not sorption, would be the primary Cl^- ingress mechanism. This week was followed by cyclic 1 week wet/1 week dry ponding with 15.0 wt percent NaCl. The salt water pondings commenced for lots 4, 5, and 6 on July 26, 2005, August 10, 2005, and December 11, 2006, respectively. Figure 9 is a photograph of a mold with CREV-SMI reinforcement prior to concrete pouring. Figure 10 shows two specimens under test, and figure 11 is a perspective view of the test site.

Figure 9. Photo. View of a mold for a CCRV-SMI specimen prior to concrete pouring.

Figure 10. Photo. Two SDS specimens under exposure.

Figure 11. Photo. SDS specimens under exposure in the outdoor test yard.

Monitoring the potential of electrically connected bars of individual specimens and of voltage drop between bar layers was performed weekly. The onset of active corrosion was defined as having occurred if a measureable voltage drop was detected for two consecutive measurement periods. This detection limit corresponded to a current of 0.1 μA. Subsequent to the BB specimens becoming active (the first specimens to do so), the potential and voltage drop measurement procedure was modified, as follows:

1. Once corrosion activity was detected according to the voltage drop criterion (see above), each of the top bars was electrically isolated temporarily from all of the other bars.

2. Individually, each of the three top bars was then connected through a 10 Ω resistor to the three bottom bars, and voltage drop was measured. Through this step, the top bar(s) that was active was identified.

3. The top bar(s) for which voltage drop was 0 was reconnected to the three bottom bars, leaving the top bar(s) that did show corrosion activity isolated. Exposure and monitoring of the remaining connected bars continued.

4. Steps 1 through 3 were repeated as successive bars became active. Once corrosion activity was detected for the last of the three top bars, testing of that slab was discontinued, and the specimen was dissected.

3.3.3 Design and Fabrication of Macrocell Slab (MS) Specimens

The design for the MS specimens is a modification of the standard G109 geometry and consisted of either a single straight or bent top bar and four straight bottom bars. The latter was positioned at two elevations beneath the top bar. This geometry is illustrated by figure 12. The standard condition was with the reinforcement wire brushed (ARWB), but one set was prepared with bars as received. The STD1 specimens were fabricated with and without a simulated crack, but specimens based upon the STD2 concrete mix were of the standard type only (no crack).

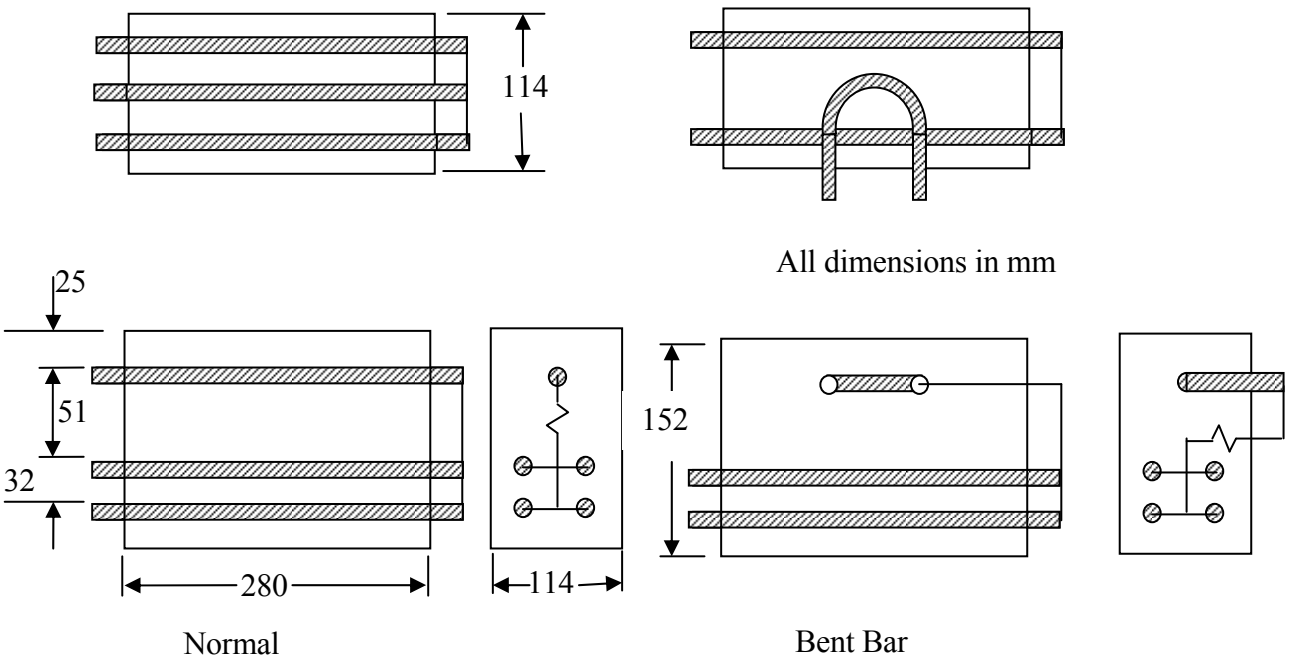

Figure 12. Chart. Geometry of the macrocell slab type specimen with both bent and straight bars.

The types of specimens that were fabricated are indicated in table 4 with individual specimens identified according to the same convention that was explained above for SDS specimens. However, "MS" is included in the nomenclature. Subsequent to curing, the specimens were inverted relative to the orientation at casting, and a 76 mm by 152 mm plastic container for

ponding was attached to what had been the bottom cast face. The top bar was wired to the four lower bars through a 1 Ω resistor via 16 gauge multi-strand wire and solder eyelet connectors. The latter was attached to bar ends using a stainless steel screw mounted into a hole drilled into the end of each bar. The specimens were subjected to a 14 days wet/14 days dry cyclic ponding with a 3.0 wt percent NaCl solution until corrosion-induced cracking occurred. Duplicate sets of three STD1 specimens were prepared with one set exposed in a screened covered outdoor location. The second set (designated STD1G) was prepared in a constant temperature (25 ^{o}C) and relative humidity (50 percent) room. In addition, a single set of three other reinforcement/ specimen types (see table 4) and STD2 specimens were prepared and exposed in the same outdoor location noted previously.

Figure 13 shows a photograph of three MS specimens, and figure 14 is a perspective view of the outdoor exposure. For both the controlled and ambient outdoor exposures, potential was recorded monthly, as was the current for the controlled temperature/relative humidity specimens. The current for the outdoor exposed specimens was recorded daily via an Agilent 34970A data acquisition system.

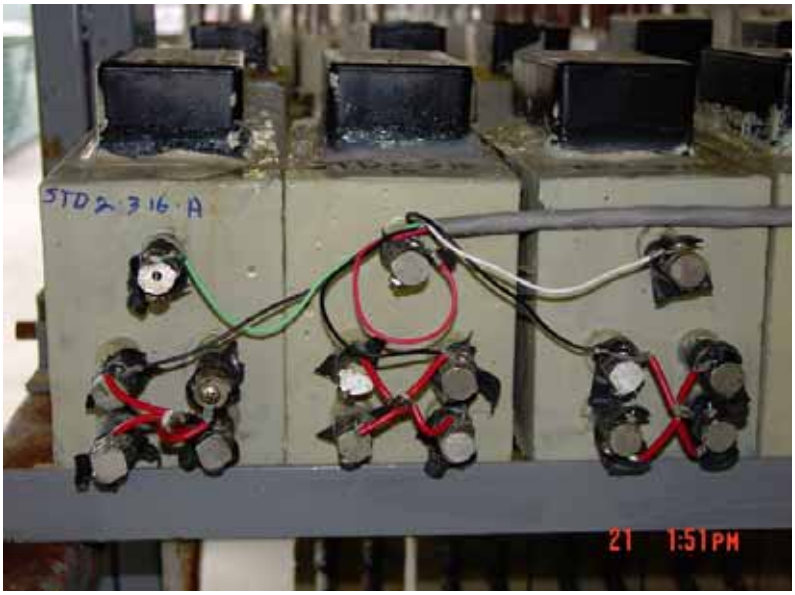

Figure 13. Photo. Three MS specimens under exposure.

Figure 14. Photo. MS slab specimens under exposure.

3.3.4 Design and Fabrication of 3-Bar Tombstone Column (3BTC) Specimens

As noted previously, the 3BTC specimens were intended to simulate a marine bridge substructure element. Three bar configurations—normal (STD), bent (BENT), and elevated (ELEV)—were prepared, as illustrated in figure 15. Concrete mixes STD2 and STD3 (table 3) were employed.

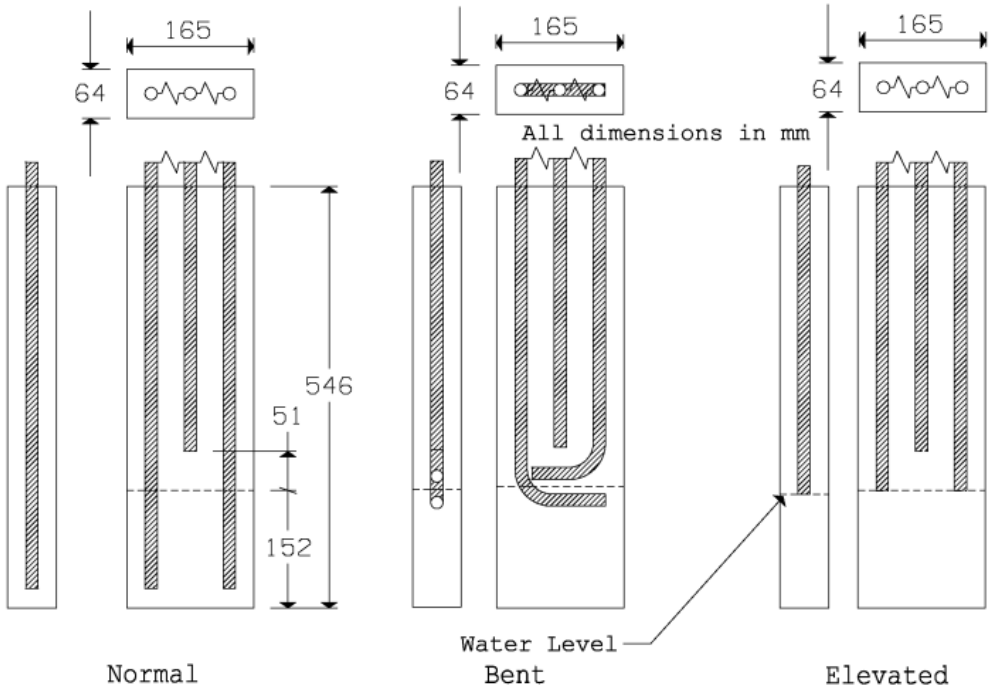

Figure 15. Chart. 3BTC specimen for each of the three bar configurations.

Figure 16 shows a photograph of bars of the bent configuration in a mold prior to concrete placement. The bar clamping and alignment method that is illustrated in the figure serves to maintain the intended cover (24 mm) to within close tolerance. The normal reinforcement

configuration has been employed by the FDOT for more than 10 years, and it is intended to provide baseline data that can be compared to results from previous studies. On the other hand, the bent bar configuration was considered particularly relevant in the case of stainless clad and possibly MMFX-2 reinforcements because of the possibility of clad or surface layer cracking. Reinforcements that were employed were BB, 3Cr12, MMFX-2, 2101, Type 316, Type 304 SS, and SMI. Six specimens with each rebar type were prepared for the STD2 and STD3 BB type specimens. Otherwise, the number of specimens was three.

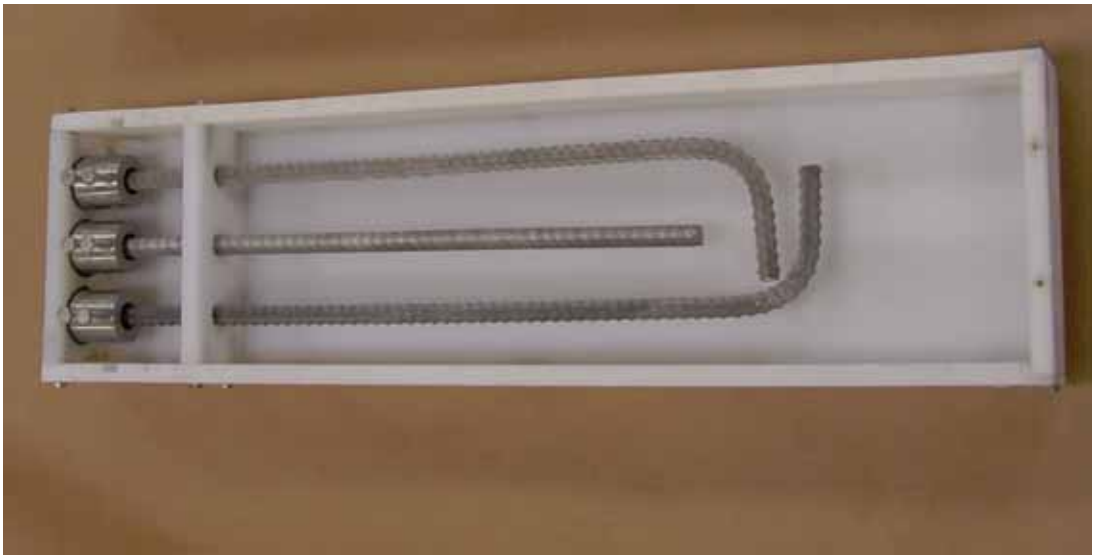

Figure 16. Photo. Type 304 rebars of the bent configuration in a mold prior to concrete placement.

Figure 17 is a photograph of a specimen after casting. Prior to exposure, a 1 Ω resistor was wired between each long bar and the other two bars using the procedure described previously for the MS specimens. Subsequent to curing, specimens were positioned vertically in a plastic tank and submerged in a 3.5 wt percent NaCl solution to a depth of 152 mm to facilitate formation of an electrochemical macrocell on each of the longer bars.

Figure 17. Photo. 3BTC specimen.

Figure 18 shows specimens under exposure in the outdoor screened room at the FDOT-SMO Corrosion Laboratory. Once exposure was initiated, potential of all three bars coupled, and voltage drop across the two resistors for each specimen was measured daily utilizing a pair of Agilent 34970A data acquisition systems. Exposure of individual specimens was terminated upon concrete cracking or appearance of visible corrosion product bleed-out.

Figure 18. Photo. 3BTC specimens under exposure.

3.3.5 Design and Fabrication of Field Column (FC) Specimens

FC specimens were based upon the STD1 concrete mix design with bars only in the as-received condition. Figure 19 illustrates the specimen geometry. The reinforcements that were employed were BB, 3Cr12, MMFX-2, 2101, Type 316.16 SS, Type 304 SS, and SMI with end caps. Each bar was electrically isolated from the others during exposure and potential measurements. The columns were exposed in the Intracoastal Waterway at Crescent Beach, FL by jetting the lower 1.2 m in sand such that mean high water was approximately 1.8 m from the specimen bottom. Placement was delayed because of environmental permitting issues, but it commenced in September 2005.

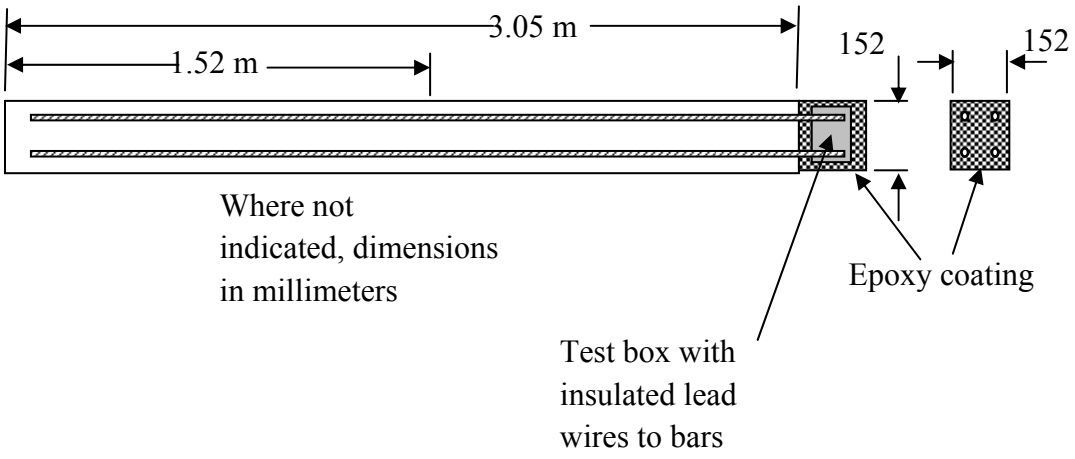

Figure 19. Chart. Geometry of the field column type specimen.

Figure 20 is a photograph of the specimens installed at the exposure site. A single potential was measured for each of the four bars by placing a copper-copper sulfate electrode in the moist sand near the base of the column. Polarization resistance (R_p) of one bar in each column was determined using an embedded T_i electrode as reference and one of the other three bars as a counter electrode. A cyclic polarization scan was performed to calculate total resistance (R_t), and solution resistance (R_s) was determined using a three-point resistance test. Finally, R_p was calculated as $R_t - R_s$. These measurements were performed at the time of initial exposure and at approximately 6-month intervals subsequently until corrosion-induced cracking or visible corrosion product bleed-out was observed.

Figure 20. Photo. Field column specimens under exposure at the Intracoastal Waterway site in Crescent Beach, FL.

Table 3.8 to table 3.13 of the interim report list all of the specimens of each of the four designs that had been deployed as of that submission.[19] Those tables are reproduced here as table 6 to table 11. Shaded cells in these tables indicate specimens that had not been fabricated at the time the earlier report was prepared, but these were included in the inventory for lots 4–6 (see table 1).

Table 6. Listing of specimens reinforced with 316.18 and 3Cr12.

Description	SDS	S3BC	3BTC	MS	FC
STD1 mix design, standard specimen	3	6	—	6	3
STD3 mix design, standard specimen	3	3	3	3	—
STD2 mix design, standard specimen	—	—	6	—	—
STD1-BCAT	3	—	—	3	—
STD1-CCON	3	—	—	3	—
STD1-CCNB	3	—	—	3	—
STD1-CREV	3	—	—	—	—
STD1-CCRV	3	—	—	—	—
STD1-BENT	—	3	—	3	—
STD3-BENT	—	—	3	—	—
STD1-BNTB	—	—	—	3	—
STD1-CBNT	—	—	—	3	—
STD1-CBNB	—	—	—	3	—
STD1-ELEV	—	3	—	—	—
STD3-ELEV	—	—	3	—	—
STD1-WB	3	—	—	—	—
STD1-ARWB	—	—	—	3	—
Total	**24**	**15**	**15**	**33**	**3**
					TOTAL: 90

— indicates that no specimen of the indicated type was fabricated.

Table 7. Listing of specimens with 2101 rebar.

Description	SDS	S3BC	3BTC	MS	FC
STD1 mix design, standard specimen	3	6	—	6	3
STD3 mix design, standard specimen	3	3	3	3	—
STD2 mix design, standard specimen	—	—	6	—	—
STD1-BCAT	3	—	—	3	—
STD1-CCON	3	—	—	3	—
STD1-CCNB	3	—	—	3	—
STD1-CREV	3	—	—	—	—
STD1-CCRV	3	—	—	—	—
STD1-BENT	—	3	3	3	—
STD3-BENT	—	—	3	—	—
STD1-BNTB	—	—	—	3	—
STD1-CBNT	—	—	—	3	—
STD1-CBNB	—	—	—	3	—
STD1-ELEV	—	3	3	—	—
STD3-ELEV	—	—	3	—	—
STD1-WB	3	—	—	—	—
STD1-ARWB	—	—	—	3	—
STD1-ACID	3	—	—	—	
STD1-ABRD	3				
Total	**30**	**15**	**15**	**33**	**3**
					TOTAL: 96

— indicates that no specimen of the indicated type was fabricated. Shaded cells indicate that specimens of his type had not been fabricated at the time of the earlier report.

Table 8. Listing of specimens reinforced with MMFX-2.

Description	SDS	S3BC	3BTC	MS	FC
STD1 mix design, standard specimen	3	6	—	6	3
STD2 mix design, standard specimen	3	3	3	3	—
STD3 mix design, standard specimen	—	—	6	—	—
STD1-BCAT	3	—	—	3	—
STD1-CCON	3	—	—	3	—
STD1-CCNB	3	—	—	3	—
STD1-CREV	3	—	—	—	—
STD1-CCRV	3	—	—	—	—
STD1-BENT	—	3	—	3	—
STD3-BENT	—	—	3	—	—
STD1-BNTB	—	—	—	3	—
STD1-CBNT	—	—	—	3	—
STD1-CBNB	—	—	—	3	—
STD1-ELEV	—	3	—	—	—
STD3-ELEV	—	—	3	—	—
STD1-WB	3	—	—	—	—
STD1-ARWB	—	—	—	3	—
STD1-USDB	3	—	—	3	—
STD1-ACID	3	—	—	—	—
STD1-ABRD	3	—	—	—	—
Total	**33**	**15**	**15**	**36**	**3**
					TOTAL: 102

— indicates that no specimen of the indicated type was fabricated.

Table 9. Listing of specimens reinforced with Stelax.

Description	SDS	S3BC	3BTC	MS	FC
STD1 mix design, standard specimen	3	6	—	6	3
STD2 mix design, standard specimen	3	3	3	3	—
STD3 mix design, standard specimen	—	—	6	—	—
STD1-CCON	3	—	—	3	—
STD1-CREV	3	—	—	—	—
STD1-CCRV	3	—	—	—	—
STD1-BENT	—	3	3	3	—
STD3-BENT	—	—	3	—	—
STD1-CBNT	—	—	—	3	—
STD1-ELEV	—	3	3	—	—
STD3-ELEV	—	—	3	—	—
STD1-WB	3	—	—	—	—
STD1-ARWB	—	—	—	3	—
STD1-USDB	3	—	—	3	—
STD1-UBDB	—	—	—	3	—
STD1-CSDB	3	—	—	3	—
STD1-CBDB	—	—	—	3	—
STD1-BCCD	3	—	—	3	—
STD1-ACID	3	—	—	—	—
STD1-ABRD	3	—	—	—	—
STD1-CVNC	3	—	—	—	—
Total	**36**	**15**	**15**	**36**	**3**
					TOTAL: 105

— indicates that no specimen of the indicated type was fabricated. Shaded cells indicate that specimens of this type had not been fabricated at the time of the earlier report.

Table 10. Listing of specimens reinforced with SMI.

Description	SDS	S3BC	3BTC	MS	FC
STD1 mix design, standard specimen	3	—	—	6	3
STD2 mix design, standard specimen	3	—	3	3	—
STD3 mix design, standard specimen	—	—	6	—	—
STD1-CCON	3	—	—	3	—
STD1-CREV	3	—	—	—	—
STD1-CCRV	3	—	—	—	—
STD1-BENT	—	—	—	3	—
STD3-BENT	—	—	3	—	—
STD1-CBNT	—	—	—	3	—
STD1-ELEV	—	—	—	—	—
STD3-ELEV	—	—	3	—	—
STD1-WB	3	—	—	—	—
STD1-ARWB	—	—	—	3	—
STD1-USDB	3	—	—	3	—
STD1-UBDB	—	—	—	3	—
STD1-CSDB	3	—	—	3	—
STD1-CBDB	—	—	—	3	—
STD1-BCCD	3	—	—	3	—
STD1-ABRD	3	—	—	—	—
STD1-CVNC	3	—	—	—	—
Total	**33**	**0**	**15**	**36**	**3**
					TOTAL: 87

— indicates that no specimen of the indicated type was fabricated. Shaded cells indicate that specimens of this type had not been fabricated at the time of the earlier report.

Table 11. Listing of specimens reinforced with black bar.

Description	SDS	S3BC	3BTC	MS	FC
STD1 mix design, standard specimen	3	6	—	9	3
STD2 mix design, standard specimen	3	6	6	3	—
STD3 mix design, standard specimen	—	—	6	—	—
CCON–STD1, cracked concrete	3	—	—	3	—
Total	**9**	**12**	**12**	**15**	**3**
					TOTAL: 51

— indicates that no specimen of the indicated type was fabricated.

3.4 SPECIMEN TERMINATIONS AND DISSECTIONS

3.4.1 Termination and Dissection of Simulated Deck Slab (SDS) Specimens

SDS specimens that became active and were designated for dissection were opened and evaluated. First, testing and exposure were terminated, and the ponding bath was removed. Next, two saw cuts were made; each of them were perpendicular to the top surface and parallel to and at mid-spacing between the center and each of the two outer bars of each layer. For each of the three resultant specimen parts, a further saw cut was made on each of the previous saw cut faces and on what had been the two specimen side faces opposite and parallel to the top rebars to a depth approximately 10 mm from each rebar. In some cases where corrosion of bottom layer BB was thought to have occurred, this procedure was also performed at the level of these bars. Each specimen section was then split open by placing a chisel in one of the previous saw cuts and tapping gently with a hammer until a fracture occurred. This split created a fracture that exposed both the rebar and its trace, which were then examined for corrosion and photographed. Figure 21 schematically illustrates the location of concrete cuts, as listed above.

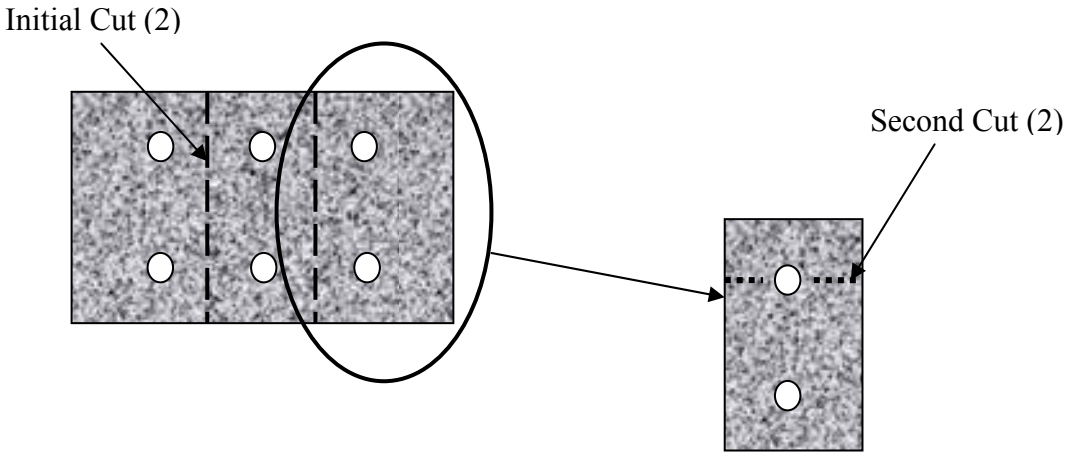

Figure 21. Chart. Concrete sectioning for SDS specimens.

3.4.2 Termination and Dissection of Macrocell Slab (MS) Specimens

Dissection procedures for these specimens were essentially the same as for the SDS specimens, as described previously.

3.4.3 Termination and Dissection of 3-Bar Tombstone Column (3BTC) Specimens

Dissection of the 3BTC specimens was performed by making a saw cut to the steel depth on the front and back faces along both longer bars starting at the bottom of the specimens and extending up about 0.25 m or more if visual cracking was apparent beyond this. A cut to the steel depth was then made on the front and back faces perpendicular to the reinforcement bars at the 0.25 m elevation across the width of the specimens or just above the highest reaching crack. Once all of the cuts were made, a hammer and chisel were used to split off the cut portion of concrete and expose the reinforcement. Figure 22 provides a schematic illustration of these cuts on a specimen.

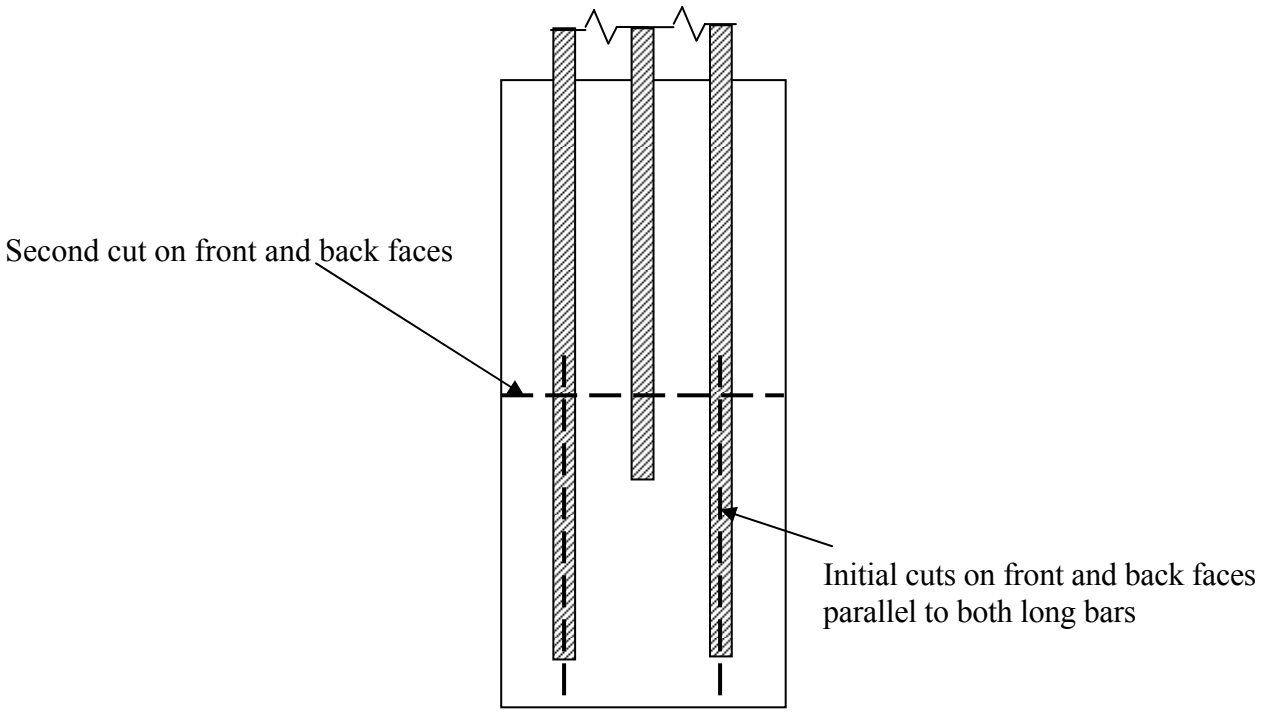

Figure 22. Chart. Concrete sectioning for 3BTC specimens.

3.4.4 Termination and Dissection of Field Column Specimens

No dissections have been made on FC specimens due to a lack of an environmental permit to remove them from the test site.

3.5 CHLORIDE ANALYSES

Concrete samples for [Cl^-] determinations were acquired from SDS specimens according to two methods. Both were performed as soon as possible once all of the top layer bars had initiated corrosion, as explained previously. The first method involved acquiring a 75-mm-diameter core

from the top concrete surface at the mid-spacing between two adjacent top layer bars. This core was then dry sliced parallel to the top surface at 6.4 mm intervals, and the individual slices were separately ground to powder. The second method involved individually mounting the concrete sections from the top portion of each specimen on a mill and milling a cut approximately 0.6 mm deep along that portion of the rebar trace that was void of corrosion products using a 10-mm-diameter square end cutter. Figure 23 illustrates this process schematically. For both methods (coring and milling), the powder samples were analyzed for [Cl^-] using the FDOT wet chemistry method.

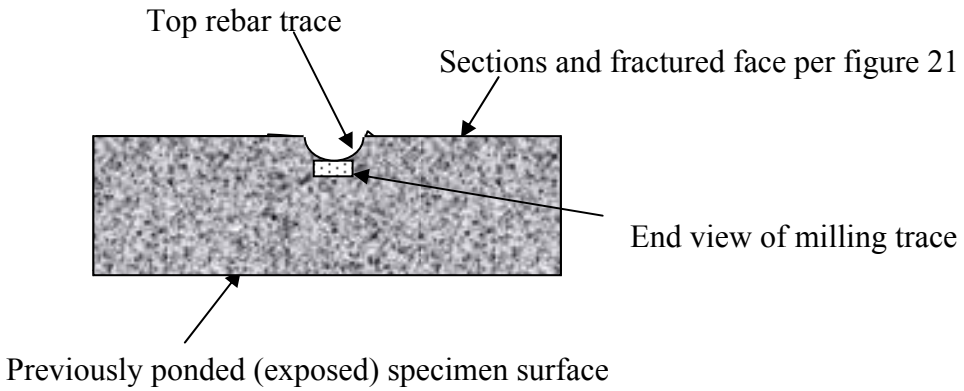

Figure 23. Chart. SDS specimen milling along rebar trace to acquire powdered concrete for chloride analysis.

4.0 RESULTS AND DISCUSSION

4.1 TIME-TO-CORROSION

4.1.1 Results for Simulated Deck Slab Specimens

4.1.1.1 General Comments Regarding SDS Specimens

Results and discussion of the corrosion exposures are presented in two subdivisions. The first section, termed *improved performance reinforcements*, includes BB, 3Cr12, MMFX-2, and 2101. The second subdivision is termed *high-performance reinforcements*, which includes 316, 304, 2304, SMI, and STAX. This distinction between subdivisions was made because the former group of reinforcements initiated corrosion within the project timeframe, whereas most of the latter did not. Data for each of these are presented and discussed below.

4.1.1.2 Results for Improved Performance Reinforcements in SDS Specimens

Data for improved performance reinforced lot 5 specimens, which initiated corrosion, were employed for defining the respective T_i values. Figure 24 shows a typical plot of potential versus exposure time, while figure 25 plots macrocell current versus exposure time, in this case for MMFX-2 reinforced specimens. In general, the somewhat abrupt potential shift from relatively positive to more negative was accompanied by the occurrence of measureable macrocell current (figure 25). The latter serves as the criterion for defining T_i for the bar in question and for its isolation from other bars, as explained previously. In all cases, a positive current indicates that the top layer of bars was anodic to the bottom layer.

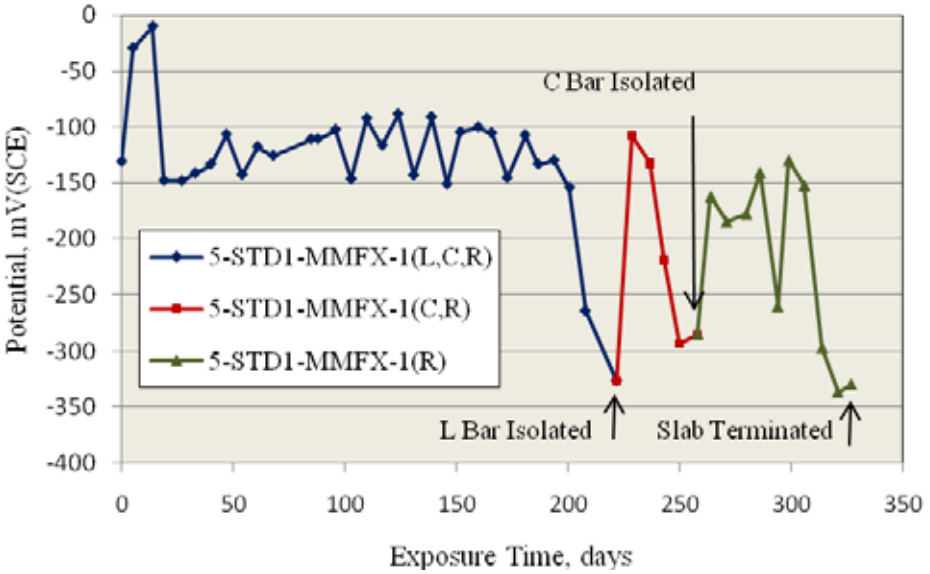

Figure 24. Graph. Potential versus time for specimens reinforced with MMFX-2 steel indicating times that individual bars became active and were isolated (L—left bar; C—center bar; R—right bar).

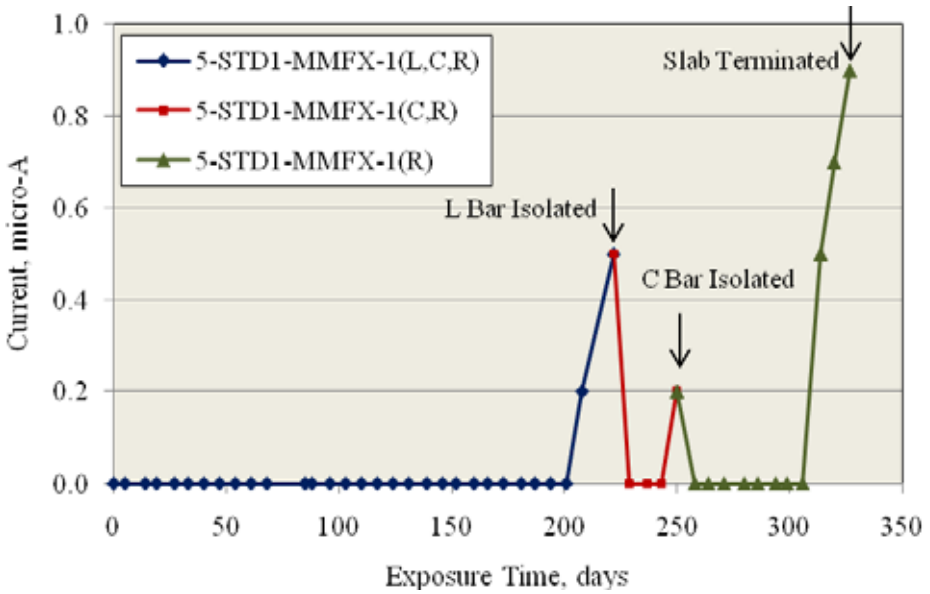

Figure 25. Graph. Macrocell current versus time for specimens reinforced with MMFX-2 steel indicating times that individual bars became active and were isolated (L—left bar; C—center bar; R—right bar).

Time-to-corrosion results for lot 5 specimens are listed in table 12. However, the procedure whereby individual bars were isolated was employed only after the 5-STD-BB slabs had become active and removed from testing. Upon dissection, all three bars in 5-STD-BB-1 and two in 5-STD-BB-2 and 5-STD-BB-3 were found to have locations of active corrosion. Bars without corrosion were treated as runouts. Also, if the extent of corrosion on a given bar was 25 mm or more wide, T_i was taken 8 days earlier than the time at termination. For example, specimen 5-STD-BB-1 was removed for exposure after 68 days. Upon dissection, the left (L) and center (C) bars where found to have corrosion products less broad than 25 mm, whereas for the right (R) bar, corrosion products were more extensive (width or length > 25 mm). While somewhat arbitrary, this data modification was thought to provide a more realistic representation of what occurred than if T_i for all bars had simply been taken as the slab termination time.

Table 12. T_i data for SDS/STD1 specimens with improved performance reinforcements (see table 4 for specimen designation nomenclature).

SDS Specimen	Bar	T_i (days)
5-STD1-BB-1	L	68
	C	68
	R	60
5-STD1-BB-2	L	60
	C	60
	R	> 68
5-STD1-BB-3	L	80
	C	> 88
	R	88
5-STD1-3Cr12-1	L	404
	C	404
	R	314
5-STD1-3Cr12-2	L	124
	C	> 124
	R	> 124
5-STD1-3Cr12-3	L	342
	C	> 342
	R	635
5-STD1-MMFX-2-1	L	264
	C	299
	R	327
5-STD1-MMFX-2-2	L	327
	C	222
	R	327
5-STD1-MMFX-2-3	L	>124
	C	124
	R	>124
5-USDB-MMFX-2-1	L	173
	C	299
	R	299
5-USDB-MMFX-2-2	L	> 749
	C	749
	R	> 749
5-USDB-MMFX-2-3	L	> 342
	C	> 343

Table 12 (continued). T_i data for SDS/STD1 specimens with improved performance reinforcements (see table 4 for specimen designation nomenclature).

SDS Specimen	Bar	T_i (days)
	R	> 344
5-STD1-2101-1	L	250
	C	264
	R	152
5-STD1-2101-2	L	124
	C	> 124
	R	124
5-STD1-2101-3	L	314
	C	628
	R	250

Figure 26 shows a cumulative distribution function (CDF) plot for the STD1 type specimen T_i data in table 12. Weibull statistics were employed because they take runouts into account in generating the best fit line, although the runout data per se are excluded from the plot. The mean T_i for these four reinforcements (the mean in Weibull statistics occurs at a CDF of 62.5 percent) is 76 days for BB, 459 days for 3Cr12, 306 days for MMFX-2, and 297 days for 2101.

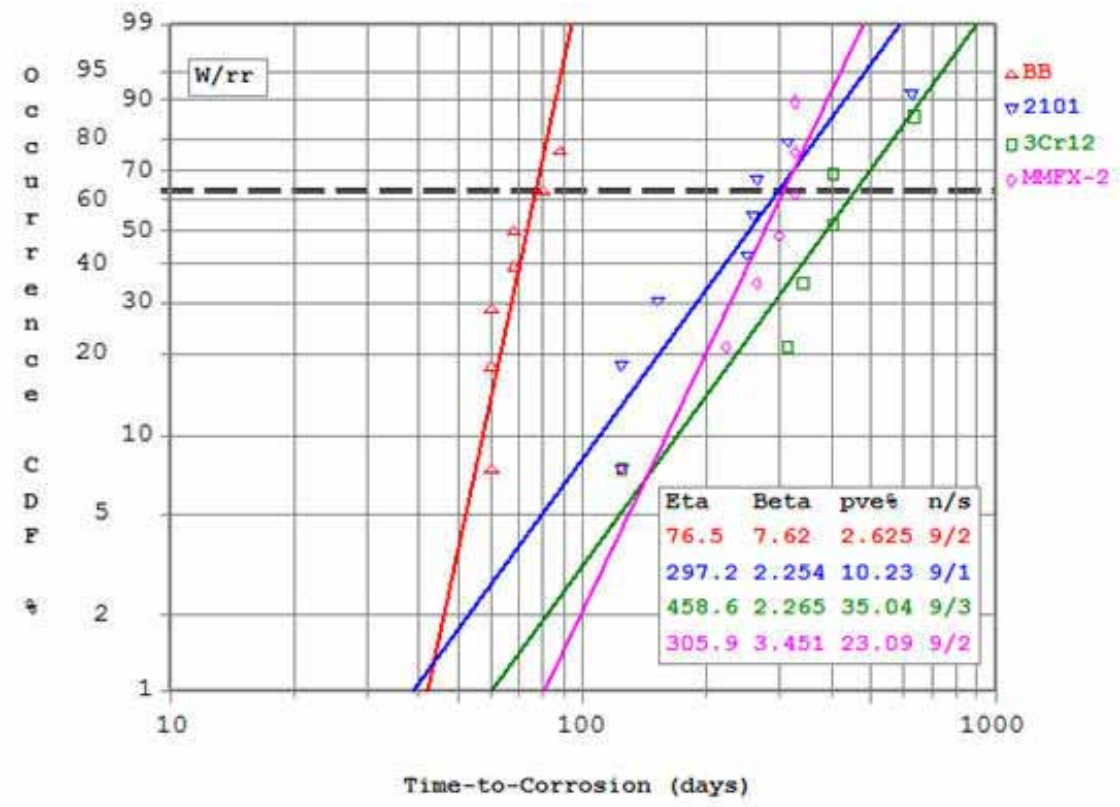

Figure 26. Graph. Weibull cumulative distribution plot of T_i for the four indicated reinforcements.

In the figure, *eta* is the mean (dashed horizontal line), *beta* is a measure of data spread or slope of the best fit line, *pve%* is a measure of the line fit to data, *n* is the total number of specimens, and *s* is the number of runouts. Table 13 lists T_i and the ratio of T_i for individual improved performance bars to BB at 2 percent, 10 percent, and 20 percent active. These percentages were selected to cover a range of values from when damage first occurred to when intervention may be required.

Table 13. Listing of T_i for improved performance reinforcements and T_i ratio to BB for SDS-STD 1 specimens at 2 percent, 10 percent, and 20 percent active.

	T_i (days)				T_i (alloy)/T_i (BB)		
Percent Active	**BB**	**3Cr12**	**MMFX-2**	**2101**	**3Cr12**	**MMFX-2**	**2101**
2	44	81	91	52	1.8	2.1	1.2
10	55	160	175	108	2.9	3.2	2.0
20	62	225	225	140	3.6	3.6	2.3

Figure 27 shows a CDF plot of T_i for the two types of specimens reinforced with MMFX-2, which includes STD and USDB (3-mm-diameter holes were drilled through the surface layer on the upper side of the top bars at 25 mm spacing). Here, the mean T_i for the STD specimens is 306 days and 809 days for the USDB specimens. It is unclear if this distinction is simply specimen-to-specimen scatter or if it reflects actual differences; however, no reason is apparent why surface damaged bars of this alloy should exhibit greater resistance to corrosion initiation than undamaged ones.

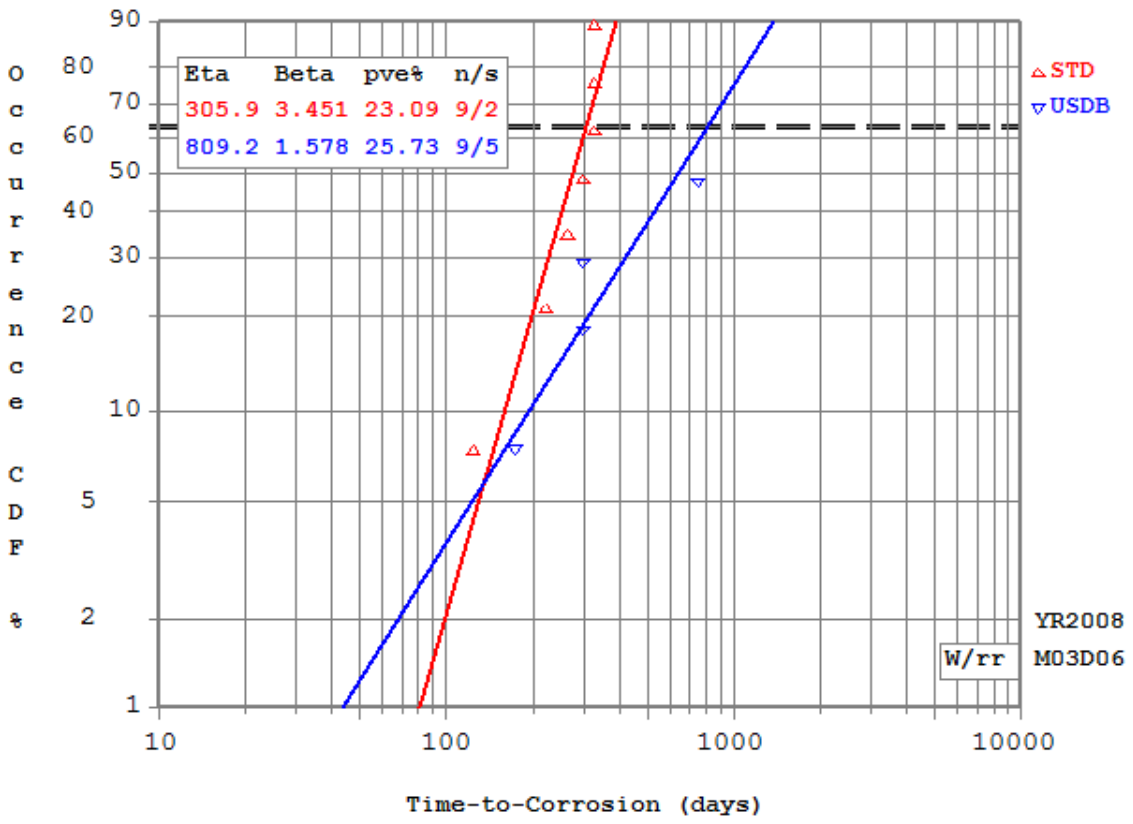

Figure 27. Graph. Weibull cumulative distribution plot of T_i for STD and USDB MMFX-2 reinforcements.

Figure 28 reproduces figure 26 but with both the STD and USDB MMFX-2 specimens included as a common data set. This transposes the MMFX-2 mean T_i from 306 days to 435 days, which is essentially the same as for 3Cr12 and at the upper bound for the alloys shown here.

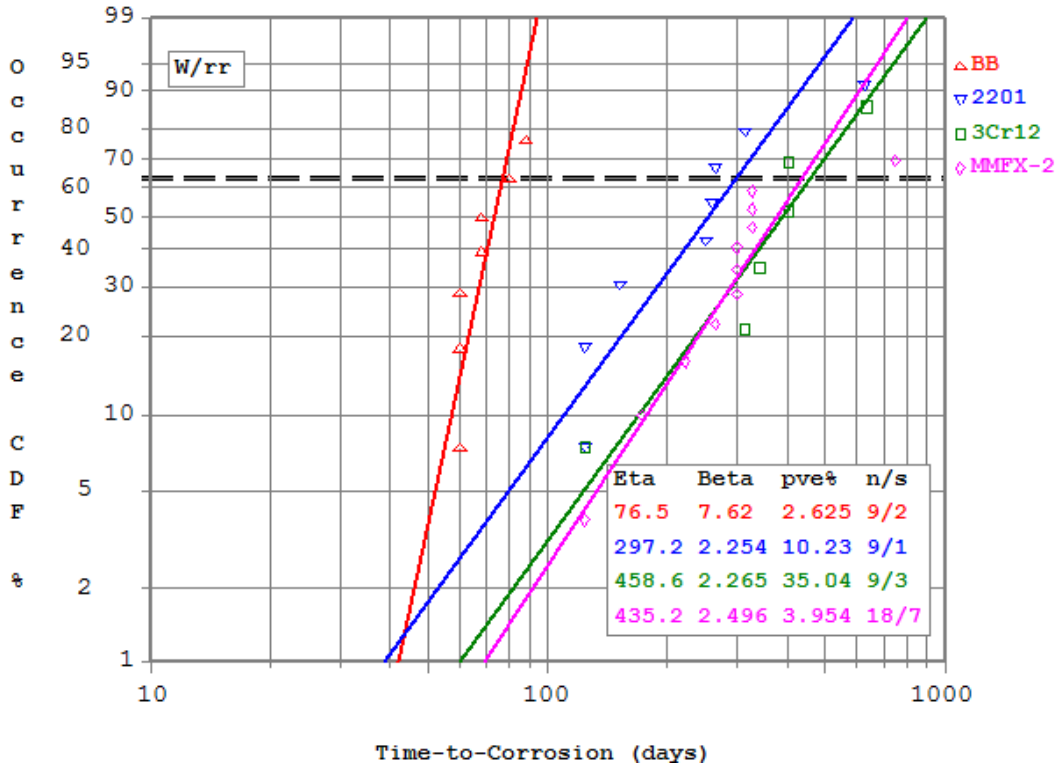

Figure 28. Graph. Weibull cumulative distribution plot of T_i treating all STD and USDB-MMFX-2 reinforced specimens as a single population.

Referencing T_i data to the mean value has little practical significance because the mean value corresponds to widespread corrosion having occurred. For this reason, table 14 lists T_i values from figure 28 corresponding to 2 percent, 10 percent, and 20 percent probability of corrosion initiation, as well as the ratio of T_i for each alloy to that for BB. Consistent with the large *beta* (less T_i scatter) in figure 28 for BB specimens compared to the three more CRR, the T_i ratio for each increased with increasing percent active. Thus, 3Cr12 and MMFX-2 were the better performers with T_i(alloy)/T_i(BB) near 2 at 2 percent active and 3.8 at 20 percent active.

Table 14. Listing of T_i for improved performance reinforcements and T_i ratio to BB for SDS-STD 1 specimens at 2 percent, 10 percent, and 20 percent active based on all MMFX-2 specimens.

	T_i (days)				T_i(alloy)/T_i(BB)		
Percent Active	BB	3Cr12	MMFX-2	2101	3Cr12	MMFX-2	2101
2	44	81	91	52	1.8	2.1	1.2
10	55	160	177	108	2.9	4.0	2.0
20	62	225	239	140	3.6	3.9	2.3

4.1.1.3 Results for High Performance Reinforcements in SDS Specimens

Table 15 lists exposure duration and macrocell current measurement results for the two types of 316SS (316.16.and 316.18, see table 1) reinforced SDS specimens that either did not initiate corrosion or that eventually did initiate corrosion on lower layer BB, as indicated by a negative macrocell current.

Table 15. Listing of exposure times and macrocell current data for Type 316SS SDS reinforced slabs.

Specimen No	Exposure Time (days)	No Curr Meas	No Zero Curr Readings	No Non-Zero Curr Readings	Max Neg Curr Recorded (μA)
1-STD1-316.16-1	1,726	178	178	0	—
1-STD1-316.16-2	1,726	178	178	0	—
1-STD1-316.16-3	1,726	178	178	0	—
1-STD2-316.16-1	1,726	178	178	0	—
1-STD2-316.16-2	1,726	178	178	0	—
1-STD2-316.16-3	1,726	178	178	0	—
3-STD1-316.18-1	1,585	1,585	1,585	0	—
3-STD1-316.18-2	1,585	1,585	1,585	0	—
3-STD1-316.18-3	1,585	1,585	1,585	0	—
2-STD2-316.18-1	1,669	1,669	1,669	0	—
2-STD2-316.18-2	1,669	1,669	1,669	0	—
2-STD2-316.18-3	1,669	1,669	1,669	0	—
3-CCON-316.18-1	1,585	1,585	1,585	0	—
3-CCON-316.18-2	1,585	1,585	1,585	0	—
3-CCON-316.18-3	1,585	1,585	1,585	0	—
2-WB-316.16-1	1,669	1,72	172	0	—
2-WB-316.16-2	1,669	1,72	172	0	—
2-WB-316.16-3	1,669	172	172	0	—
3-CCON-316.16-1	1,585	157	157	0	—
3-CCON-316.16-2	1,585	157	157	0	—
3-CCON-316.16-3	1,585	157	157	0	—
3-CREV-316.16-1	1,585	157	157	0	—

Table 15 (continued). Listing of exposure times and macrocell current data for Type 316SS SDS reinforced slabs.

Specimen No	Exposure Time (days)	No Curr Meas	No Zero Curr Readings	No Non-Zero Curr Readings	Max Neg Curr Recorded (μA)
3-CREV-316.16-2	1,585	157	157	0	—
3-CREV-316.16-3	1,585	157	157	0	—
3-CCRV-316.16-1	1,585	157	157	0	—
3-CCRV-316.16-2	1,585	157	157	0	—
3-CCRV-316.16-3	1,585	157	157	0	—
2-BCAT-316.16-1	1,669	172	144	28	0.4
2-BCAT-316.16-2	1,669	172	124	48	0.2
2-BCAT-316.16-3	1,196	159	147	12	0.2
2-CCNB-316.16-1	1,669	172	101	71	0.3
2-CCNB-316.16-2	1,669	172	124	48	0.3
2-CCNB-316.16-3	1,669	172	86	86	0.3

—indicates that no specimen of the indicated type was fabricated.

Figure 29 shows a plot of macrocell current versus exposure time for specimens with a bottom BB mat.

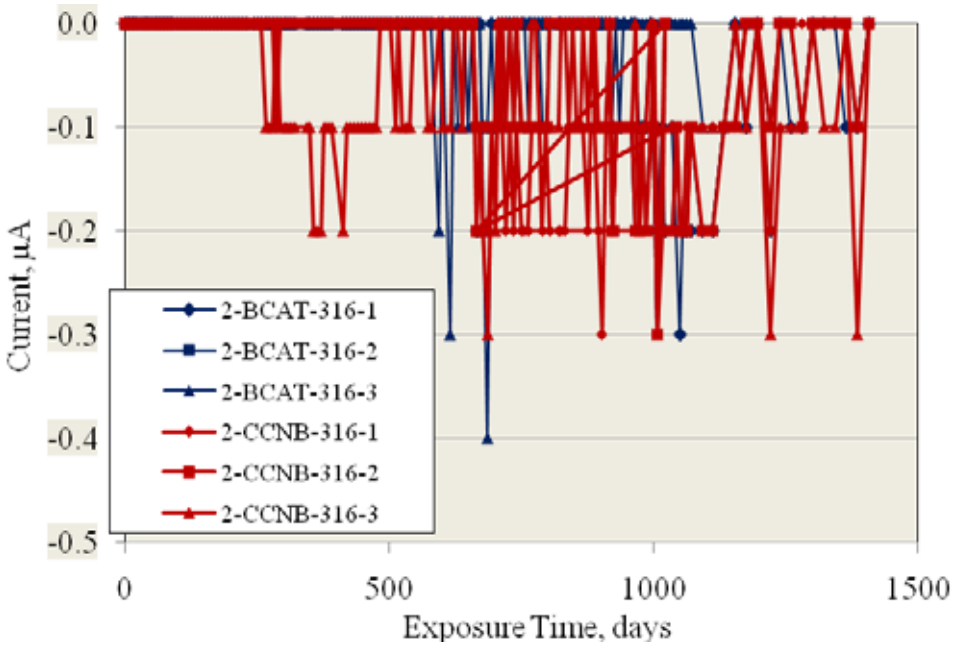

Figure 29. Graph. Macrocell current history for 316 reinforced slabs with BB lower steel.

Table 16 lists data for Type 304SS reinforced slabs and indicates the same response as for the 316 (no macrocell current except for specimens fabricated with lower mat BB, which did eventually initiate corrosion).

Table 16. Listing of exposure times and macrocell current data for Type 304SS reinforced slabs.

Specimen No	Exposure Time (days)	No Curr Meas	No Zero Curr Readings	No Non-Zero Curr Readings	Max Neg Curr Recorded (μA)
6-STD1-304-1	440	22	22	0	—
6-STD1-304-2	440	22	22	0	—
6-STD1-304-3	440	22	22	0	—
6-STD2-304-1	440	22	22	0	—
6-STD2-304-2	440	22	22	0	—
6-STD2-304-3	440	22	22	0	—
6-WB-304-1	440	22	22	0	—
6-WB-304-2	440	22	22	0	—
6-WB-304-3	440	22	22	0	—
6-CCON-304-1	440	22	22	0	—
6-CCON-304-2	440	22	22	0	—
6-CCON-304-3	440	22	22	0	—
6-CREV-304-1	440	22	22	0	—
6-CREV-304-2	440	22	22	0	—
6-CREV-304-3	440	22	22	0	—
6-CCRV-304-1	440	22	22	0	—
6-CCRV-304-2	440	22	22	0	—
6-CCRV-304-3	440	22	22	0	—
6-BCAT-304-1	440	22	22	1	0.2
6-BCAT-304-2	440	22	22	7	0.7
6-BCAT-304-3	440	22	22	5	0.6
6-CCNB-304-1	440	22	22	3	0.9
6-CCNB-304-2	440	22	22	3	0.8
6-CCNB-304-3	440	22	22	1	0.1

— indicates that no specimen of the indicated type was fabricated.

Table 17 lists parameters and macrocell current measurement results for SDS slabs reinforced with STAX. The data indicate that isolated instances of measurable current occurred on occasion. However, for the most part, the macrocell current was 0 μA. Specimen configurations for this reinforcement type were limited to those shown because of material stock limitations.

Table 17. Corrosion activity for Stelax reinforced SDS specimens.

Specimen No	Exposure Time (days)	No Curr Meas	No Zero Curr Readings	No Non-Zero Curr Readings	Current Recorded (μA)
1-STD1-Stelax-1	1,726	178	177	1	0.1
1-STD1-Stelax-2	1,726	178	164	14	-0.2 to 0.3
1-STD1-Stelax-3	1,726	178	171	7	0.1
1-STD2-Stelax-1	1,726	178	178	0	0
1-STD2-Stelax-2	1,726	178	178	0	0
1-STD2-Stelax-3	1,726	178	178	0	0

Results for SMI reinforced SDS slabs—other than those with a bar crevice, BB lower layer, concrete crack, or clad defects (or combinations of these)—are listed in table 18. In general, the macrocell current that occurred in some cases was small and infrequent.

Table 18. Listing of SMI reinforced SDS specimens and macrocell current results.

Specimen No	Exposure Time (days)	Total No Curr Meas	No Zero Curr Readings	No Non-Zero Curr Readings	Maximum Current Recorded (μA)
4-STD1-SMI-1	944	112	112	0	—
4-STD1-SMI-2	944	112	112	0	—
4-STD1-SMI-3	944	112	112	0	—
4-STD2-SMI-1	944	112	112	0	—
4-STD2-SMI-2	944	112	112	0	—
4-STD2-SMI-3	944	112	112	0	—
4-CCON-SMI-1	944	112	111	1	0.1
4-CCON-SMI-2	944	112	112	0	—
4-CCON-SMI-3	944	112	112	6	0.1
4-CREV-SMI-1	944	112	112	0	—
4-CREV-SMI-2	994	112	111	1	0.6
4-CREV-SMI-3	994	112	112	0	—
4-CCRV-SMI-1	994	112	112	0	—
4-CCRV-SMI-2	994	112	103	9	0.6
4-CCRV-SMI-3	994	112	112	0	—
4-USDB-SMI-1	994	112	112	0	—
4-USDB-SMI-2	994	112	111	1	0.2
4-USDB-SMI-3	994	112	112	0	—

— indicates that no specimen of the indicated type was fabricated.

Table 19 lists the results for the other SMI specimens, which exhibited a distinct T_i. As indicated, T_i was 0 days for specimens of the CSDB condition (simulated concrete crack and 3-mm-diameter holes through the cladding spaced at 25-mm intervals on the top of upper bars), 20 days to 29 days for BCCD specimens (holes drilled through the cladding and BB bottom layer), and 139 days to 230 days for CVNC (top layer bars with a crevice and no caps on embedded bar ends).

Table 19. Results for SMI reinforced SDS specimens that exhibited a defined T_i followed by measureable macrocell corrosion.

Specimen No	T_i (days)	Exposure Duration (days)
4-BCCD-SMI-1	29	944
4-BCCD-SMI-2	20	944
4-BCCD-SMI-3	20	944
4-CSDB-SMI-1	0	944
4-CSDB-SMI-2	0	944
4-CSDB-SMI-3	0	944
6-CVNC-SMI-1	139	440
6-CVNC-SMI-2	230	440
6-CVNC-SMI-3	139	440

Figure 30 provides a plot of macrocell current versus time for SDS-SMI specimen sets.

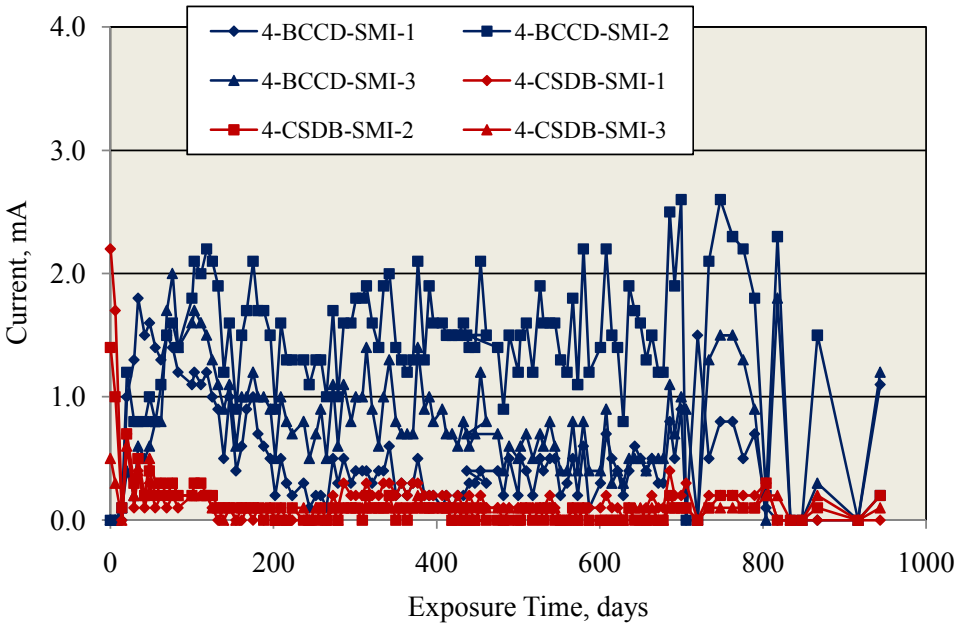

Figure 30. Graph. Current-time history for SDS-SMI specimens that initiated corrosion.

Three Type 2304SS reinforced STD1 specimens have been under test for 929 days with no macrocell current activity. Table 20 lists all high performance alloy reinforcement/specimen

types that did not initiate corrosion within the exposure time and the corresponding ratio of T_i for each to the mean T_i for STD1 BB specimens (76 days, figure 24 and figure 26). Because exposure times were different for different specimen sets, the ratios vary from one alloy to the next but are as high as > 22.

Table 20. Ratio of T_i for CRR that did not initiate corrosion to the mean T_i for BB specimens.

Alloy/Specimen Type	T_i (alloy)/T_i (BB)
STD1-316.16	> 22
STD2-316.16	> 22
STD1-316.18	> 21
STD2-316.18	> 22
CCON-316.16	> 21
CCON-316.18	> 21
WB-316.16	> 22
CREV-316.16	> 21
CCRV-316.16	> 21
STD1-304	> 6
STD2-304	> 6
WB-304	> 6
CCON-304	> 6
CREV-304	> 6
CCRV-304	> 6
STD1-Stelax	> 22
STD2-Stelax	> 22
STD1-SMI	> 12
STD2-SMI	> 12
STD1-2304	> 12

4.1.2 Results for Macrocell Slab (MS) Specimens

4.1.2.1 Results for Improved Performance Reinforcements in MS Specimens

Outdoor Exposures. The potential and macrocell current versus time trends for STD1-MS specimens with improved performance reinforcements were generally similar to those indicated previously for comparable SDS specimens (figure 24 and figure 25), as shown by figure 31 to figure 34. These plots show that macrocell current was nearly 0 µA initially but abruptly increased in most, but not all, cases; the potential correspondingly became more negative. Time-to-corrosion was defined for SDS specimens as initial occurrence of measureable, sustained macrocell current. Because there was only a single top bar (anode) for this specimen type, no bar isolation procedure was performed as was done for SDS specimens.

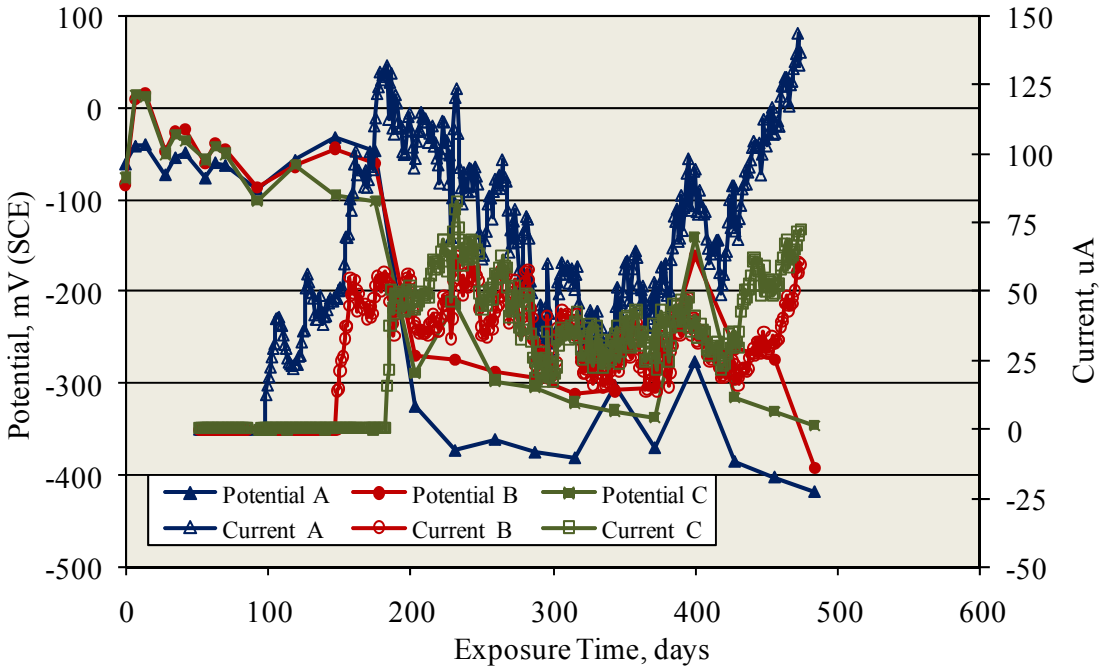

Figure 31. Graph. Potential and macrocell current results for MS-STD1-BB specimens.

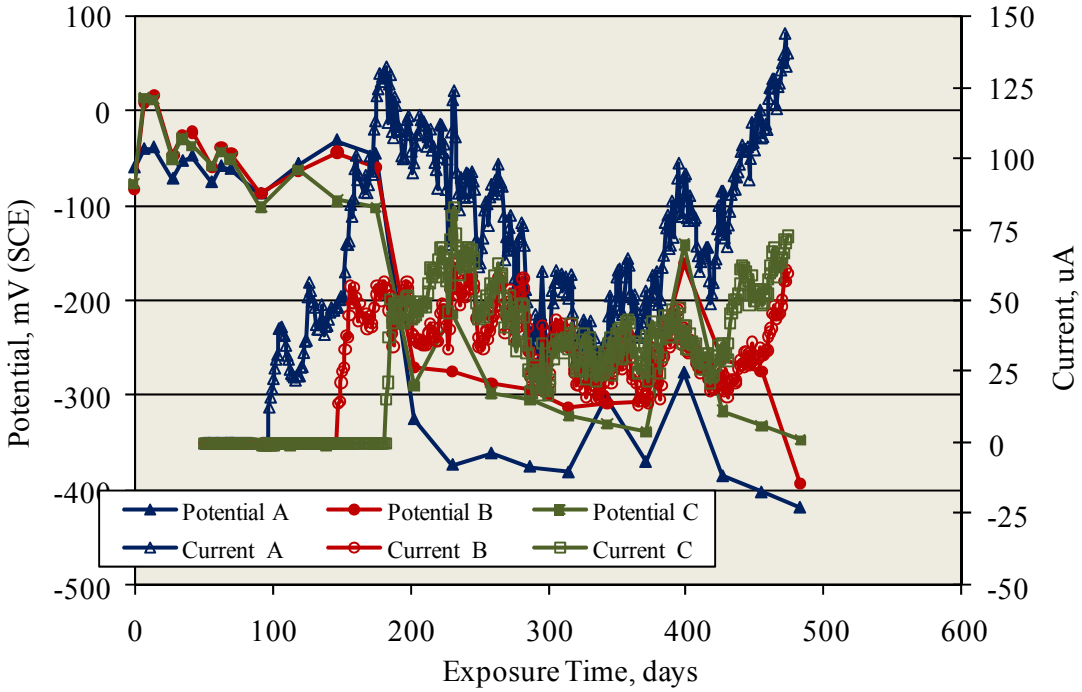

Figure 32. Graph. Potential and macrocell current results for MS-STD1-3Cr12 specimens.

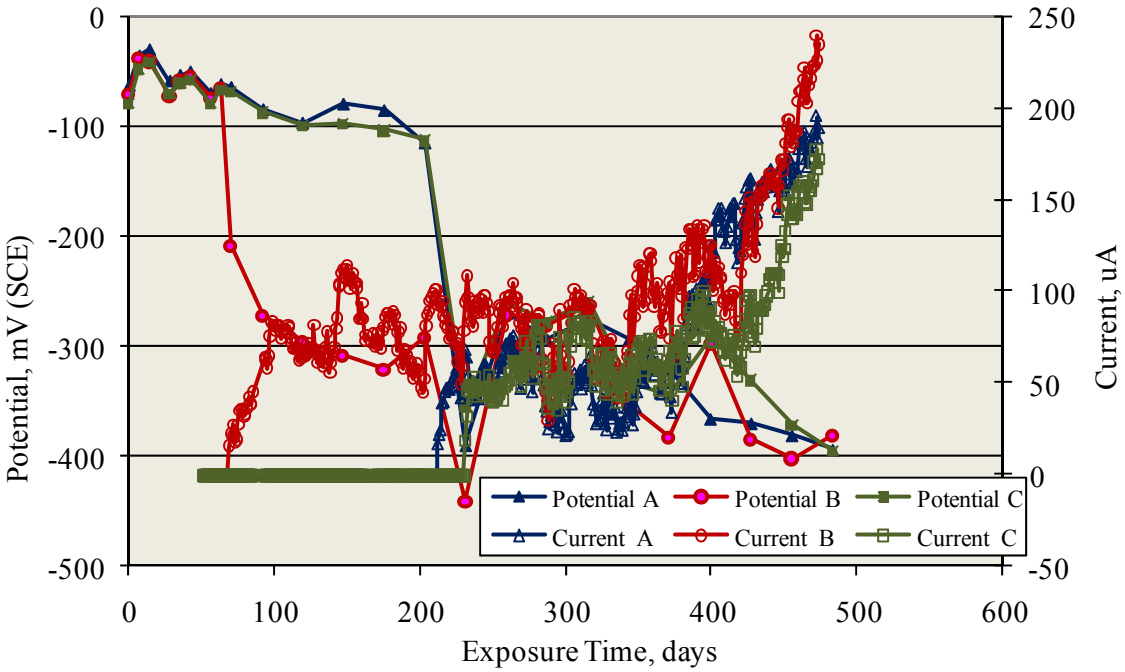

Figure 33. Graph. Potential and macrocell current results for MS-STD1-MMFX-2 specimens.

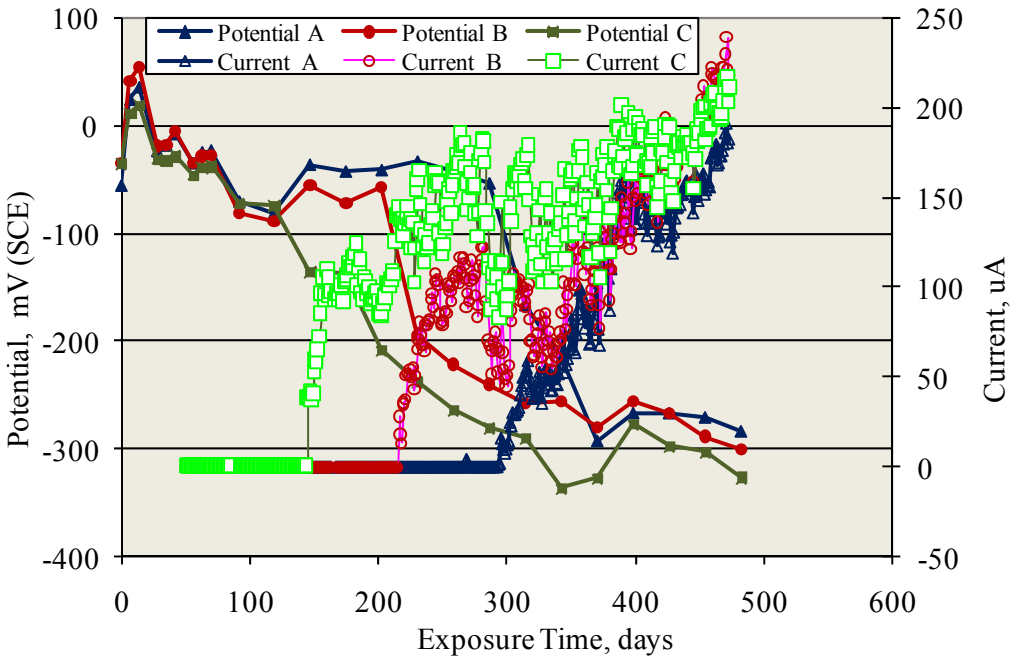

Figure 34. Graph. Potential and macrocell curent results for MS-STD-1-2101 specimens.

Table 21 lists the T_i values for MS-STD1 specimens reinforced with BB, 3Cr12, MMFX-2, and 2101.

Table 21. Listing of T_i values for MS-STD1 specimens with improved performance reinforcements.

T_i (days)			
BB	**3Cr12**	**MMFX-2**	**2101**
97	121	68	144
147	212	211	215
182	488	230	295

Figure 35 shows a normal distribution CDF plot of T_i. In contrast to results for the SDS specimens (figure 26 and figure 28), the extent to which T_i was enhanced for the improved performance reinforcements in STD1 concrete is modest, particularly when corrosion initiation percentages were low, and the single 3Cr12 datum at 488 days was neglected.

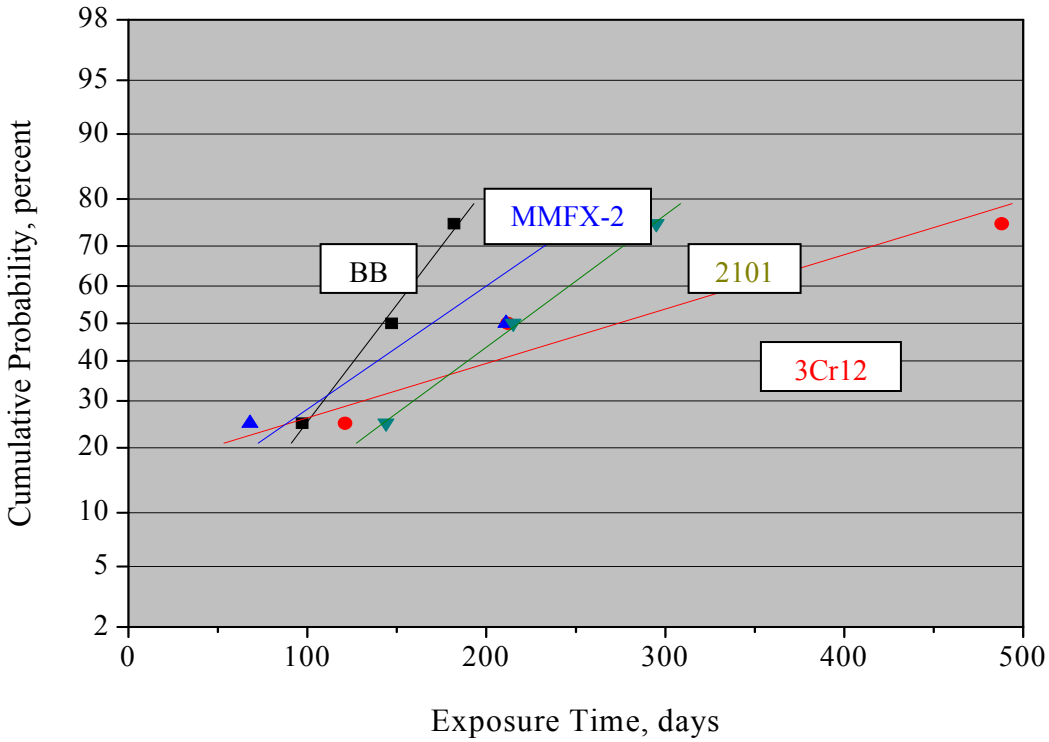

Figure 35. Graph. Cumulative probability plot of T_i for STD1-MS specimens with improved performance reinforcements.

Table 22 shows T_i values for other STD1-MS specimen types reinforced with 3Cr12, MMFX-2, and 2101.

Table 22. Listing of T_i values (days) for MS specimens with improved performance reinforcements other than STD.

	3Cr12	MMFX-2	2101
ARWB	430	85	52
	433	223	137
	1,229	244	195
BENT	57	152	178
	92	229	201
	228	284	345
BCAT	222*	149*	93
	505	1,314	142
	980	1,254*	163
BNTB	173	91	178
	185	93	254*
	346	222	466
CCON	< 43	< 43	69
	< 43	208	85
	< 43	458	158
CBNB	0	0	63
	0	0	159
	0	0	293*
CBNT	0	0	< 43
	0	0	75
	0	0	498
CCNB	0	< 43	110
	0	< 43	142
	0	450	411
UBDB	—	232	—
	—	> 358	—
	—	> 358	—
USDB	—	179	—
	—	300	—
	—	324	—
CBDB	—	50	—
	—	138	—
	—	267	—

* Corrosion initiated at one or more lower black bars;

— indicates that no specimen of the indicated type was fabricated.

Table 22 shows T_i values for other STD1-MS specimen types reinforced with 3Cr12, MMFX-2, and 2201. Figure 34 shows a Weibull CDF plot of T_i that includes data for both the STD (table 21 and figure 36) and BENT, BNTB, BCAT, and USDB (table 22) specimen types based on the assumption that data for each alloy conform to a common population. The results show that T_i is approximately the same for all reinforcements at a relatively low activation percentage but with T_i for 3Cr12, MMFX-2, and 2101 diverging to slightly higher values as the active percentage increases. For specimens with a simulated crack (CBDB, CBNB, CBNT, and CCNB; table 22), corrosion initiated in less than 43 days for 3Cr12 and MMFX-2, but it was greater for 2101.

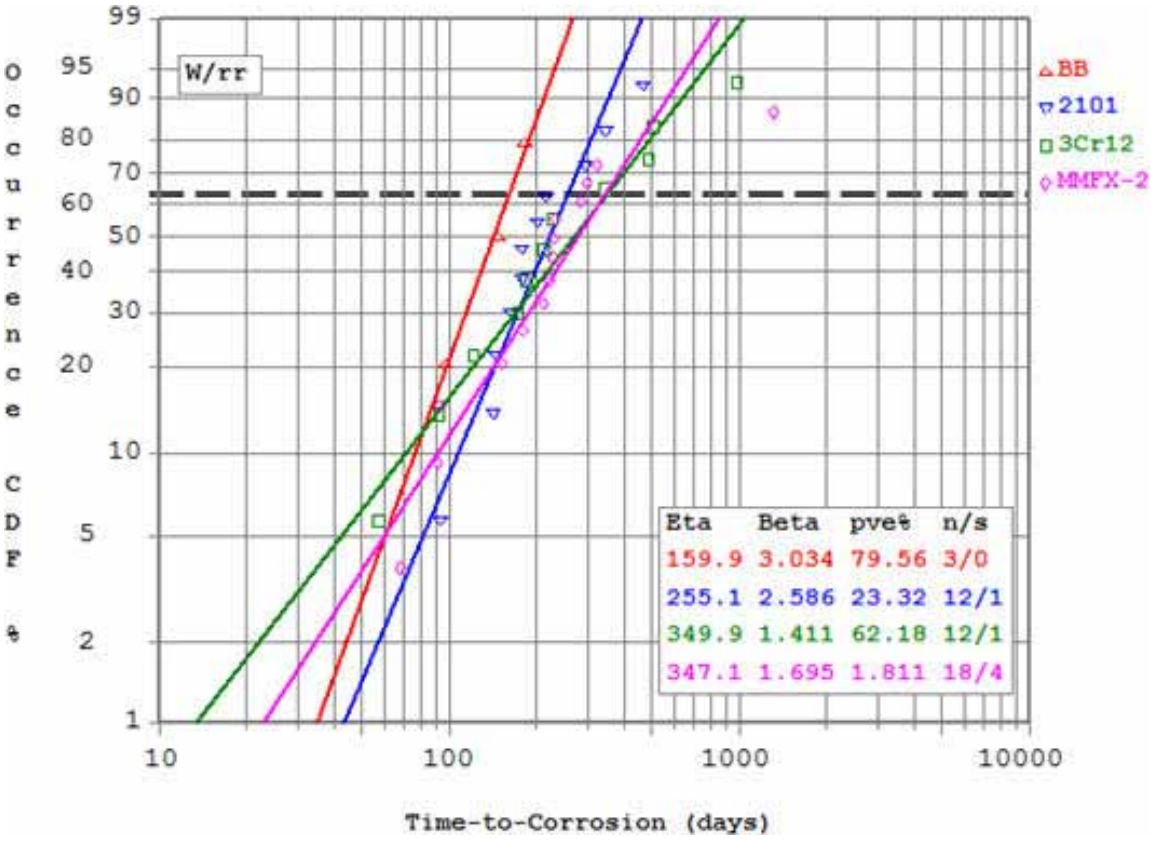

Figure 36. Graph. Weibull CDF plot of T_i for MS-STD1, -BCAT, -BENT, -BNTB, -UBDB, and -USDB specimens.

Data for STD2-MS specimens were not always conducive to definitively identifying T_i. Thus, figure 37 and figure 38 show potential and macrocell current data for the three BB MS specimens, and figure 39 and figure 40 show the data for the three 3Cr12 specimens. As for the SDS specimens, positive macrocell current corresponds to an anodic top bar. Corrosion was assumed to have initiated at the time at which this current increased to above the background level, which was near 0 μA. For MS-BB-1 in figure 38, a negative current occurred after 168 days, indicating that a lower bar (or bars) had initiated corrosion with the top bar serving as a cathode. This situation continued to 405 days, at which time the top bar activated and was anodic to the four lower bars. In the intermediate period, the top bar was cathodically polarized by one or more lower bars. This polarization is expected to have elevated the critical chloride concentration for corrosion initiation of the top bar. For MS-BB-2, corrosion initiated on the top bar after 180 days (positive macrocell current), but this polarity reversed at 275 days. These results indicate that a lower bar had

activated, and its potential was more negative than that for the top bar. Corrosion of the top bar reinitiated after 483 days. Specimen MS-BB-3 behaved in a more conventional manner in that macrocell current was 0 μA until the top bar activated after 488 days.

In analysis of these data, a specimen was considered to have initiated corrosion upon initial occurrence of either a positive or negative current. For 3Cr12, current excursions were both positive and negative as for BB specimens, but they were smaller in magnitude and subsequently often reverted to near 0 μA, indicating repassivation. Specimen MS-3Cr12-1 was terminated after 1,233 days, and no corrosion was apparent upon dissection. Because of these complexities, data for 3Cr12 specimens was excluded in the T_i analysis. Specimens reinforced with MMFX-2 and 2101, on the other hand, exhibited better defined corrosion initiation for the top bar only. This is illustrated by figure 41 for STD2-MMFX-2 MS specimens, where specimen B initiated corrosion after 974 days, although the corresponding potential decrease was relatively modest (≤ 100 mV). Specimen C was removed after 1,221 days, and dissection revealed no corrosion. Specimen A remains under testing with no indication of corrosion initiation.

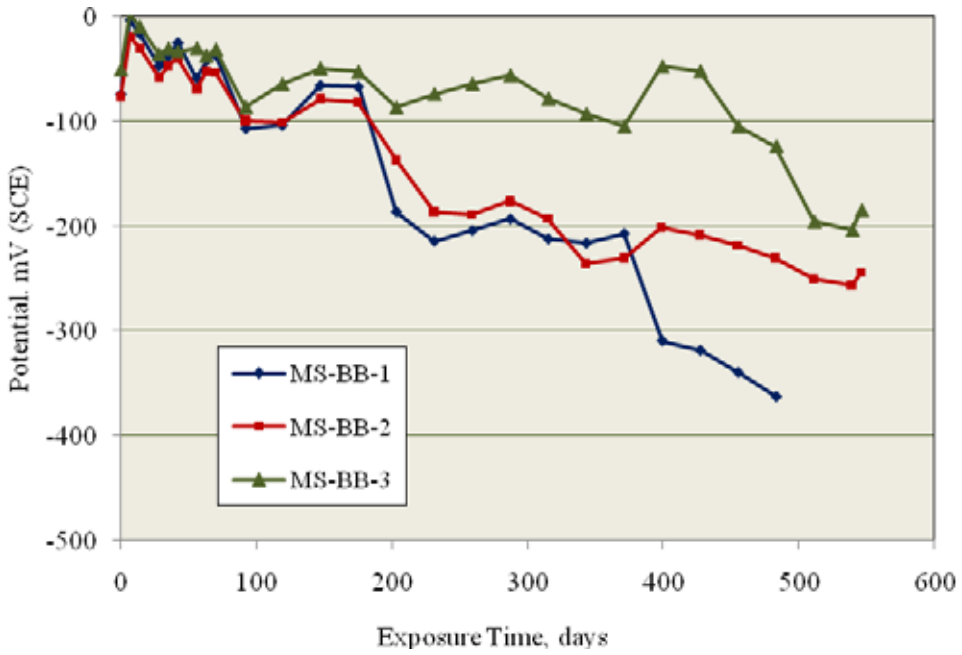

Figure 37. Graph. Potential versus time for STD2 black bar MS specimens.

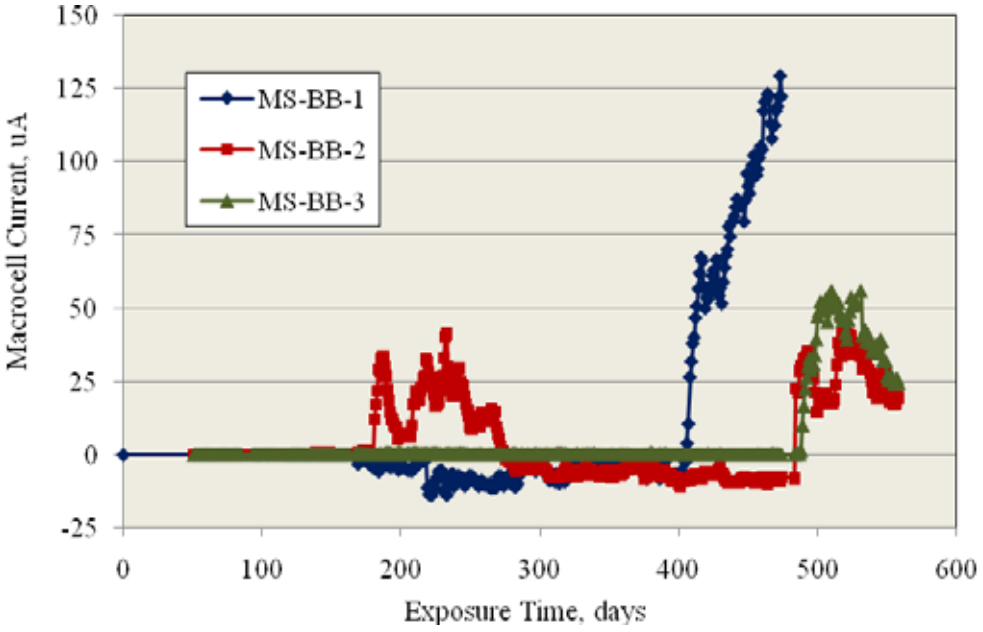

Figure 38. Graph. Macrocell versus time for STD2 black bar MS specimens.

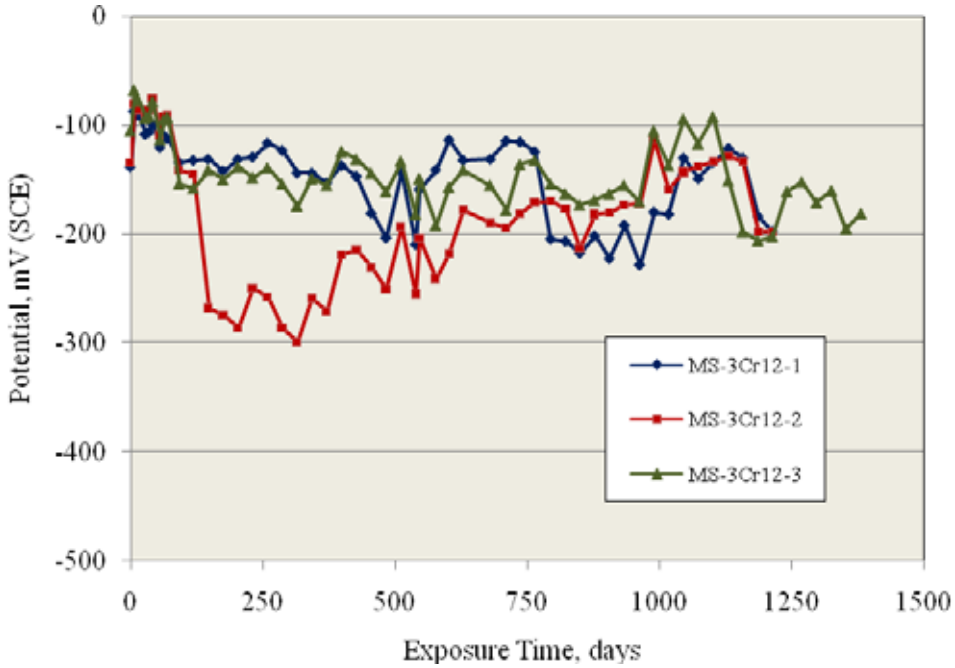

Figure 39. Graph. Potential versus time for STD2 3Cr12 MS specimens.

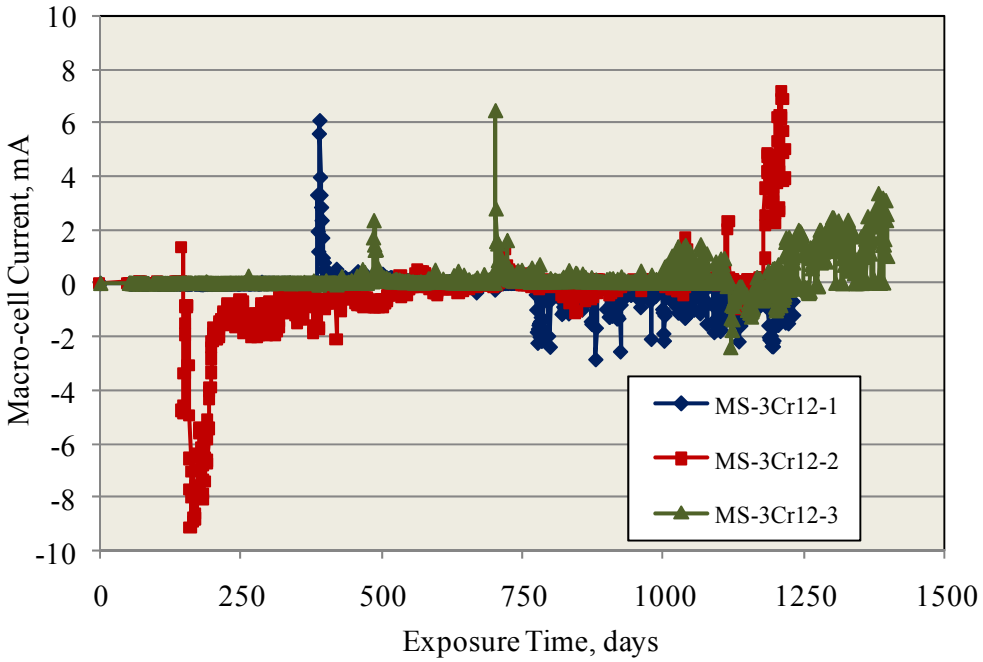

Figure 40. Graph. Macrocell current versus time for STD2 3Cr12 MS specimens.

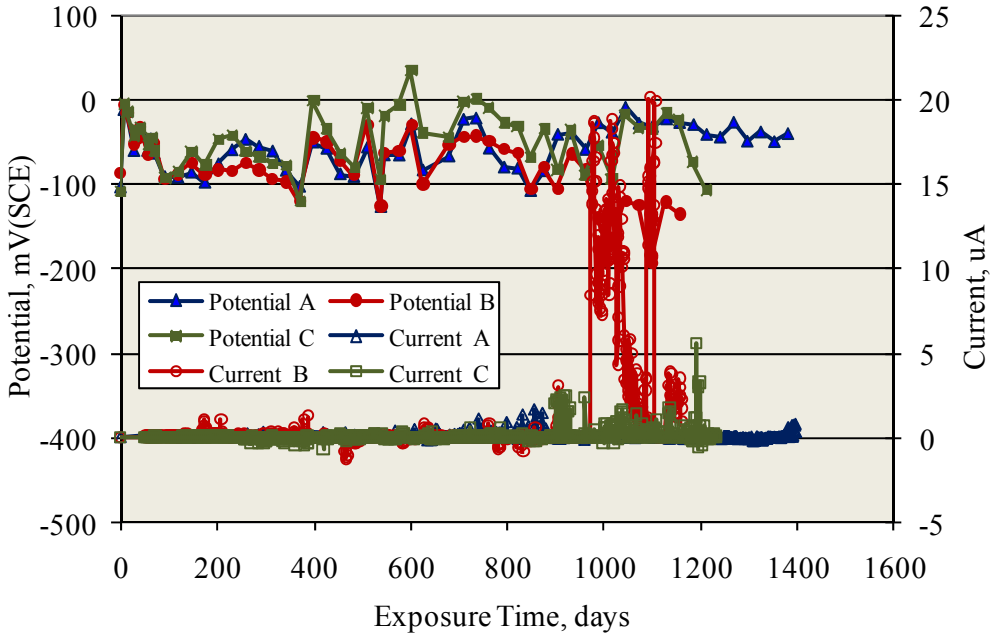

Figure 41. Graph. Potential and macrocell current versus time for STD2 MMFX-2 MS specimens.

Based on the previously stated protocol, table 23 lists T_i values for the MS STD2 specimens. In the case of 3Cr12, one specimen was removed after 1,233 days and dissected; however, no corrosion was apparent. A second specimen apparently initiated corrosion after 1,181 days as an increase in macrocell current from near zero to a range of 4 µA to 7 µA occurred. The third specimen remains

under test after 1,399 days with macrocell current in the range 0 μA to 2 μA. It is unclear if corrosion has initiated in this case.

Table 23. Listing of T_i values for MS-STD2 specimens with improved performance reinforcements.

BB	3Cr12	MMFX-2	2101
168	1,181	974	855
180	> 1,233	> 1,221	1,017
488	> 1,399	> 1,387	> 1,224

Figure 42 shows a CDF plot of T_i where data for 3Cr12 have been omitted because of the uncertainties mentioned previously. Corrosion initiation for BB specimens was considered to have occurred at the initial onset of macrocell current, either positive or negative. Runout data (indicated by arrows at data points in figure 40) were treated as if corrosion had initiated at the indicated time.

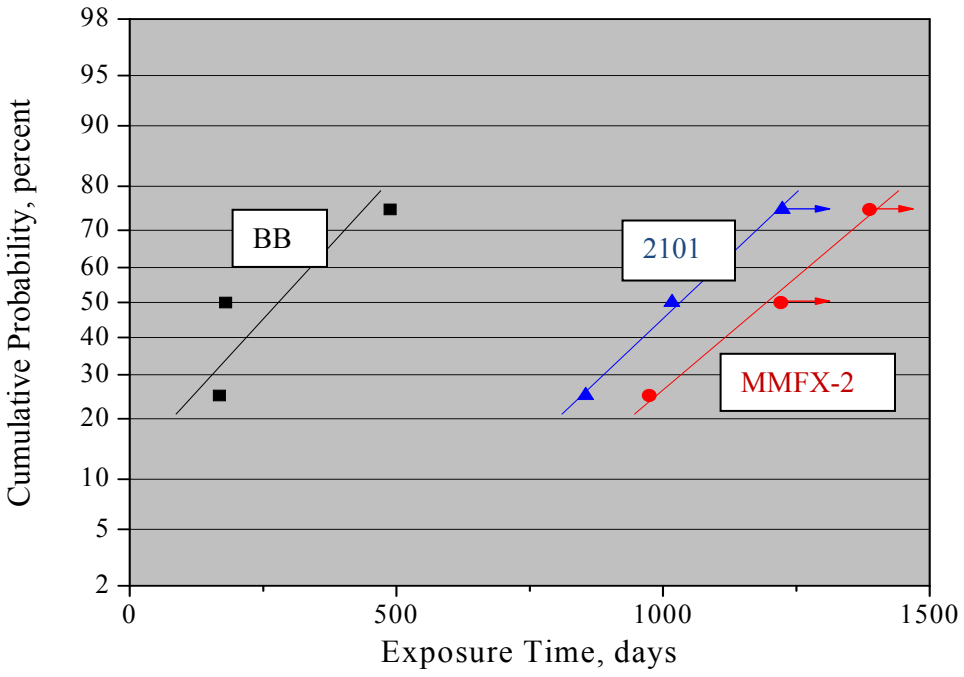

Figure 42. Graph. Normal CDF plot of T_i for MS-STD2 specimens that exhibited a well-defined corrosion initiation.

Because of the limited data, it was necessary in generating this plot to treat runouts (two of the three MMFX-2 data and one of three for 2101) as having initiated corrosion at the time of termination, although either no corrosion was detected upon dissection of these specimens or the specimens remain under test. The data were insufficient for application of Weibull statistics. An attempt was made to project T_i(alloy)/T_i(BB), as was done above for SDS specimens; however, it was complicated by the fact that the best fit line through the three BB data points indicates negative

T_i at small percentages active. For this reason, it was assumed that T_i at 2 percent, 10 percent, and 20 percent active was the value for the first BB specimen to become active (168 days). Doing this yields the T_i(alloy)/T_i(BB) results in table 24. However, if data for the lower percentages active were available, the ratios would be greater than indicated.

Table 24. Listing of T_i(alloy)/T_i(BB) for STD2-MS-MMFX-2 and -2101 reinforced specimens.

Percent Active	T_i(alloy)/T_i(BB)	
	MMFX-2	2101
2	3.4	2.7
10	> 4.8	3.9
20	> 5.7	> 4.8

The higher values for these ratios compared to the STD1 results (table 21, figure 35, and figure 36) suggest that when comparing STD2 to STD1, better quality concrete (lower permeability) may be required to realize significantly greater T_i for these improved performance reinforcements compared to BB. Figure 43 shows a schematic plot of [Cl^-] at a particular depth into concrete versus exposure time, assuming Fickian diffusional transport. The figure illustrates that T_i(alloy)/T_i(BB) for relatively low permeability concrete exceeds T_i(alloy)/T_i(BB) in high permeability concrete.

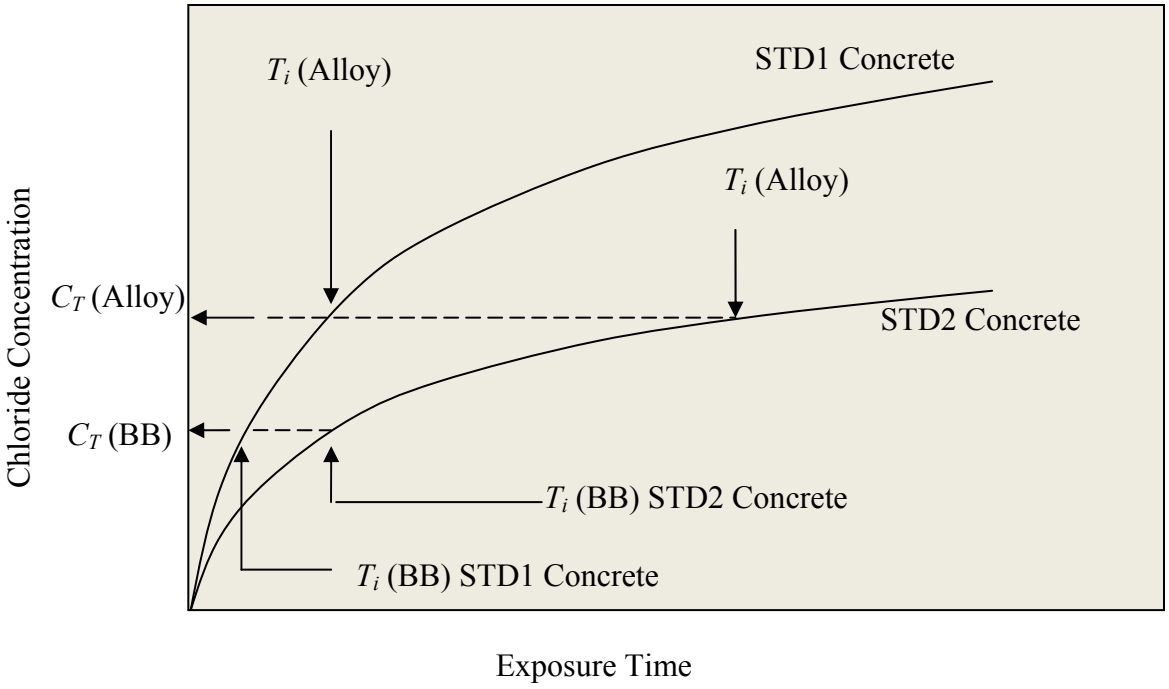

Figure 43. Chart. T_i for BB and an improved performance reinforcement in STD1 and STD2 concretes.

Controlled Temperature and Relative Humidity Exposures. Table 25 lists the T_i for individual specimens that underwent this exposure—all of which were of the STD1 mix design (designated STD1G in this case)—along with comparable STD1 data (table 21) and the average for each specimen type. This table shows that the average T_i for STD1G and STD1 was approximately the same for BB; however, for the three additional CRR, T_i for STD1G exceeded that for STD1. Variations in temperature and relative humidity, as occurred for the outdoor exposures, may have promoted sorptive transport of the ponding solution in the STD1 specimens, such that C_T was reached at the bar depth in a shorter time than for the STD1G specimens. It is possible that the relatively low C_T for BB specimens precluded this effect being apparent for this reinforcement.

Table 25. Listing of T_i for STD1G and STD1-MS specimens along with the three specimen average for each of the two exposures.

STD1G				STD1			
BB	**3Cr12**	**MMFX-2**	**2101**	**BB**	**3Cr12**	**MMFX-2**	**2101**
64	320	201	348	97	121	68	144
201	433	201	433	147	212	211	215
201	516	376	680	182	488	230	295
Average							
155	423	259	487	142	274	170	218

4.1.2.2 Results for High Performance Reinforcement in MS Specimens

Outdoor Exposures. Figure 44 to figure 48 show plots of potential and macrocell current versus time for 316.16SS, 316.18SS, 304SS, STAX, and SMI reinforced STD1-MS specimens. With the exception of the 316.16 data, for which macrocell current excursions were relatively small, the plots consist of occasional current "bursts" to as high as 38 μA (figure 47) followed by repassivation. For STD2-MS-304, -316.16, and -316.18 specimens, macrocell current excursions were of lesser magnitude and more infrequent than for STD1. In the case of STD2-MS-SMI and -STAX, the excursions were about the same as for STD1.

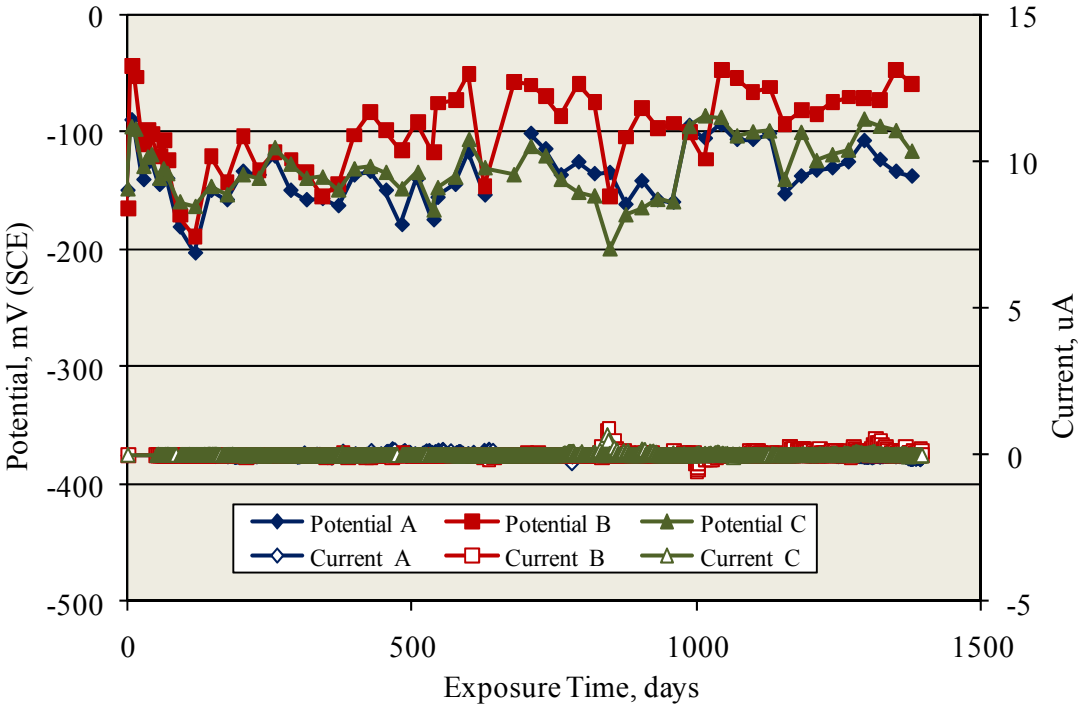

Figure 44. Graph. Potential and macrocell current history for MS-STD1-316.16 specimens.

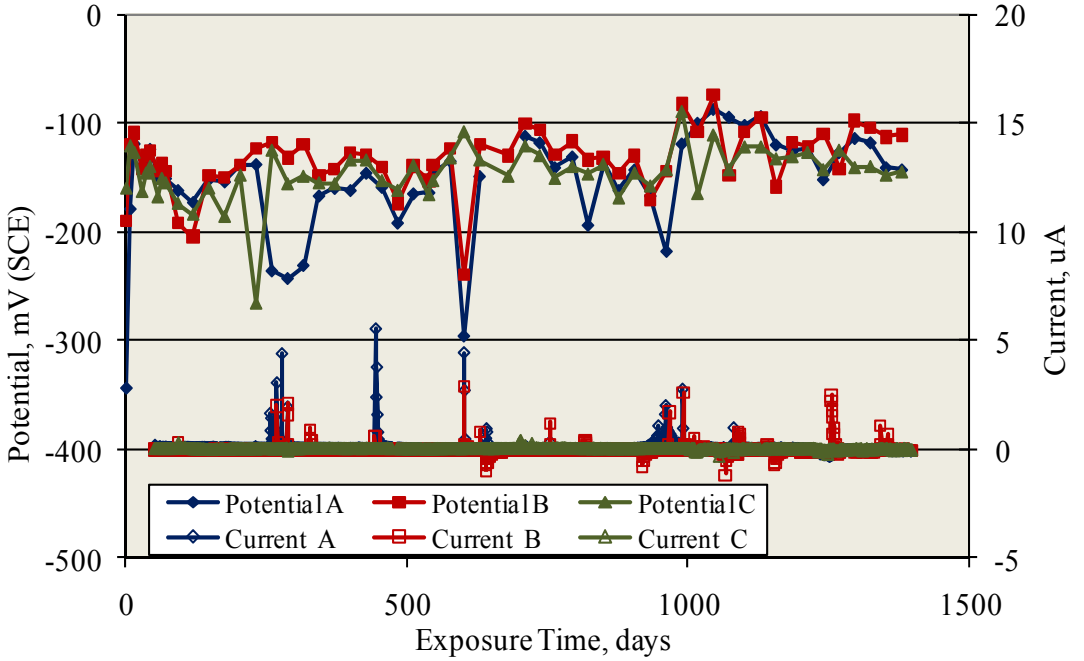

Figure 45. Graph. Potential and macrocell current history for MS-STD1-316.18 specimens.

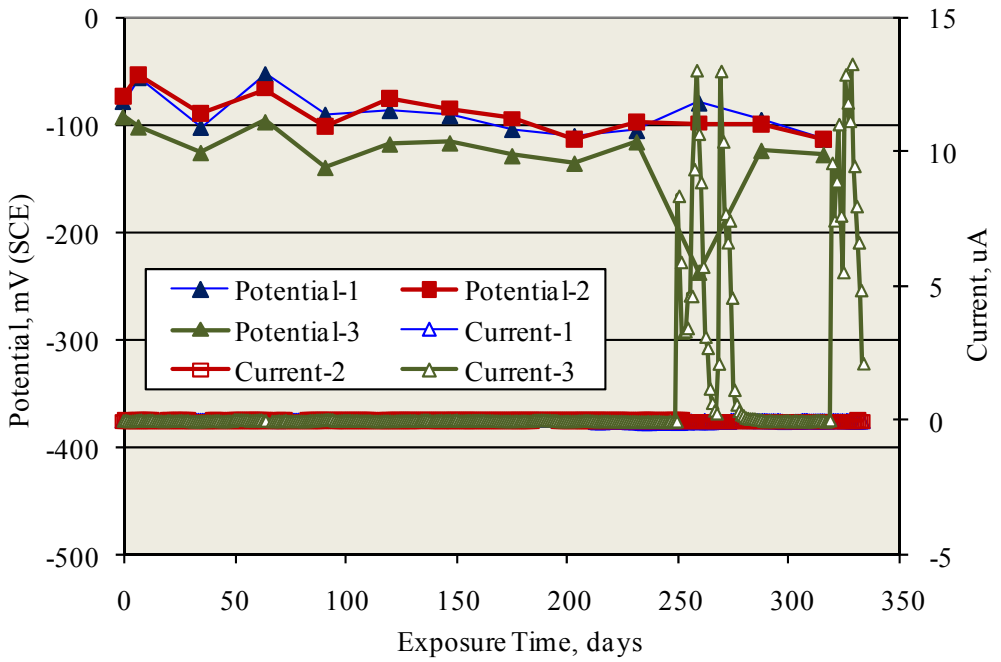

Figure 46. Graph. Potential and macrocell current history for MS-STD1-304 specimens.

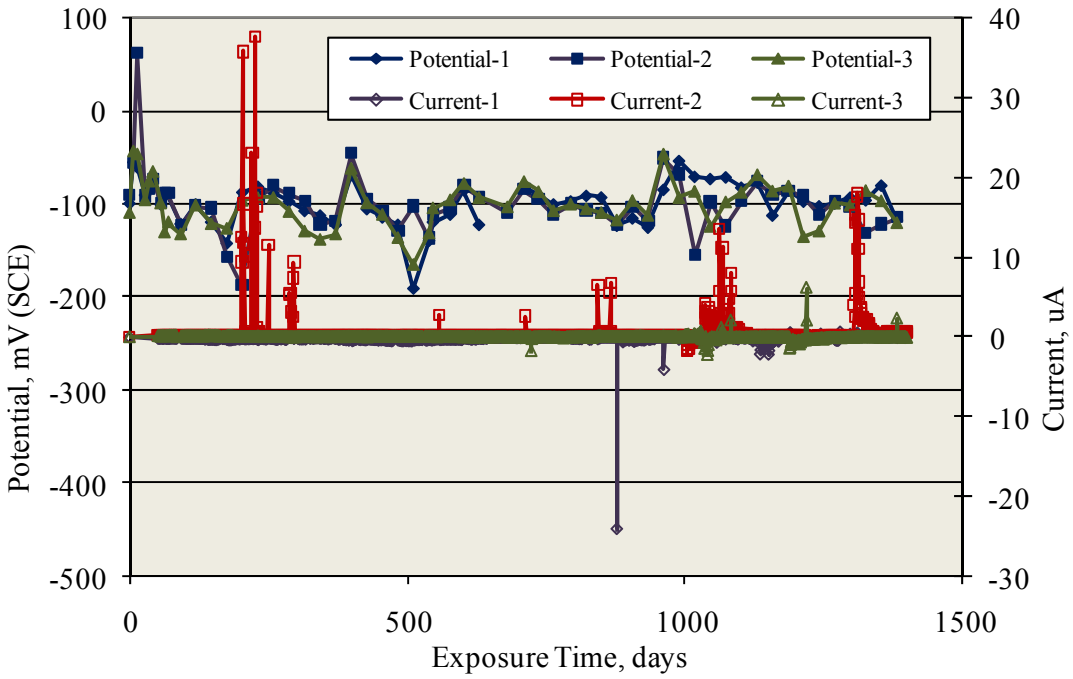

Figure 47. Graph. Potential and macrocell current history for MS-STD1-STAX specimens.

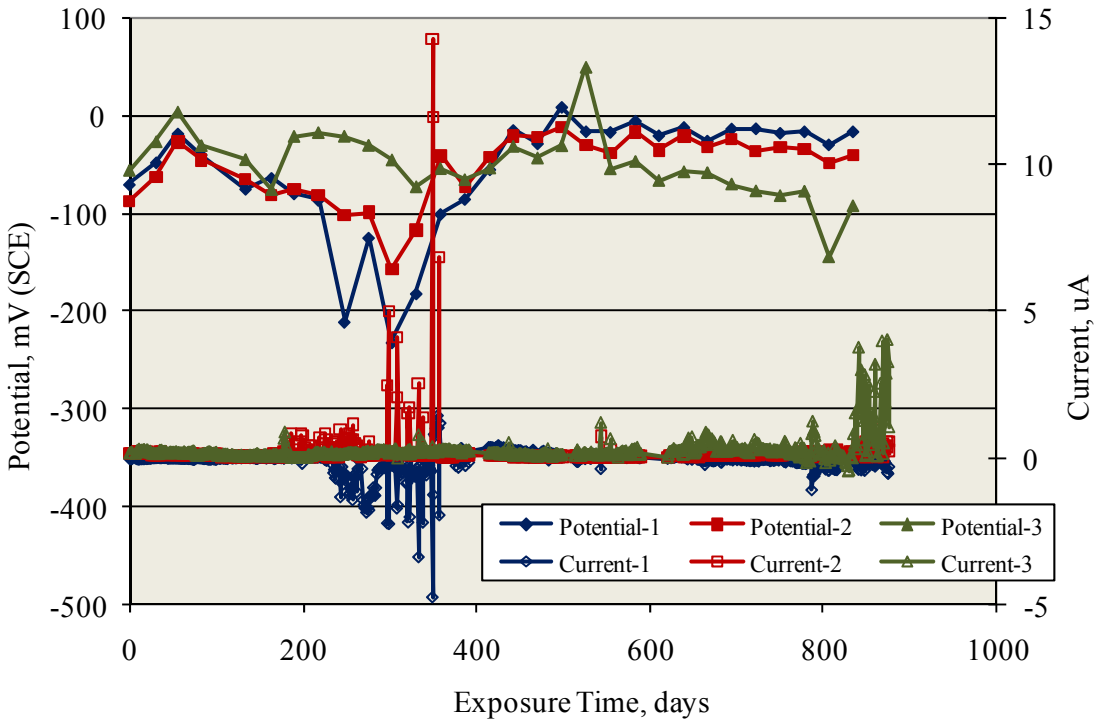

Figure 48. Graph. Potential and macrocell current history for MS-STD1-SMI specimens.

Table 26 lists the maximum and minimum currents that were recorded for the STD1 and STD2 specimens, where the positive current corresponds to the cathodic top bar to a lower bar (or bars) and negative to the anodic top bar.

Table 26. Listing of maximum and minimum macrocell currents for high alloy STD1-MS specimen.

Specimen Type	Macrocell Current (μA)									
	316.16		316.18		304		SMI		STAX	
	Max	**Min**	**Max**	**Min**	**Max**	**Min**	**Max**	**Min**	**Max**	**Min**
STD1	1.2	-5.5	0.4	-0.9	0	-13.3	4.8	-14.3	4.1	-37.7
STD2	2.8	-1.4	0.7	-6.2	0	-0.6	8	-3.7	1.3	-24.2

Results for the other specimen types are presented according to type of reinforcement. Thus, table 27 lists the maximum and minimum macrocell currents for 316.16 reinforced specimens.

Table 27. Maximum and minimum macrocell currents for Type 316.16 specimens other than STD1 and STD2.

Specimen Type	Macrocell Current (μA)		Exposure Time (days)
	Max	Min	
ARWB	1.1	-0.7	1,370
BENT	1.3	-12.7	1,380
CCON	0.9	-1.9	1,383
BCAT	3.1	-42.7	1,388
BNTB	13.9	-20.4	1,378
CBNB	15.2	-32.9	1,376
CBNT	3.2	-12.0	1,376
CCNB	4.0	-46.1	1,380

Figure 49 shows potential and macrocell current versus time for the CCNB specimens, which had the largest and most frequent current excursions. For 316.18, the only non-STD specimen type was CCON, for which the maximum and minimum macrocell currents were 7.0 μA and -14.2 μA, respectively.

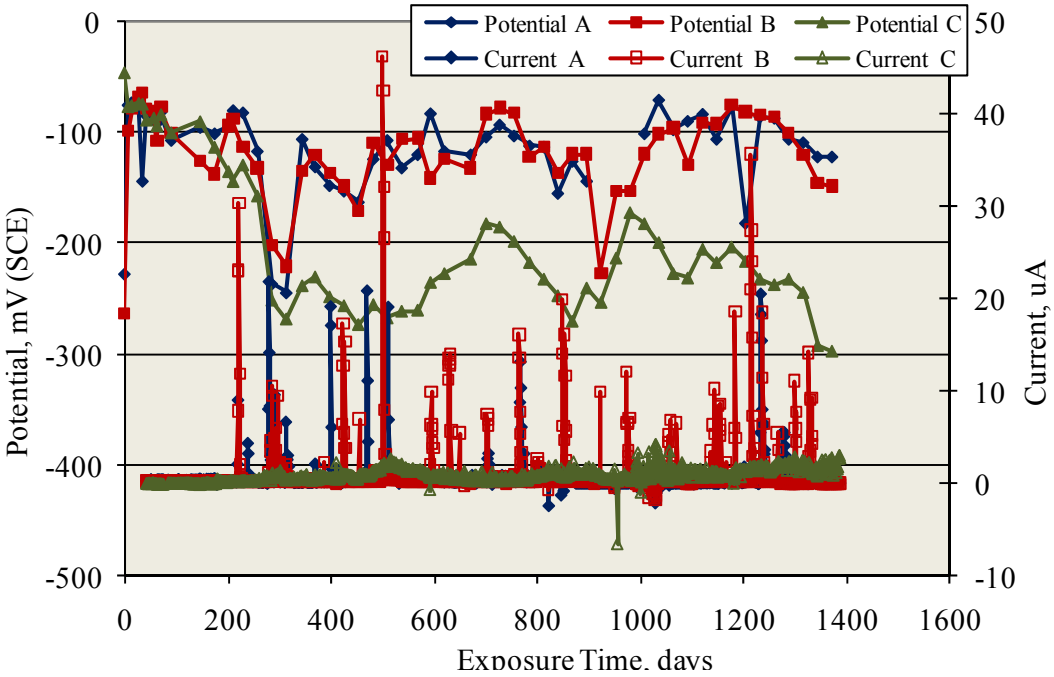

Figure 49. Graph. Potential and macrocell current history for MS-CCNB-316.16 specimens.

Table 28 lists results for non-STD 304 reinforced specimens.

Table 28. Maximum and minimum macrocell currents for Type 304 specimens other than STD1 and STD2.

Specimen Type	Macrocell Current (μA)		Exposure Time (days)
	Max	Min	
ARWB	0.2	-0.2	303
BENT	0.0	-0.1	302
CCON	0.9	-11.3	330
BCAT	0.1	-0.4	331
BNTB	0.9	-3.3	302
CBNB	0.0	-15.0	303
CBNT	0.0	-2.0	302
CCNB	0.2	-48.6	303

Figure 50 plots potential and macrocell current for the CCNB specimens with this reinforcement (same specimen type as for 316.16; see figure 49), which exhibited the largest current excursions.

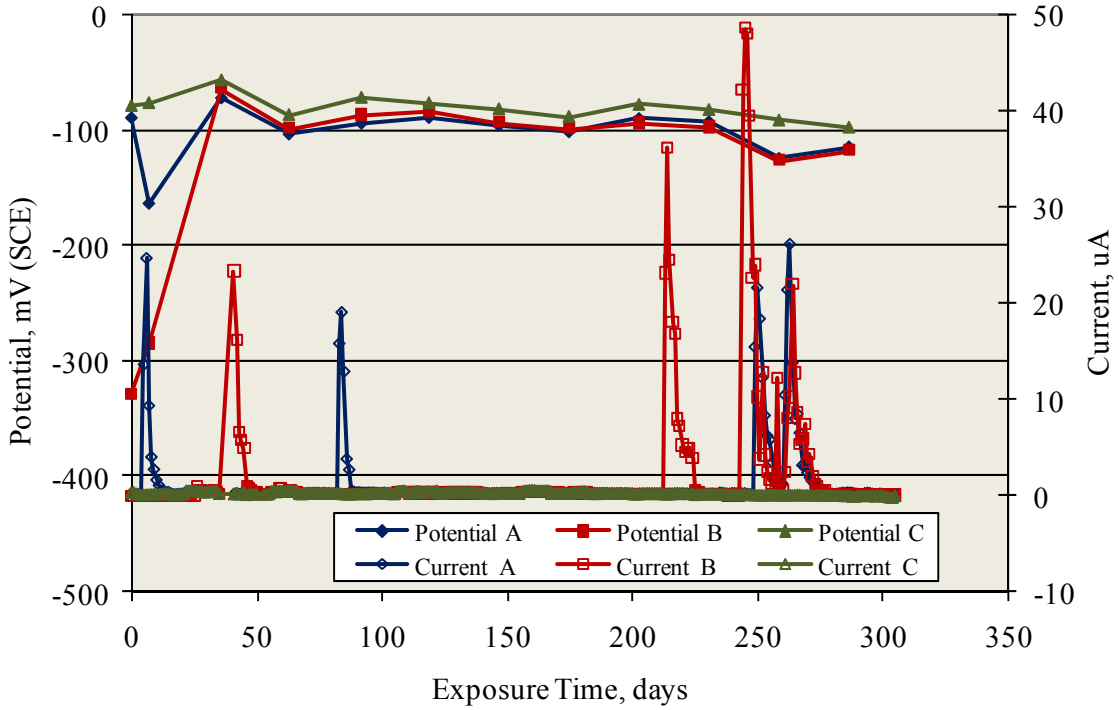

Figure 50. Graph. Potential and macrocell current history for MS-CCNB-304 specimens.

Table 29 shows the maximum and minimum macrocell currents recorded for SMI reinforced specimens. For this alloy, the CSDB and USDB specimens exhibited relatively large current excursions.

Table 29. Maximum and minimum macrocell currents for SMI specimens other than STD1 and STD2.

Specimen Type	Macrocell Current (μA)		Exposure Time (days)
	Max	Min	
ARWB	1.2	-2.7	302
BENT	16.1	-17.7	302
CCON	3.4	-3.6	330
CBNT	3.5	-13.7	302
BCCD	10.6	-6.4	877
CSDB	3.7	-32.2	917
UBDB	4.4	-28.7	903
USDB	2.8	-9.7	887

Figure 51 and figure 52 show the time history for MS-CSDB-SMI speciments. For each reinforcement, the time of exposure is also shown because it varied for the different cases. Exposure time for 316.18 specimens was 1,387 days.

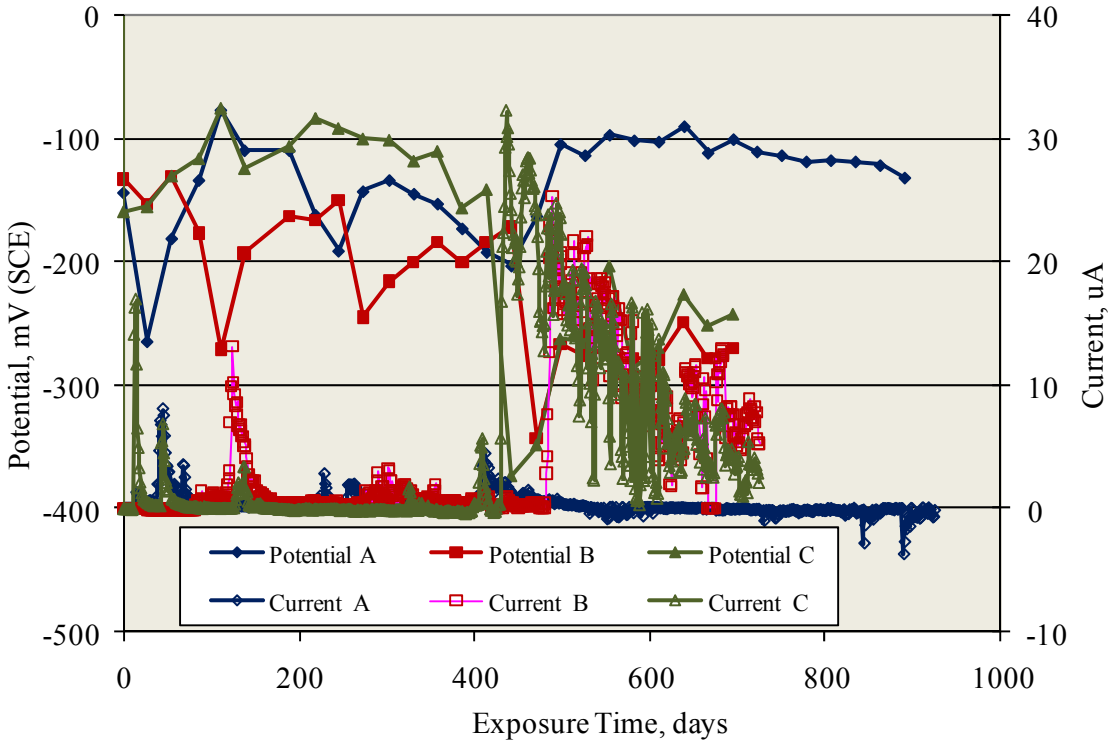

Figure 51. Graph. Potential and macrocell current history for MS-CSDB-SMI specimens.

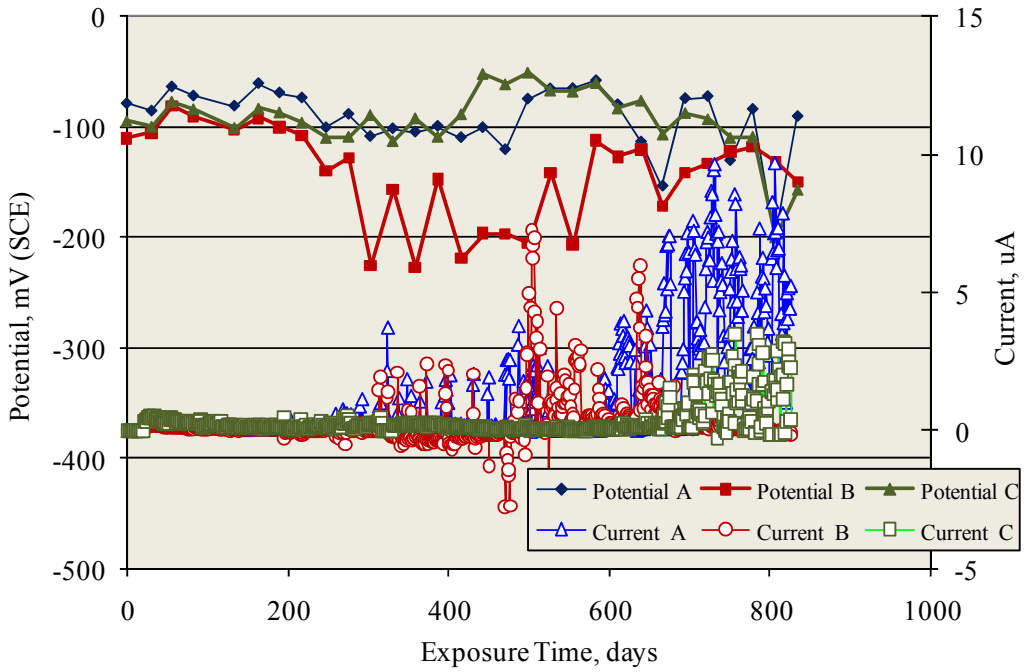

Figure 52. Graph. Potential and macrocell current history for MS-USDB-SMI specimens.

Calculations were made to determine the corrosion rate associated with the current excursions. To do this, charge transfer was computed as the area under the current-time plots. The charge transfer served as input to Faraday's Law from which mass loss and wastage rate were determined.

Table 30 to table 40 show the results for specimens with relatively high charge transfer. In some cases, the calculations were made for both cathodic and anodic current excursions since these correspond to anodic activity on one or more of the lower bars. The columns labeled "Avg Corr Rate" list corrosion rates based upon the total exposure time, assuming wastage occurred uniformly over the entire exposed surface. For "Avg Corr Rate During Current Spike," the calculations were based on the time during which current excursions occurred. The column "Local Corr Rate," on the other hand, assumes that wastage during the macrocell current spikes occurred solely within a 1-mm^2 area such that the corrosion was localized, and all current activity occurred at the same location. While localization is likely, activation sites were probably random. Otherwise, successive activation and repassivation events would have occurred repeatedly at a single location. While this assumption is probably unrealistic, the calculation on which it is based does constitute a worst case situation. In most cases, this localized attack was at a rate of several mm/yr or less; however, for CSDB-MS-316.16-B, corrosion rate exceeded 22 mm/yr.

Table 30. Corrosion rate calculations for STD1-MS specimens with relatively high current excursions.

Rebar Type	Avg Corr Rate (mm/yr)	Avg Corr Rate During Current Spike (mm/yr)	Local Corr Rate (mm/yr)
316.16-A	1.01E-05	1.24E-04	0.78
316.16-B	5.16E-06	6.33E-05	0.40
304-C	1.52E-04	1.08E-03	6.82
SMI-C	2.34E-05	3.49E-05	0.22
SMI-B	3.90E-05	5.80E-05	0.37
STAX-B	8.54E-05	1.02E-05	0.06

Table 31. Corrosion rate calculations for the STD2-MS specimens with relatively high current excursions.

Rebar Type	Avg Corr Rate (mm/yr)	Avg Corr Rate During Current Spike (mm/yr)	Local Corr Rate (mm/yr)
STAX-B	2.13E-04	6.20E-04	3.93

Table 32. Corrosion rate calculations for CCON-MS specimens with relatively high current excursions.

Rebar Type	Avg Corr Rate (mm/yr)	Avg Corr Rate During Current Spike (mm/yr)	Local Corr Rate (mm/yr)
316.18-A	1.60E-05	6.51E-05	0.10
316.18-B	3.91E-05	2.80E-04	0.25

Table 33. Corrosion rate calculations for BENT-MS specimens with relatively high current excursions.

Rebar Type	Sense of Current	Avg Corr Rate (mm/yr)	Avg Corr Rate During Current Spike (mm/yr)	Local Corr Rate (mm/yr)
316.16-A	Anodic	3.19E-05	1.49E-04	0.94
316.16-B	Anodic	2.24E-05	1.42E-04	0.90
316.16-C	Anodic	4.17E-05	1.13E-04	0.71
SMI-A	Anodic	1.42E-04	3.19E-04	2.02
	Cathodic	1.62E-04	5.74E-04	3.63
SMI-B	Anodic	1.72E-04	3.00E-04	1.90
	Cathodic	4.45E-05	4.05E-04	2.57
SMI-C	Anodic	2.47E-06	2.40E-04	1.52
	Cathodic	9.35E-05	1.58E-08	0.59

Table 34. Corrosion rate calculations for the BCAT-MS specimen with relatively high current excursions.

Rebar Type	Avg Corr Rate (mm/yr)	Avg Corr Rate During Current Spike (mm/yr)	Local Corr Rate (mm/yr)
316.18-A	1.28E-04	2.32E-04	1.47

Table 35. Corrosion rate calculations for CBNT-MS specimens with relatively high current excursions.

Rebar Type	Avg Corr Rate (mm/yr)	Avg Corr Rate During Current Spike (mm/yr)	Local Corr Rate (mm/yr)
316.18-A	2.96E-05	3.24E-04	0.19
SMI-A	8.34E-05	3.39E-04	2.14
SMI-B	1.27E-04	2.08E-04	0.80

Table 36. Corrosion rate calculations for CBNB-MS specimens with relatively high current excursions.

Rebar Type	Sense of Current	CBNB		
		Avg Corr Rate (mm/yr)	Avg Corr Rate During Current Spike (mm/yr)	Local Corr Rate (mm/yr)
316.16-A	Anodic	3.25E-05	2.69E-04	1.70
	Cathodic	6.79E-04	3.49E-03	22.11
316.16-B	Anodic	1.62E-04	4.67E-04	2.96
	Cathodic	2.37E-04	4.10E-04	2.60
316.16-C	Anodic	3.74E-06	1.92E-04	1.21
	Cathodic	5.20E-04	6.81E-04	4.31

Table 37. Corrosion rate calculations for CSDB-MS specimens with relatively high current excursions.

Rebar Type	Avg Corr Rate (mm/yr)	Avg Corr Rate During Current Spike (mm/yr)	Local Corr Rate (mm/yr)
SMI-A	6.82E-05	1.62E-04	1.02
SMI-B	6.82E-05	8.98E-05	0.57

Table 38. Corrosion rate calculations for CCNB-MS specimens with relatively high current excursions.

Rebar Type	Avg Corr Rate (mm/yr)	Avg Corr Rate During Current Spike (mm/yr)	Local Corr Rate (mm/yr)
316.18-A	9.61E-05	1.38E-04	0.61
316.18-B	9.61E-05	1.63E-04	1.03

Table 39. Corrosion rate calculations for CCNB-MS specimens with relatively high current excursions.

Rebar Type	Avg Corr Rate (mm/yr)	Avg Corr Rate During Current Spike (mm/yr)	Local Corr Rate (mm/yr)
SMI-A	1.84E-04	2.31E-04	1.46
SMI-B	5.36E-05	1.42E-04	0.90
SMI-C	5.72E-05	4.25E-01	0.00

Table 40. Corrosion rate calculations for the BCAT-MS specimen with relatively high current excursions.

Rebar Type	Avg Corr Rate (mm/yr)	Avg Corr Rate During Current Spike (mm/yr)	Local Corr Rate (mm/yr)
SMI-A	4.73E-04	6.47E-04	4.10

Controlled Temperature and Relative Humidity Exposures. Table 41 lists maximum and minimum macrocell currents for specimens in this category. Upon comparison to data in table 26, it is apparent that the magnitude of these was less than for specimens exposed outdoors. In most cases, only a single excursion was recorded. Apparently, variable temperature or humidity (or both) enhanced macrocell activity for the higher alloyed reinforcements to a greater extent than when temperature and relative humidity were controlled, although the magnitude of the effect was not of practical significance.

Table 41. Listing of maximum and minimum macrocell currents for MS-STD1G specimens.

Specimen Type	Macrocell Current (μA)									
	316.16		316.18		304		SMI		STAX	
	Max	**Min**	**Max**	**Min**	**Max**	**Min**	**Max**	**Min**	**Max**	**Min**
STD1G	0	-3.9	0.3	-3.6	0	-0.1	0.3	-0.1	0.5	-0.1

Table 42 lists the high-performance reinforcement MS specimens that were tested. It also shows the T_i ratio for MS specimens to the average T_i for STD1-MS-BB specimens (142 days), assuming that the temporal current activity did not constitute corrosion initiation. Because exposure time varied depending on set number, the ratios also differed from one alloy to the next depending upon when testing commenced, with the largest ratio being >9.8.

Table 42. Listing of exposure times and T_i(alloy)/T_i(BB) for high performance reinforced MS specimens.

Exposure Time (days)				
316.16	**316.18**	**304**	**SMI**	**STAX**
1,399	1,383–1,399	305–333	305–924	1,399
T_i(alloy)/T_i (BB)				
>9.8	>9.7–>9.8	> 2.1–> 2.3	> 2.1–> 6.5	> 9.8

4.1.3 Results for 3-Bar Tombstone Column (3BTC) Specimens

4.1.3.1 Results for Improved Performance Reinforcements in 3BTC Specimens

As noted in section 3.3.4, either three or six standard 3BTC specimens of the STD2 and STD3 mix designs and selected reinforcement types were prepared. The potential of all of the bars that were connected as well as the voltage drop across the resistor between each long bar (designated as bar 1 and bar 2) and the other two bars (designation of the shorter bar was 3) were measured daily. Typical examples of the potential and macrocell current versus time behavior that were observed are illustrated by figure 53 to figure 56. In all cases, a relatively abrupt potential transition to more negative values occurred at a specific time, and this was considered as indicating corrosion initiation. Concurrently, a positive macrocell current excursion for one of the two measurement pairs and a negative excursion for the other were noted; however, the relative polarity of individual bars sometimes changed subsequently such that the macrocell current versus time trends conformed to one of several types of behavior. Thus, in figure 53 (3BCT-BB specimen A), the potential shift and corrosion current (bar 3) occurred at 89 days. However, after 102 days, current

from bar 3 was cathodic and remained so until 224 days after which it was anodic until until 476 days. Current from bar 1, on the other hand, was cathodic subsequent to bar 3 activating.

The second example is provided by figure 54 (3BCT-BB specimen B), where corrosion initiated on bar 3 at 80 days with bar 1 serving as the cathode. The fact that the current for the former was less than for the latter indicates that bar 2 must also have been an anode. These relative polarities remained throughout the test. In figure 55 (3BTC-BB specimen D), corrosion initiated after 84 days with the current from both bars 1 and 3 initially being cathodic, indicating that bar 2 was the anode. However, the current from bar 3 to bar 1 and bar 2 reversed after 99 days such that it was now an anode as well and remained so thereafter. However, the current from bar 1 to bar 2 and bar 3 became anodic at 290 days. Lastly, in figure 56 (3BTC-BENT-3Cr12 specimen C), corrosion initiated after 152 days with positive current from bar 3 to bar 1 and bar 2. This demonstrated that bar 3 was an anode with a negative current from bar 1 to bar 2 and bar 3, indicating that bar 1 was a cathode. The current remained positive for bar 3 to 742 days, at which time it became an anode (positive current). Current from bar 1 to bar 2 and bar 3 was anodic for a period after 757 days. These polarities remained until day 838 for bar 1 and day 893 for bar 3, at which times, both currents reversed.

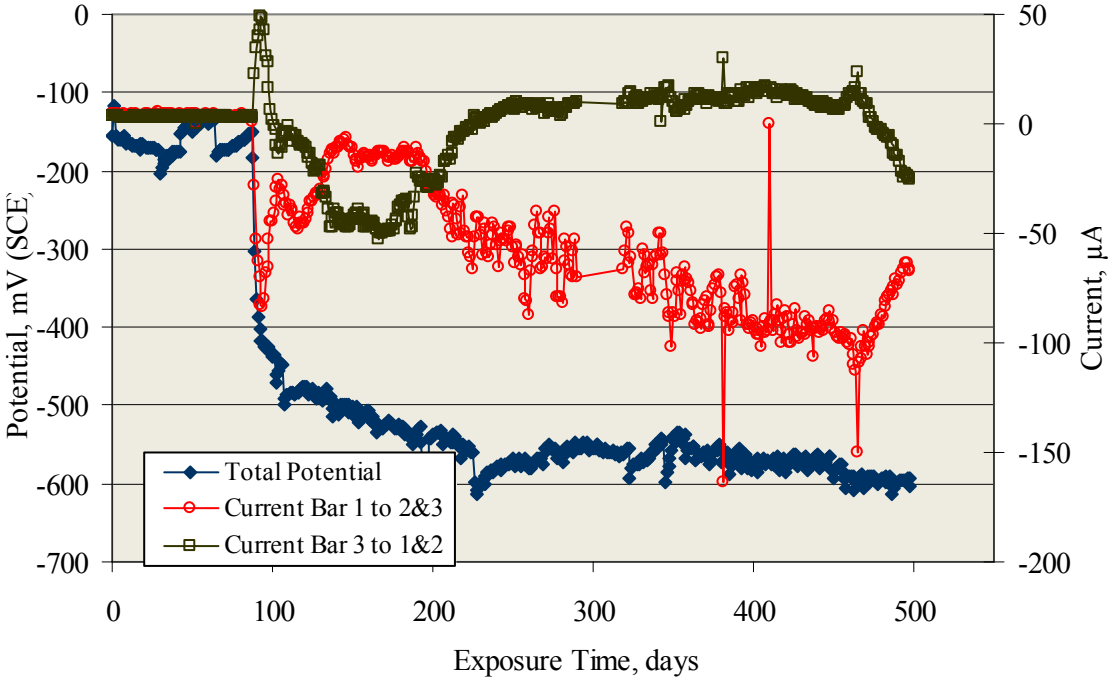

Figure 53. Graph. Potential and macrocell current between indicated bars for 3BCT-BB specimen A.

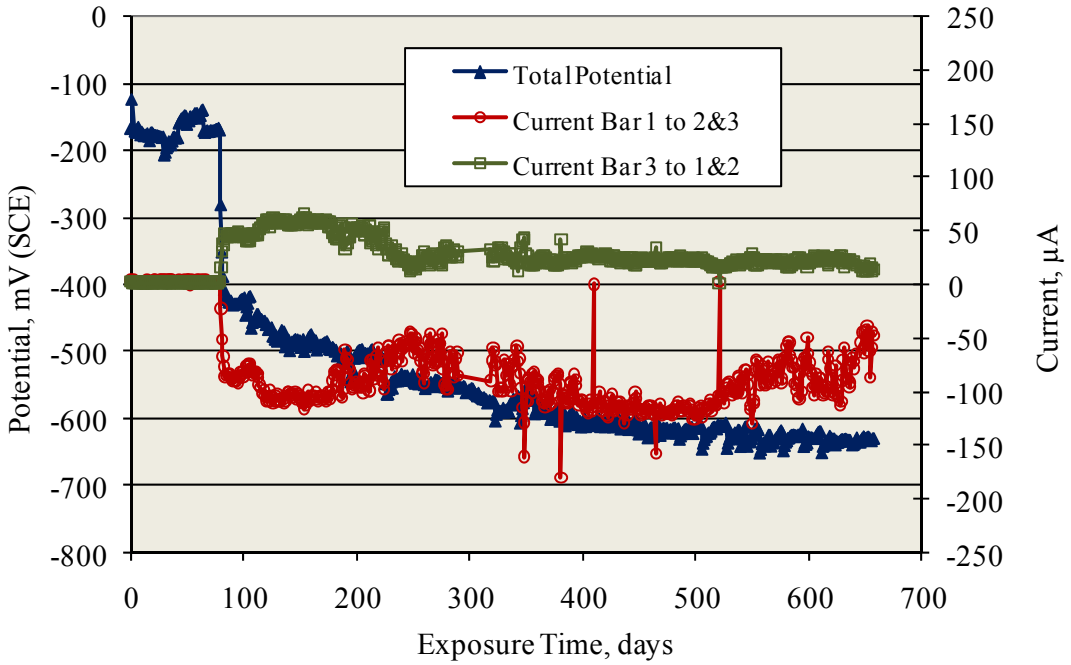

Figure 54. Graph. Potential and macrocell current between indicated bars for 3BCT-BB specimen B.

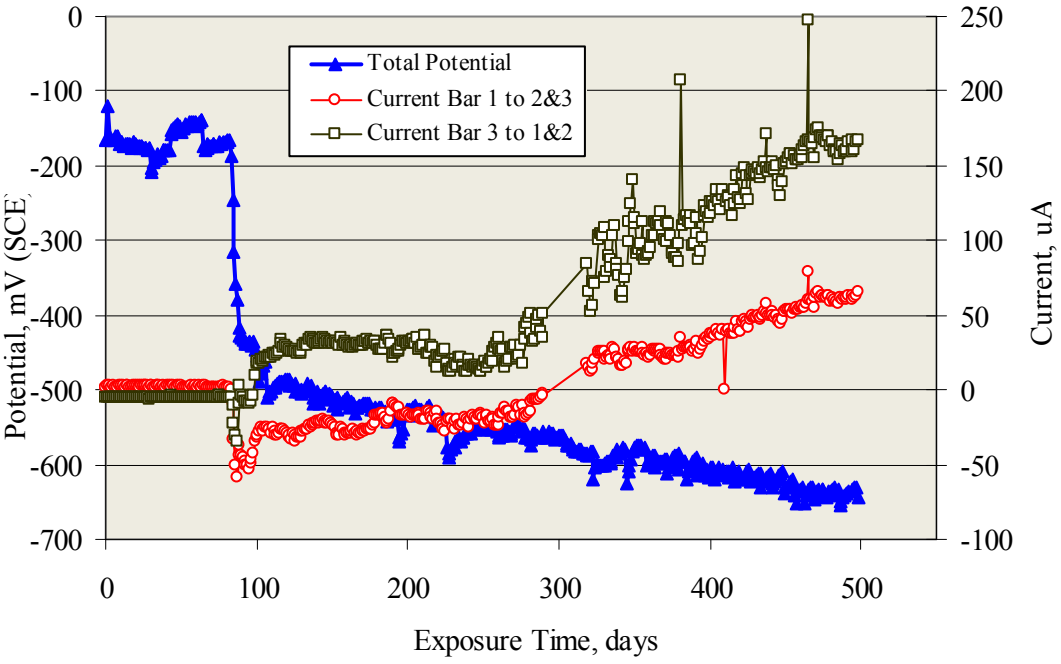

Figure 55. Graph. Potential and macrocell current between indicated bars for 3BCT-BB specimen D.

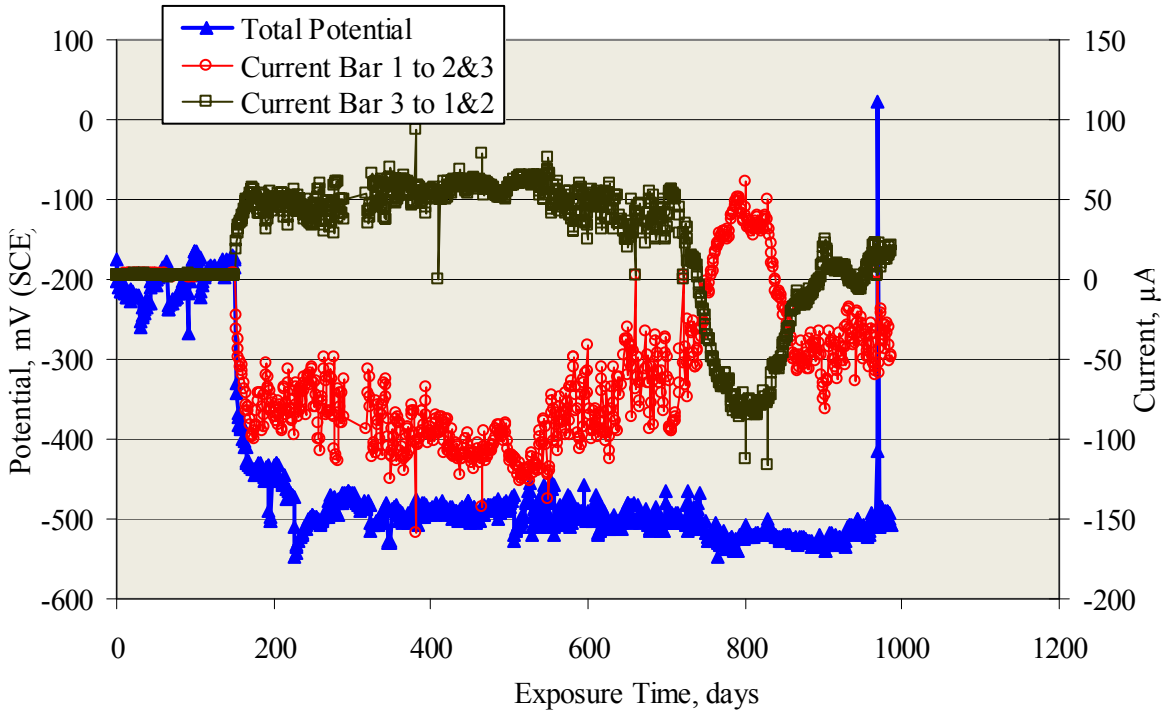

Figure 56. Graph. Potential and macrocell current between indicated bars for 3BCT-BENT-3Cr12-C.

Table 43 lists the improved performance 3BTC specimens, and it provides the T_i for each.

Table 43. Listing of 3BTC specimens with improved performance reinforcements and the T_i for each.

Black Bar												
Concr Mix	**STD2**						**STD3**					
Spm No	A	B	C	D	E	F	A	B	C	D	E	F
T_i	88	80	65	84	80	70	64	60	55	56	70	58
Avg	78						61					

3Crl2															
Concr Mix	**STD2**			**STD3**						**BENT**			**ELEV**		
Spm No	A	B	C	A	B	C	D	E	F	A	B	C	A	B	C
T_i	89	296	419	170	203	179	236	361	206	98	160	152	75	373	177
Avg	268			226						137			208		

A1035															
Concr Mix	**STD2**			**STD3**						**BENT**			**ELEV**		
Spm No	A	B	C	A	B	C	D	E	F	A	B	C	A	B	C
T_i	520	406	366	279	349	165	154	248	316	239	351	248	172	304	336
Avg	431			252						279			271		

2101															
Concr Mix	**STD2**			**STD3**						**BENT**			**ELEV**		
Spm No	A	B	C	A	B	C	D	E	F	A	B	C	A	B	C
T_i	197	286	248	91	200	221	65	55	95	192	168	117	106	164	57
Avg	244			121						159			109		

Normal cumulative distribution function plots of T_i for 3BTC-BB, -3Cr12, -MMFX-2, and -2101 reinforcements in both concretes (STD2 and STD3) are presented in figure 57 to figure 61. The first of these (figure 57) illustrates T_i distribution for the reinforcements in STD2 concrete, and the next figure illustrates STD3.

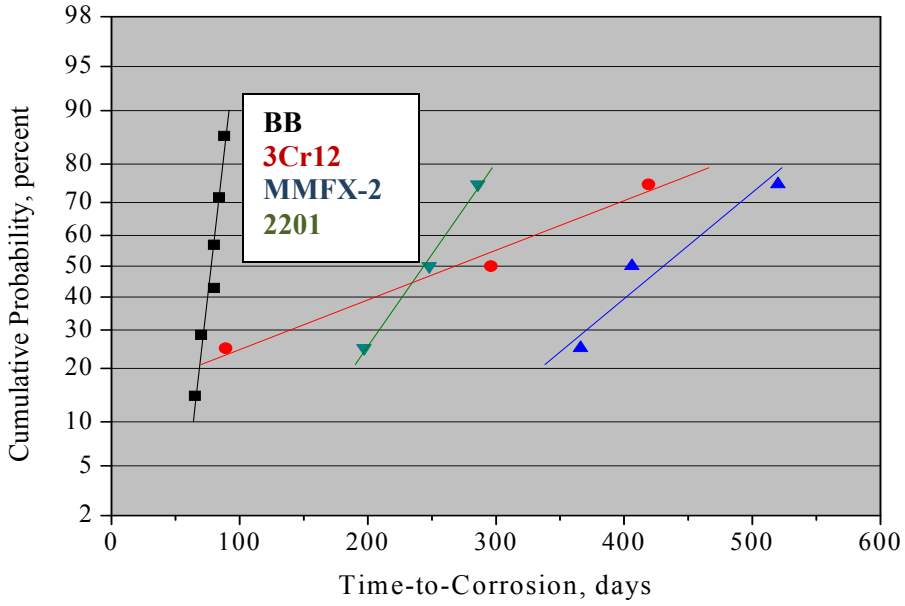

Figure 57. Graph. Cumulative probability plot of T_i for 3BTC-STD2 specimens for each reinforcement.

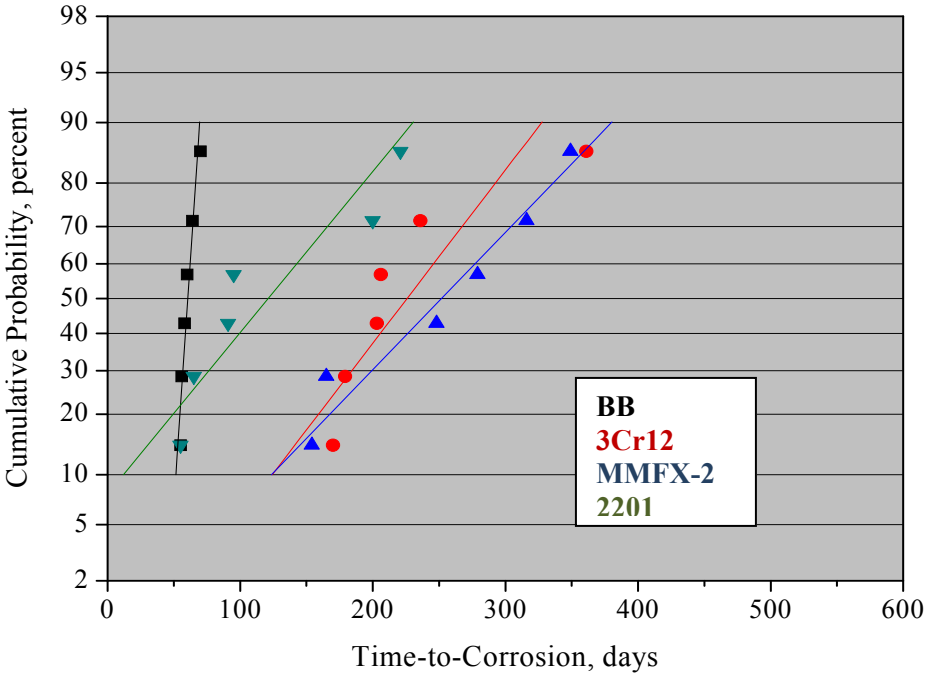

Figure 58. Graph. Cumulative probability plot of T_i for 3BTC-STD3 specimens with each reinforcement.

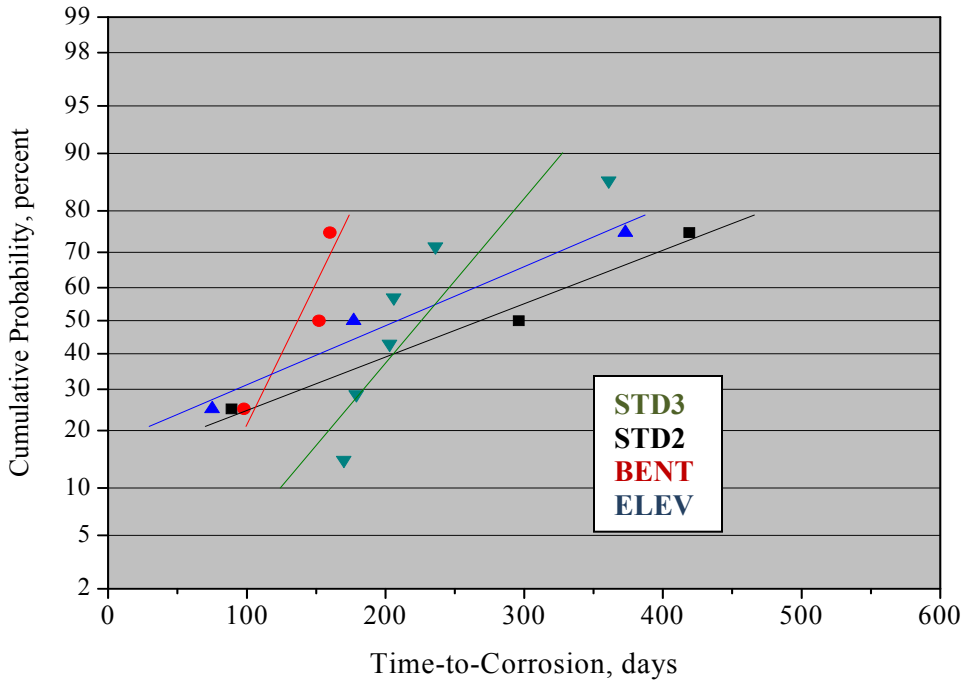

Figure 59. Graph. Cumulative probability plot of T_i for 3BTC-3Cr12 specimens.

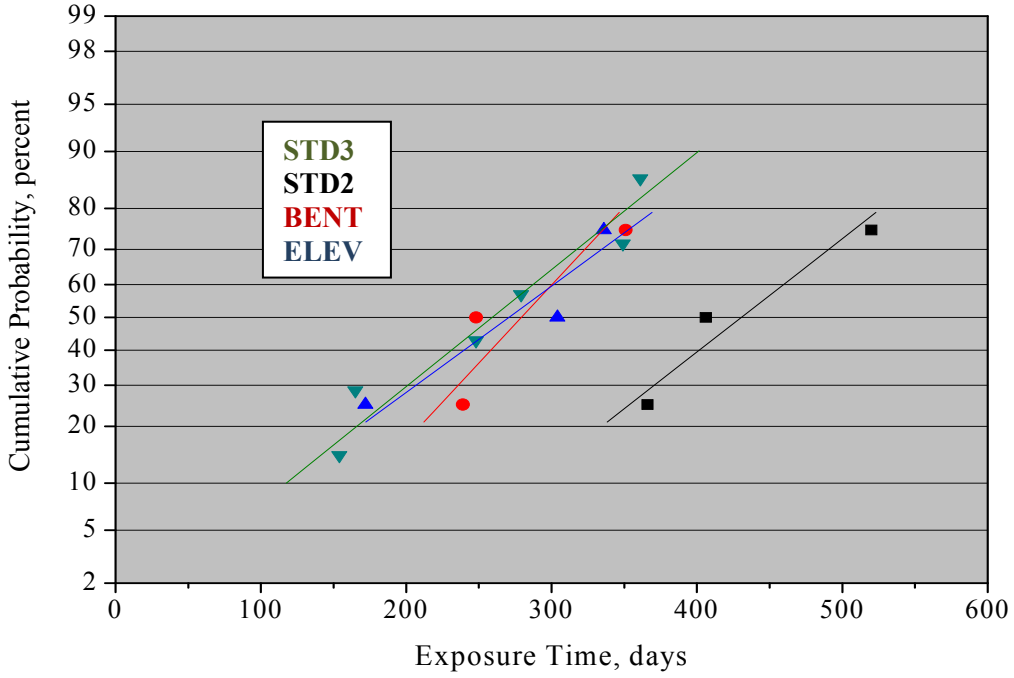

Figure 60. Graph. Cumulative probability plot of T_i for 3BTC-MMFX-2 specimens.

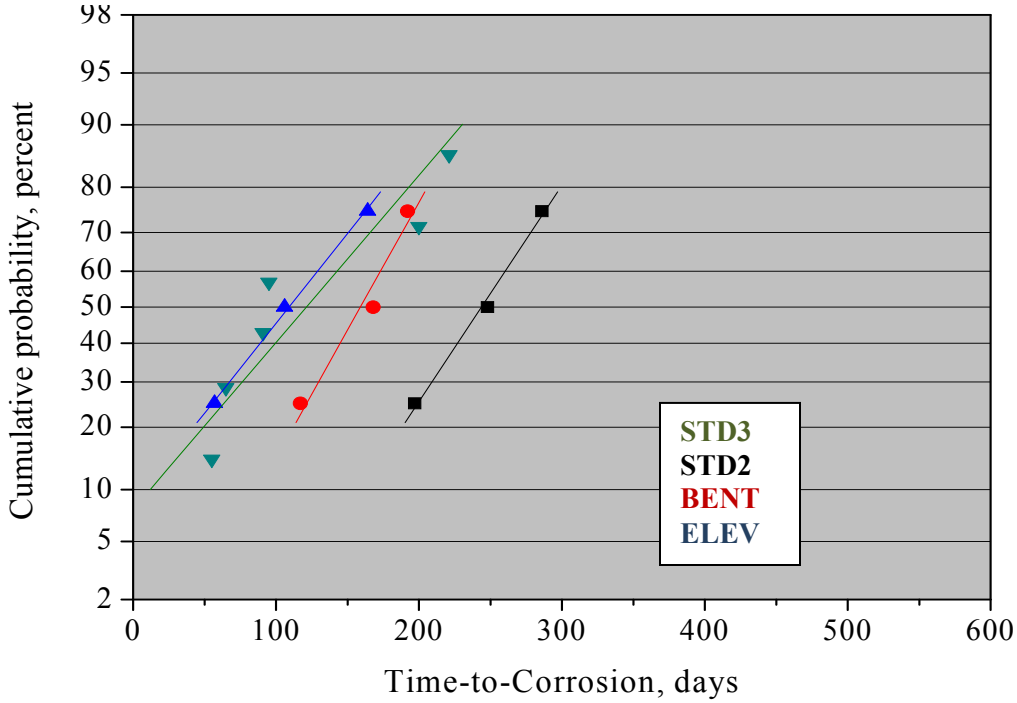

Figure 61. Graph. Cumulative probability plot of T_i for 3BTC-2101 specimens.

Table 44 and table 45 list T_i and T_i(alloy)/T_i(BB) values at 2 percent, 10 percent, and 20 percent corrosion activity for the STD2 and STD3 3BTC specimens, as determined by extrapolating the best fit line for each specimen data set in figure 57 and figure 58. This determination was not made in cases where the extrapolation yielded an unrealistically low or negative T_i value. For all reinforcements, T_i is greater in STD2 than STD3 concrete, which is consistent with the former having lower w/c than the latter (0.41 compared to 0.50; see table 3). Also, the T_i ratio of each corrosion resistant reinforcement to BB at different percentages active was higher for the STD2 than STD3 concrete, which is consistent with results from the MS specimens. Thus, T_i(alloy)/T_i(BB) for MMFX-2 in STD3 concrete ranged from 0.9 to3.4. Whereas in STD2, it ranged from 3.7 to 5.2. The results indicate T_i ordering of these alloys relative to BB (highest to lowest) as MMFX-2 ≈ 3Cr12 > 2101 > BB.

Figure 59 to figure 61, on the other hand, plot normal CDF of T_i for the different bar configurations (straight, bent, and elevated) for 3Cr12, MMFX-2, and 2101 in STD3 concrete with the STD2 data included for comparison. In the latter two cases (MMFX-2 and 2101; figure 60 and figure 61), the difference in T_i distribution for the different bar configurations may be within the range of experimental scatter. The data are more distributed in the case of 3Cr12, however, with the ordering of T_i being (highest to lowest) STD2 > ELEV ≈ STD3 > BENT. Even here, it is unclear if the differences are real of if they simply reflect data scatter.

Table 44. T_i data and T_i (alloy)/T_i (BB) at 2 percent, 10 percent, and 20 percent cumulative active for improved performance 3BTC specimens in STD2 concrete.

Cumulative Percentage Active	Reinforcement Type				T_i (alloy)/T_i (BB)	
	BB	3Cr12	MMFX-2	2101	MMFX-2	2101
2	53	—	198	112	3.7	2.1
10	61	—	282	160	5.3	3.0
20	65	—	337	190	6.4	3.6

— indicates that data for 2101 were not conducive for analysis.

Table 45. T_i data at 2 percent, 10 percent, and 20 percent cumulative active for 3BTC specimens with improved performance reinforcements in STD3 concrete.

Cumulative Percentage Active	Reinforcement Type				T_i (alloy)/T_i (BB)	
	BB	3Cr12	MMFX-2	2101	3Cr12	MMFX-2
2	48	56	45	—	1.2	0.9
10	49	127	128	—	2.6	2.7
20	51	156	162	—	3.3	3.4

— indicates that data for 2101 were not conducive for analysis.

Table 46 to table 48 list the T_i values at 2 percent, 10 percent, and 20 percent active according to the extrapolation of the best fit line in figure 59 to figure 61.

Table 46. T_i data at 2 percent, 10 percent, and 20 percent cumulative active for 3BTC specimens reinforced with 3Cr12.

Cumulative Percentage Active	3Cr12			
	STD2	STD3	BENT	ELEV
2	—	56	45	—
10	—	127	78	—
20	—	156	100	—

— indicates that no STD2 or ELEV specimens were tested.

Table 47. T_i data at 2 percent, 10 percent, and 20 percent cumulative active for 3BTC specimens reinforced with MMFX-2.

Cumulative Percentage Active	MMFX-2			
	STD2	STD3	BENT	ELEV
2	107	29	105	23
10	281	114	173	117
20	336	162	208	170

Table 48. T_i data at 2 percent, 10 percent, and 20 percent cumulative active for 3BTC specimens reinforced with 2101.

Cumulative Percentage Active	2101			
	STD2	STD3	BENT	ELEV
2	101	—	44	—
10	155	—	87	—
20	189	—	111	—

— indicates that no STD2 or ELEV specimens were tested.

4.1.3.2 Results for High Performance Reinforcements in 3BTC Specimens

For all high performance reinforcements that were included in 3BTC specimens (316.16, 304, and SMI), potential remained relatively positive for the duration of the exposures, and no sustained decreases occurred as was the case for specimens with improved performance bars. Figure 62 and figure 63 illustrate the two general types of macrocell current responses that were observed. In both cases, macrocell current, either from bar 1 to bar 2 and bar 3 or bar 3 to bar 1 and bar 2, was typically several microamperes starting from initial exposure. In the former case (figure 62), the two sets of current measurements are approximately the same magnitude but opposite sign, such that bar 3 was the anode, bar 1 was the cathode, and bar 2 provided little apparent contribution. For figure 63, however, both currents were negative, indicating that they served as cathodes to an anodic bar 2. Also, current spikes followed by repassivation are more apparent here than in figure 62. The latter behavior (figure 63) was more typical and reflects bar 2 having a more negative potential than bar 1 and bar 3, although all bars remained passive.

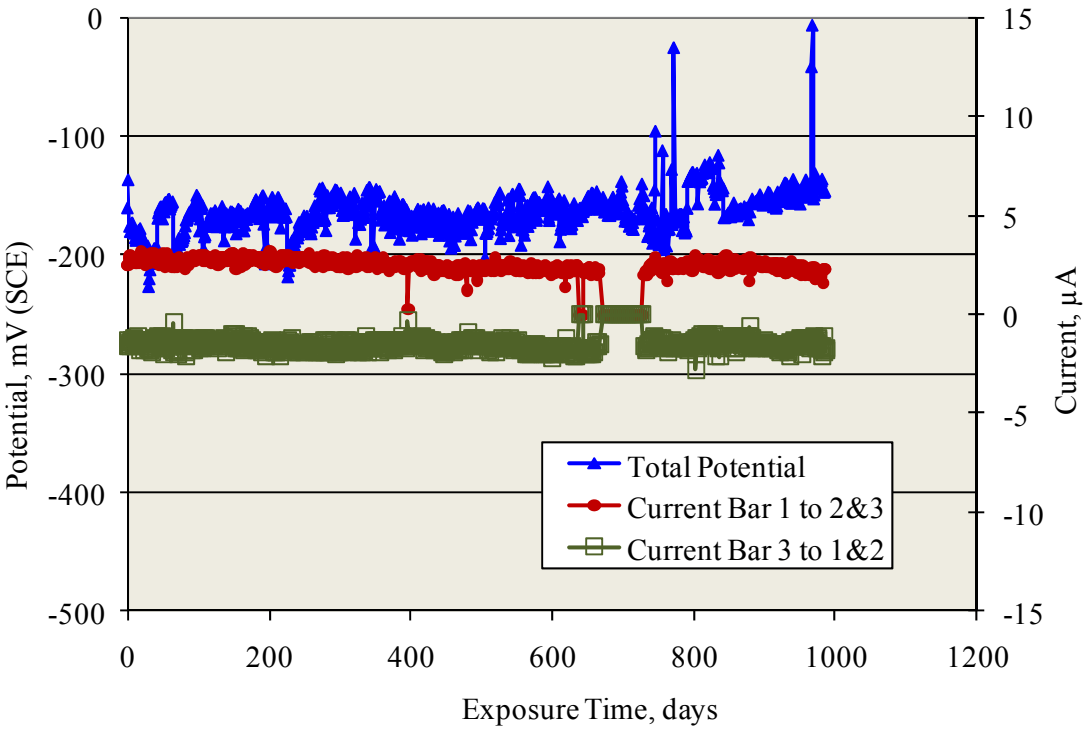

Figure 62. Graph. Potential and macrocell current versus time for 3BTC-SMI-specimen B in STD 3 concrete.

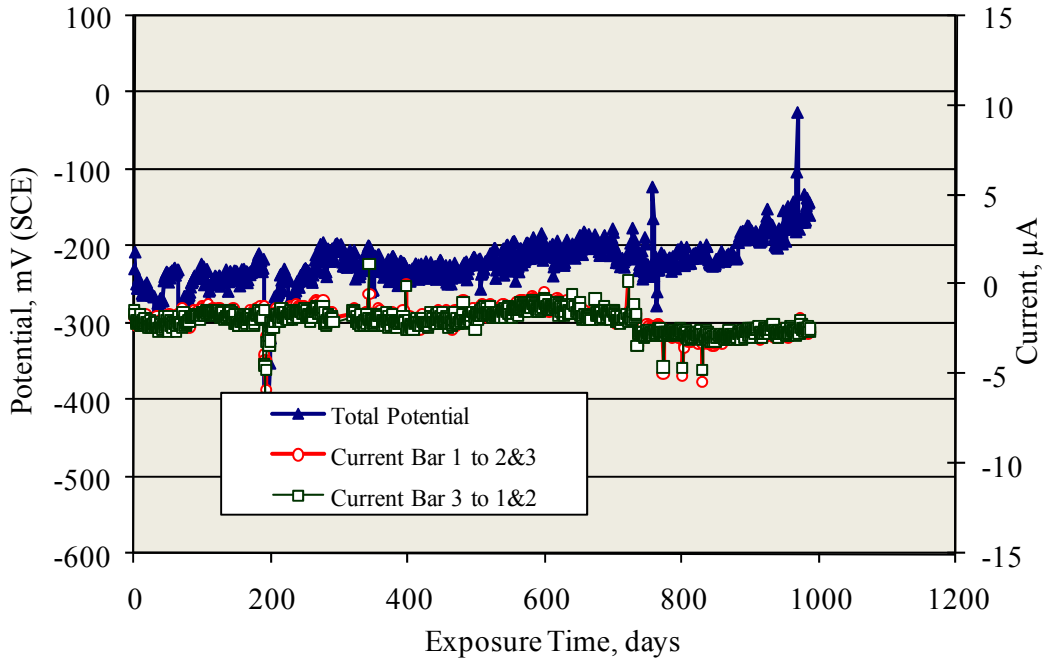

Figure 63. Graph. Potential and macrocell current versus time for 3BTC-316.16-ELEV specimen A.

Table 49 lists the maximum and minimum currents recorded during the exposure of each specimen. As for the higher alloyed MS specimens, corrosion rate associated with these current excursions was minimal.

Table 49. Maximum and minimum macrocell currents recorded for the high alloy reinforcement 3BTC specimens.

Specimen Type/Number	Macrocell Current (μA)					
	316.16		304		SMI	
	Max	**Min**	**Max**	**Min**	**Max**	**Min**
STD2-A	0.2	-4.1	-1.8	-4.9	-0.4	-4.7
STD2-B	0.3	-4.4	-1.8	-6.6	-0.3	-6.7
STD2-C	0.3	-4.7	-1.5	-4.4	-0.2	-7.5
STD3-A	-0.3	-5.0	2.1	-11.1	-0.7	-8.0
STD3-B	-0.3	-5.7	0.3	-6.9	-0.3	-3.2
STD3-C	0.0	-6.8	-0.3	-4.9	-0.5	-3.7
STD3-D	0.6	-4.2	1.1	-4.4	0.1	-9.1
STD3-E	1.6	-5.5	-0.3	-5.7	0.1	-6.3
STD3-F	-0.1	-3.8	-0.1	-7.0	0.2	-4.5
BENT-A	-0.2	-4.0	-0.3	-5.1	-0.4	-3.8
BENT-B	-0.3	-4.3	-0.4	-5.2	-0.1	-3.8
BENT-C	-0.3	-4.6	-0.3	-6.1	-0.2	-3.7
ELEV-A	1.2	-6.3	0.3	-5.7	-0.5	-4.2
ELEV-B	0.1	-6.7	-6.3	0.2	-0.3	-5.5
ELEV-C	-0.4	-4.9	0.1	-5.0	-0.6	-6.1

4.1.4 Results for Field Column Specimens

Figure 64 to figure 70 show potential versus exposure time plots for field column specimens with each type of reinforcement (BB, 3Cr12, MMFX-2, 2101, 316.16, 304, and SMI). The letters W, G, R, and Y in the specimen designation identify each of the four reinforcing bars in each column specimen. Data for the improved performance (3Cr12, MMFX-2, and 2101) and BB specimens (figure 64 to figure 67) exhibit a potential shift to relatively negative values. This often occurred within the first few days of exposure. The high permeability concrete (STD1 mix design)

facilitated by rapid sorptive Cl^- transport and possible defects in the concrete or cracks caused the threshold concentration for this species to be achieved relatively early in the exposures. The potential time behavior for one of the three 316.16SS reinforced specimens (-C; see figure 64) was similar to that of the improved performance reinforced specimens. However, this particular specimen was damaged upon installation, and the negative potentials compared to the other two 316.16 reinforced specimens probably resulted from this.

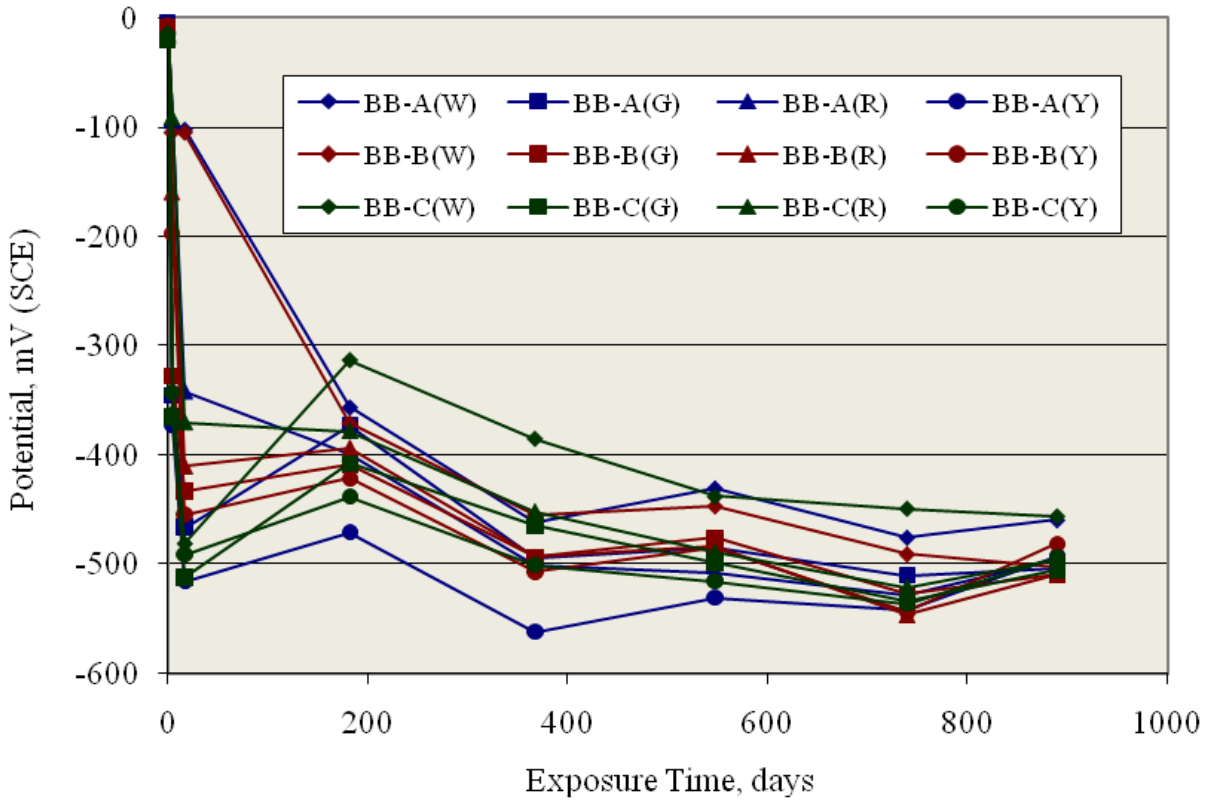

Figure 64. Graph. Potential versus exposure time plot for field columns with BB reinforcement.

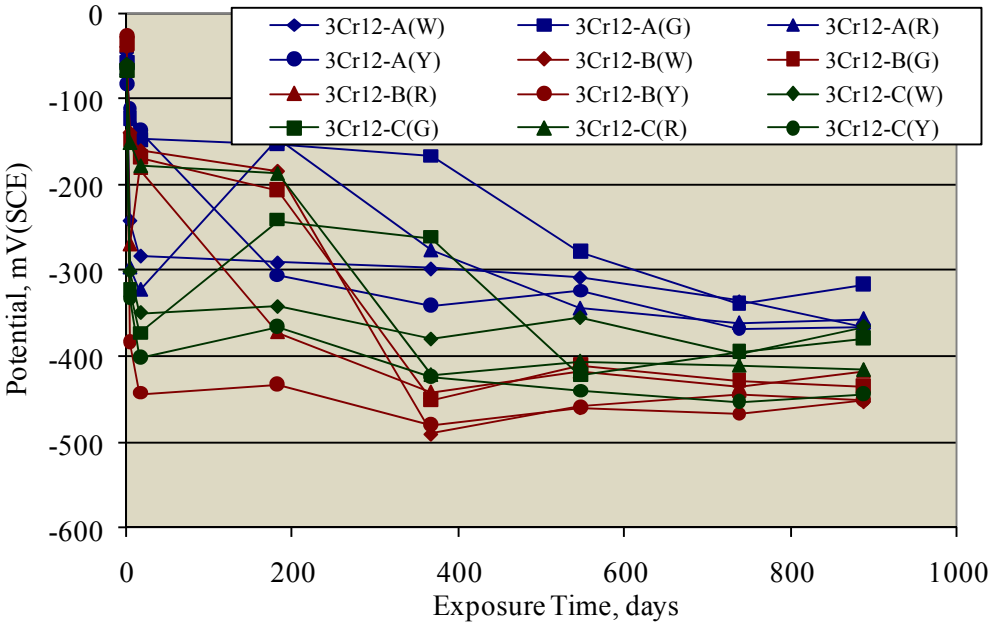

Figure 65. Graph. Potential versus exposure time plot for field columns with 3Cr12 reinforcement.

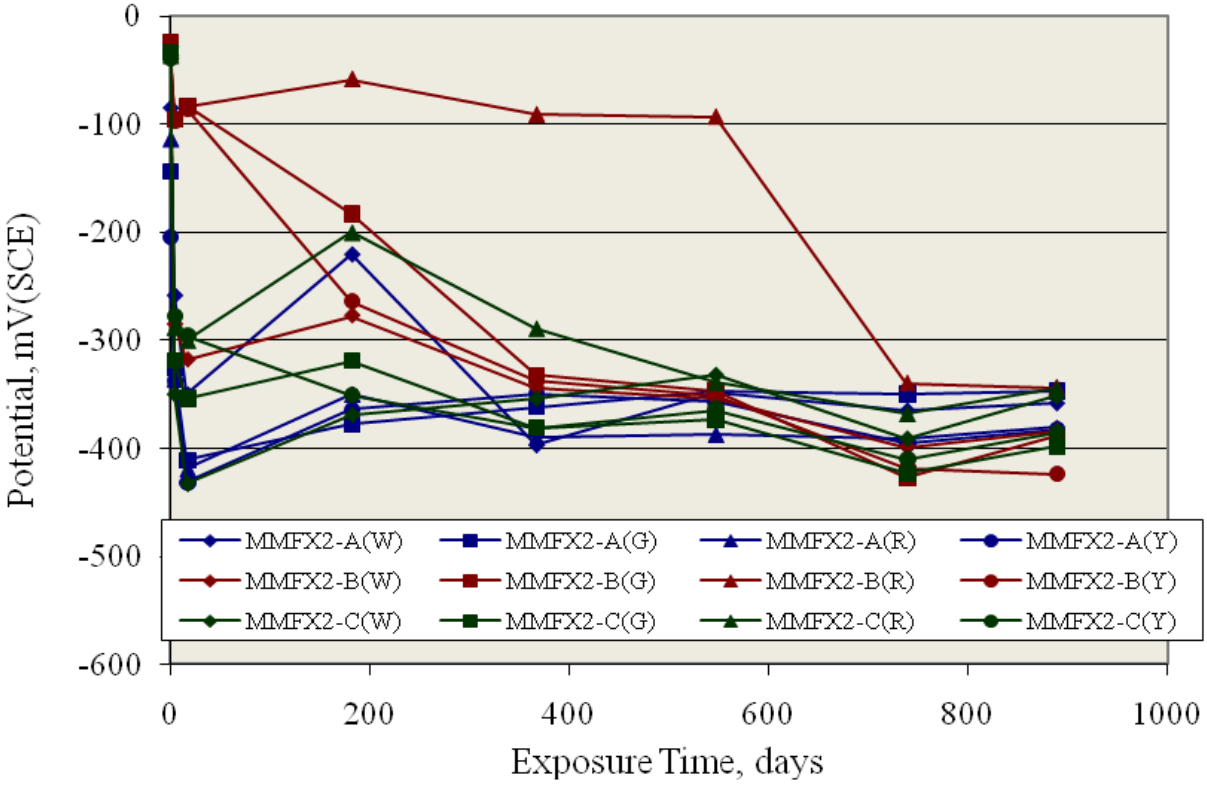

Figure 66. Graph. Potential versus exposure time plot for field columns with MMFX-2 reinforcement.

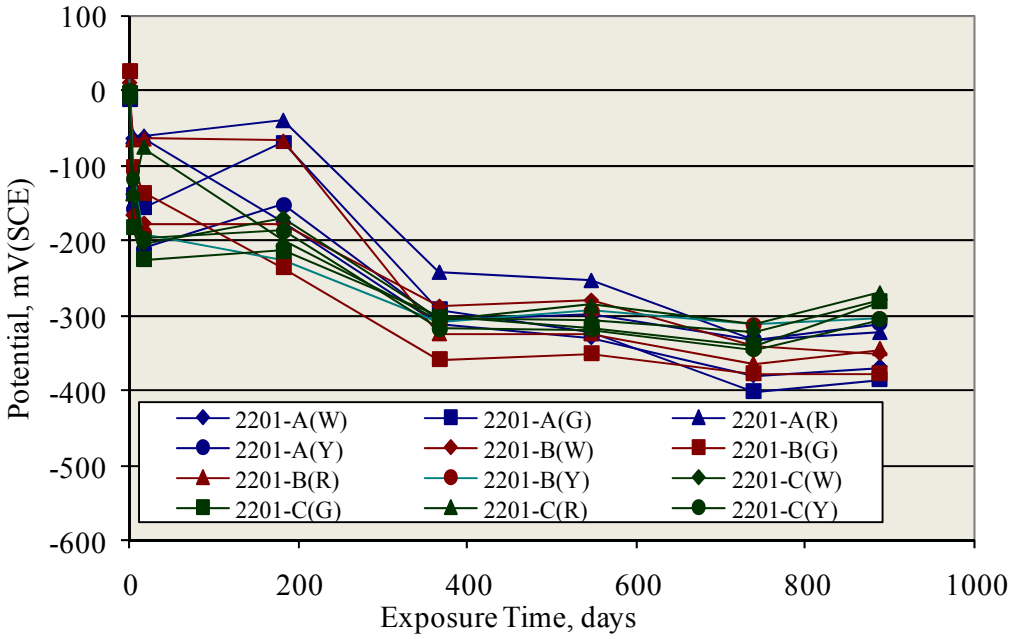

Figure 67. Graph. Potential versus exposure time plot for field column with 2101 reinforcement.

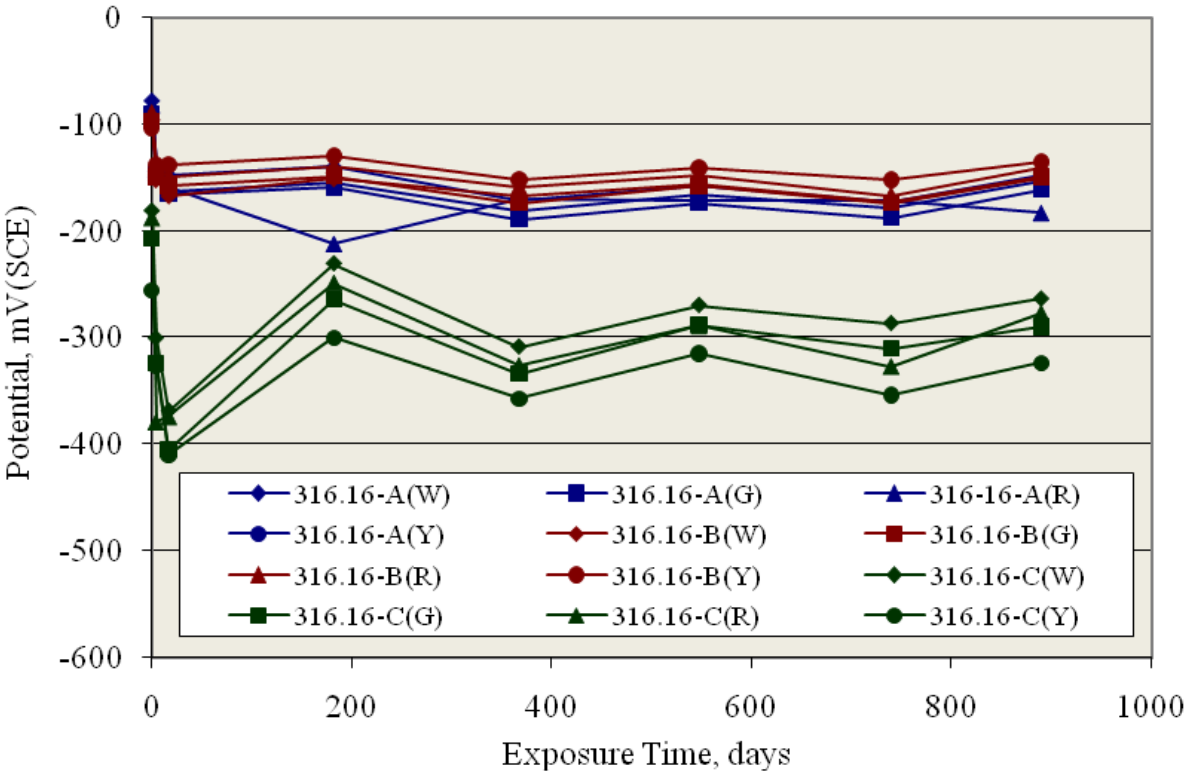

Figure 68. Graph. Potential versus exposure time plot for field columns with 316.16 reinforcement.

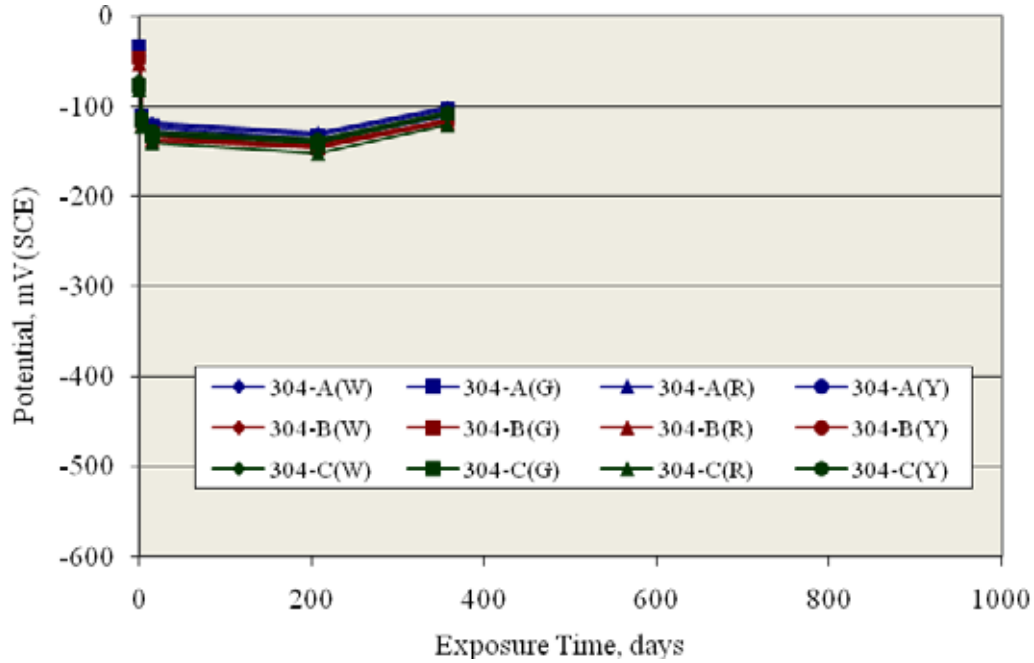

Figure 69. Graph. Potential versus exposure time plot for field columns with 304 reinforcement.

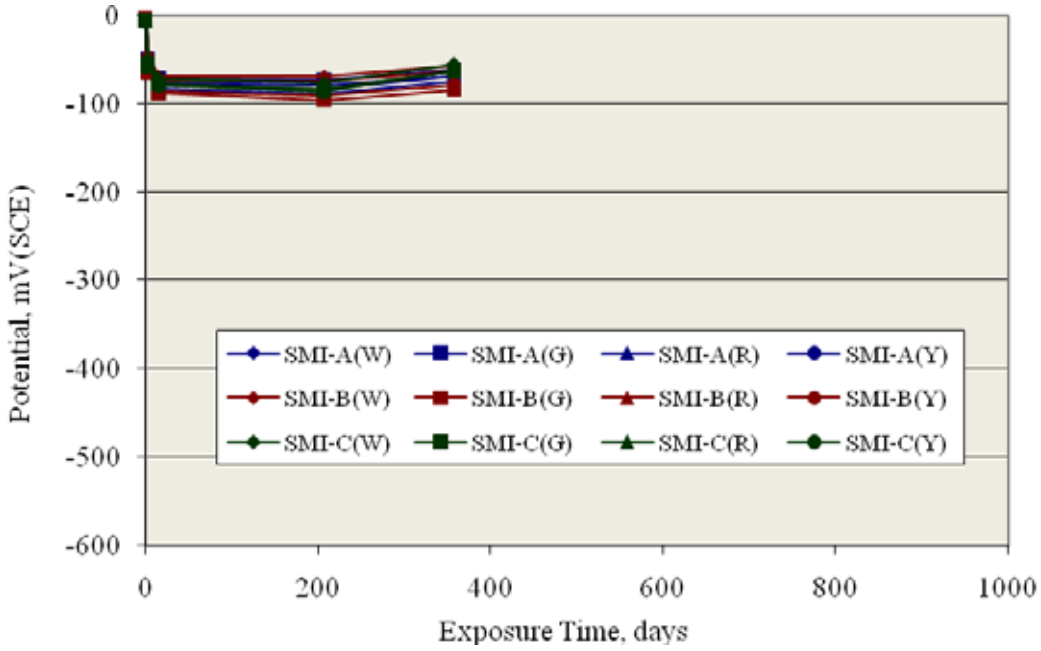

Figure 70. Graph. Potential versus exposure time plot for field columns with SMI reinforcement.

Results of the R_p determinations are presented in figure 71, which illustrates improved performance reinforcements, and in figure 72, which shows the high alloy results. For the former, R_p decreased with exposure time according to a generally common trend. Because corrosion rate is inversely proportional to R_p, the relatively low values are consistent with the corresponding potential

data (figure 64 to figure 67) and support the likelihood that corrosion had initiated. Polarization resistances for the high performance bar specimens (figure 72) were generally more than an order of magnitude or more greater than for the improved performance bars. Also, these values remained relatively constant with time and ordered (high to low) as 316.16, 304, and SMI. Specimen 316.16-C, which was discussed previously, is an exception to this. Because surface area of the working electrode for the R_p measurements was unknown, the units are in ohms rather than the more conventional ohms per square centimeter.

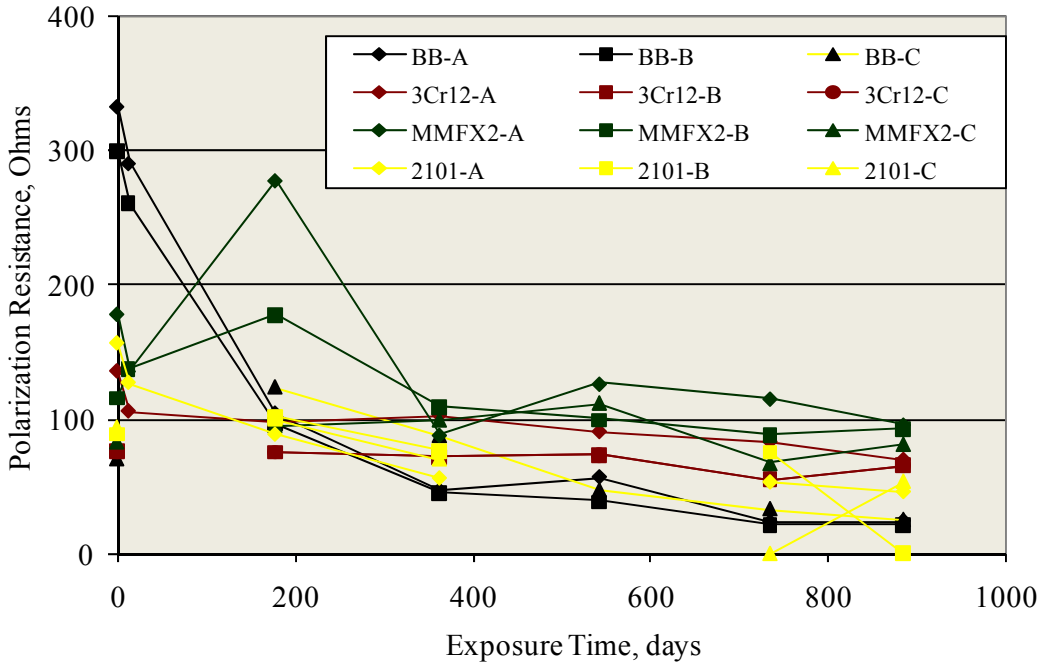

Figure 71. Graph. Polarization resistance versus exposure time plot for field columns with improved performance reinforcements.

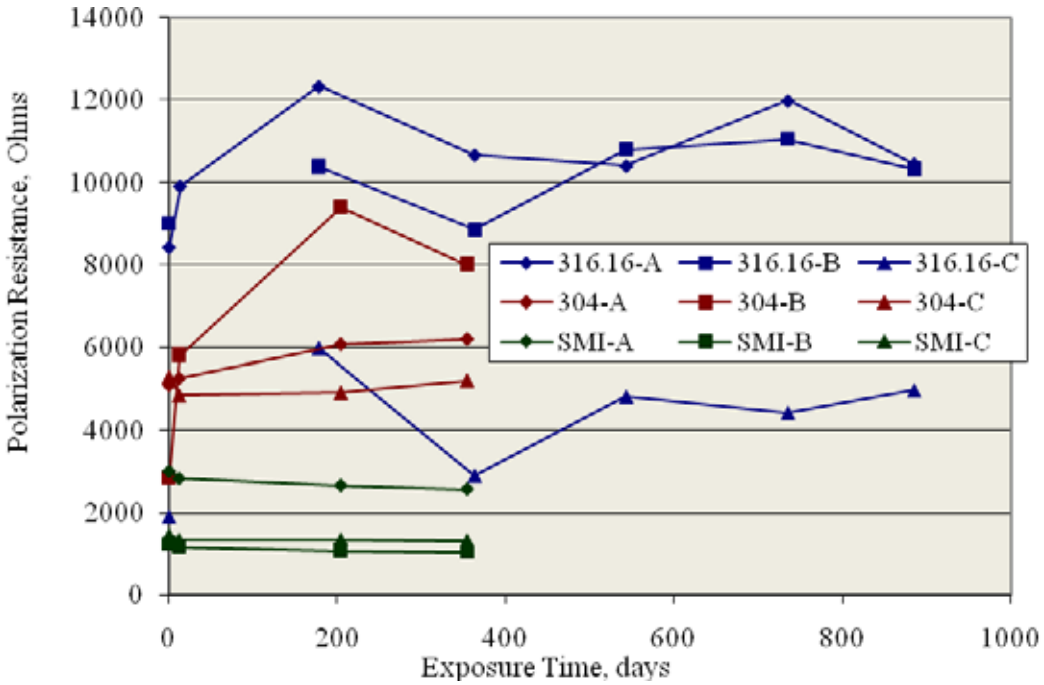

Figure 72. Graph. Polarization resistance versus exposure time plot for field columns with high alloy reinforcements.

Figure 73 and figure 74 show plots of R_p versus potential for the improved and high performance bar specimens. In the former plot, the data generally tracked from high R_p and relatively positive potential to low R_p and more negative potential, according to the decrease in both parameters as the exposures progressed. This trend is displaced somewhat to lower a R_p at a given potential for 2101 and to a higher R_p for MMFX-2. For the high performance specimens (figure 74), 316.16-C and 304-C exhibited potentials near -300 mV(SCE), whereas for other specimens, potentials were positive to -200 mV(SCE). The SMI bars have the most positive potentials compared to the other reinforcements in this category, despite R_p being relatively low. Because of the limited data, no attempt was made to estimate T_i for the different bar types.

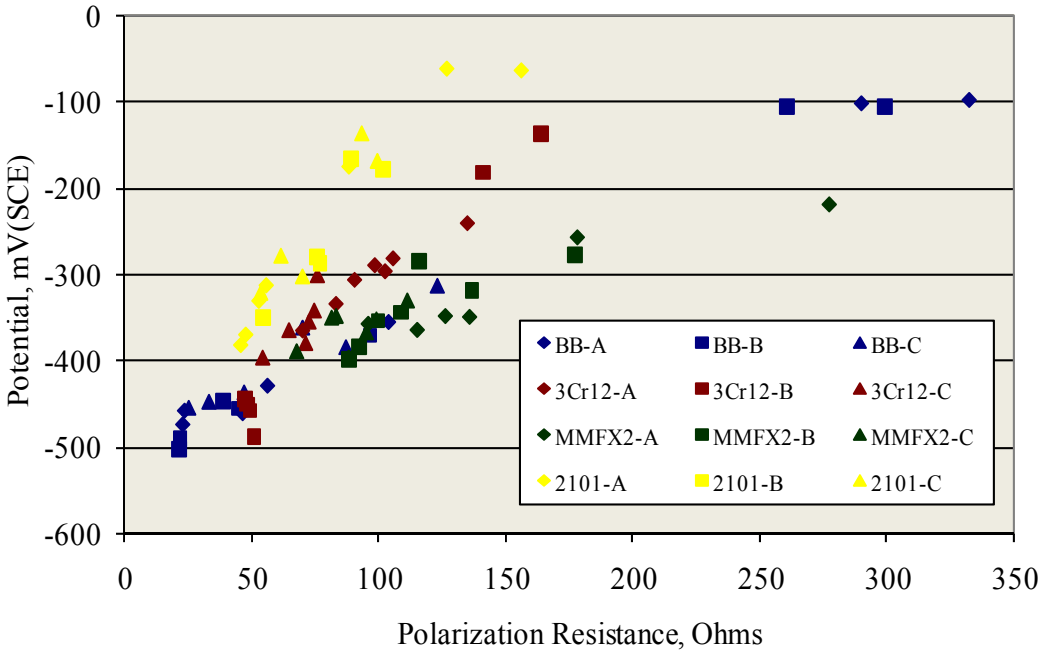

Figure 73. Graph. Plot of polarization resistance versus potential for field columns with improved performance reinforcements.

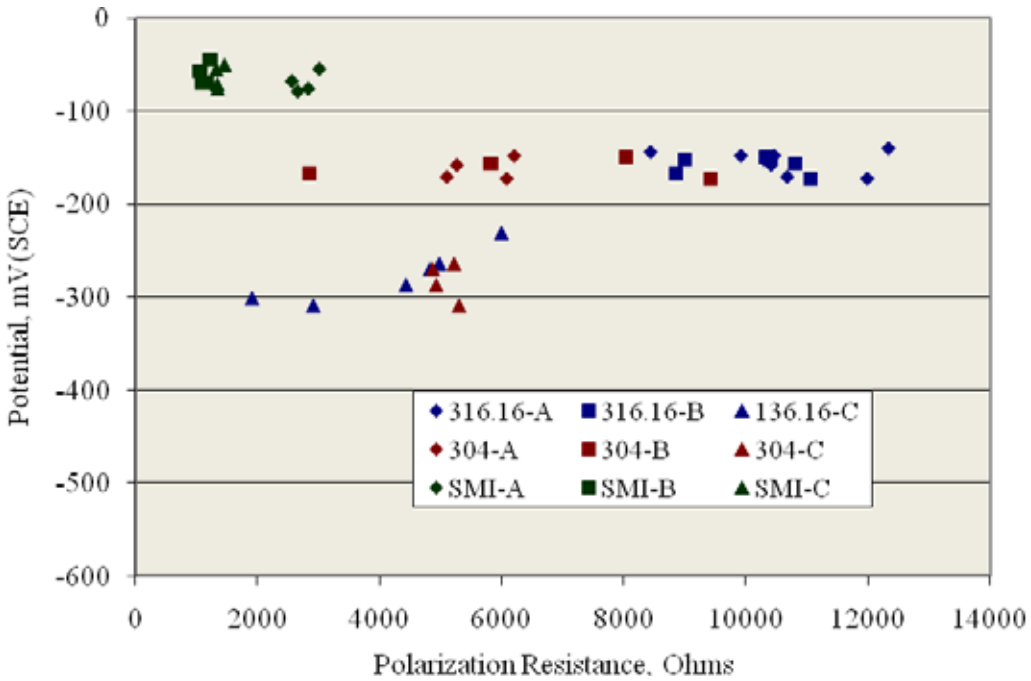

Figure 74. Graph. Plot of polarization resistance versus potential for field columns with high alloy reinforcements.

During each visit to the exposure site, researchers inspected the specimens for visible indications of corrosion damage and cracking. It was determined that each of the three BB field columns exhibited a crack in line with one of the four reinforcing bars after approximately 1 year of

exposure. At the end of 2 years, each of the cracks had grown, and the three 2101 field columns also exhibited cracks. Table 50 summarizes observations at these two times, and figure 75 and figure 76 show photographs of cracking on a BB and 2101 reinforced field column specimen after 735 days of exposure.

Table 50. Summary of field observations for cracks that developed on field column specimens.

Exposure Time (days)	Bar Type	Specimen No	Description
363	BB	A	One crack (0.46 m long) extending from 0.71 m to 1.17 m from the pile top.
		B	One crack (0.20 m long) extending from 0.63 m to 0.83 m above mud line.
		C	One crack (0.42 m long) with corrosion bleed-out extending from 0.43 m to 0.85 m above mud line.
735	BB	A	Crack had grown from 0.46 m to 0.63 m in length.
		B	Crack had grown from 0.20 m to 0.64 m in length.
		C	Crack had grown from 0.42 m to 0.71 m in length.
	2101	A	One crack (0.13 m long) extending from 0.61 m to 0.74 m from the pile top.
		B	Three cracks (0.20 m, 0.35 m, and 0.33 m long), each opposite a separate bar.
		C	Two cracks (0.11 m and 0.13 m long), each opposite a separate bar.

Figure 75. Photo. Cracking on a BB reinforced field column after 735 days of exposure.

Figure 76. Photo. Cracking on a 2101 reinforced field column after 735 days of exposure.

4.2 CRITICAL CHLORIDE THRESHOLD CONCENTRATION FOR CORROSION INITIATION, C_T

4.2.1 Chloride Analyses

Table 51 to table 57 list [Cl^-] analysis results for samples acquired both by coring and milling of SDS specimens. In all cases, [Cl^-] determined from milled samples was from locations along the bar trace where the reinforcement remained passive.

Table 51. Listing of [Cl^-] results for black bar reinforced specimens as acquired from coring.

Depth (m)	Chloride Concentration					
	5-STD1-BB-1		5-STD1-BB-2		5-STD1-BB-3	
	kg/m^3	wt/o cem	kg/m^3	wt/o cem	kg/m^3	wt/o cem
3.20E-03	11.31	4.08	13.20	4.77	11.47	4.14
9.60E-03	10.82	3.91	12.64	4.56	9.64	3.48
1.60E-02	9.42	3.40	9.22	3.33	7.28	2.63
2.24E-02	8.48	3.06	7.00	2.53	4.24	1.53
2.88E-02	6.00	2.17	0.10	0.03	2.13	0.77
3.52E-02	4.71	1.70	0.09	0.03	0.05	0.02
4.16E-02	3.05	1.10	0.09	0.03	0.00	0.00
4.80E-02	1.92	0.69	0.13	0.05	0.08	0.03
5.44E-02	0.12	0.04	0.07	0.02	0.03	0.01
6.08E-02	0.85	0.31	-0.02	-0.01	-0.06	-0.02

Table 52. Listing of [Cl^-] results for 3Cr12 reinforced specimens as acquired from cores.

Depth (m)	Chloride Concentration	
	5-STD1-3Cr12-2	
	kg/m^3	wt/o cem
3.20E-03	8.98	3.24
9.60E-03	8.60	3.11
1.60E-02	7.22	2.61
2.24E-02	5.53	2.00
2.88E-02	3.44	1.24
3.52E-02	1.76	0.63
4.16E-02	0.49	0.18
4.80E-02	0.38	0.14
5.44E-02	0.10	0.03
6.08E-02	0.09	0.03

Table 53. Listing of [Cl^-] results for 3Cr12 reinforced specimens as acquired from millings.

Bar Designation	Depth (m)	Chloride Concentration	
		5-STD1-3Cr12-2	
		kg/m^3	wt/o cem
L	2.49E-02	7.87	2.84
C	2.49E-02	9.80	3.54
R	2.49E-02	8.60	3.10

Table 54. Listing of [Cl⁻] results for MMFX-2 reinforced specimens as acquired from coring.

Depth (m)	Chloride Concentration							
	5-STD1-MMFX-2-1		5-STD1-MMFX-2-2		5-STD1-MMFX-2-3		5-USDB-MMFX-2-1	
	kg/m^3	wt% cem	kg/m^3	wt% cem	kg/m^3	wt% cem	kg/m^3	wt% cem
3.20E-03	8.03	2.90	7.88	2.85	16.42	5.93	7.88	2.85
9.60E-03	10.27	3.71	8.62	3.11	17.17	6.20	8.45	3.05
1.60E-02	8.39	3.03	8.09	2.92	12.72	4.59	7.99	2.88
2.24E-02	6.64	2.40	6.49	2.34	9.58	3.46	5.66	2.04
2.88E-02	5.22	1.88	4.89	1.77	5.86	2.11	4.80	1.73
3.52E-02	3.84	1.39	3.82	1.38	2.78	1.00	3.44	1.24
4.16E-02	2.49	0.90	2.63	0.95	0.51	0.19	1.93	0.70
4.80E-02	1.35	0.49	2.02	0.73	0.13	0.05	0.62	0.22
5.44E-02	0.52	0.19	0.75	0.27	0.16	0.06	0.38	0.14
6.08E-02	0.11	0.04	0.11	0.04	1.30	0.47	0.29	0.10

Table 55. Listing of [Cl-] results for MMFX-2 reinforced specimens as acquired from milling.

Bar Des	Depth (m)	Chloride Concentration							
		5-STD1-MMFX-2-1		5-STD-1-MMFX-2-2		5-STD1-MMFX-2-3		5-USDB-MMFX-2-1	
		kg/m^3	wt% cem	kg/m^3	wt% cem	kg/m^3	wt% cem	kg/m^3	wt% cem
L	2.49E-02	7.52	2.71	11.31	4.08	13.29	4.80	12.01	4.34
C	2.49E-02	6.94	2.50	16.33	5.90	11.83	4.27	8.46	3.06
R	2.49E-02	8.96	3.23	11.31	4.08	12.70	4.59	8.41	3.04

Table 56. Listing of [Cl^-] results for 2101 reinforced specimens as acquired from coring.

Depth (m)	Chloride Concentration			
	5-STD1-2101-1		5-STD1-2101-2	
	kg/m^3	wt% cem	kg/m^3	wt% cem
3.20E-03	12.28	4.43	8.37	3.02
9.60E-03	11.96	4.32	6.72	2.43
1.60E-02	9.84	3.55	5.54	2.00
2.24E-02	7.69	2.78	3.87	1.40
2.88E-02	5.71	2.06	1.73	0.63
3.52E-02	4.83	1.75	0.68	0.25
4.16E-02	2.74	0.99	0.02	0.01
4.80E-02	1.08	0.39	-0.01	-0.01
5.44E-02	-0.31	-0.11	0.02	0.01
6.08E-02	-0.27	-0.10	-0.05	-0.02

Table 57. Listing of [Cl^-] results for 2101 reinforced specimens as acquired from and milling.

Bar Designation	Depth (m)	Chloride Concentration			
		5-STD1-2101-1		5-STD1-2101-2	
		kg/m^3	wt% cem	kg/m^3	wt% cem
L	2.49E-02	12.74	4.60	10.77	3.89
C	2.49E-02	11.66	4.21	10.60	3.83
R	2.49E-02	10.23	3.69	11.60	4.19

Figure 77 plots [Cl^-] versus depth for all cores, and figure 78 to figure 80 show individual [Cl^-] versus depth data for both cores and millings for 3Cr12, MMFX-2, and 2101 specimens for which these determinations were made. The core data generally indicate decreasing [Cl^-] with depth into concrete as expected with differences in individual profiles, which were presumably a consequence of spatial concrete inhomogeneity. No trends are apparent from these data that suggest that

differences in concrete age at the time of coring were a factor. Scatter of milling [Cl^-] data for individual specimens occured by a factor of 1.25 for 3Cr12 and 2101 specimens but 2.4 for MMFX-2; however, for individual MMFX-2 specimens, the range was 1.1 to 1.4. Differences in coarse aggregate volume percentage (CAVP) in the powder samples acquired by milling and the relatively small sample size (1.0–1.5 g) were probably responsible. Invariably, [Cl^-] for milled samples exceeded that for cores. This is attributed to a combination of the bar obstruction and CAVP effects.[21,22,23]

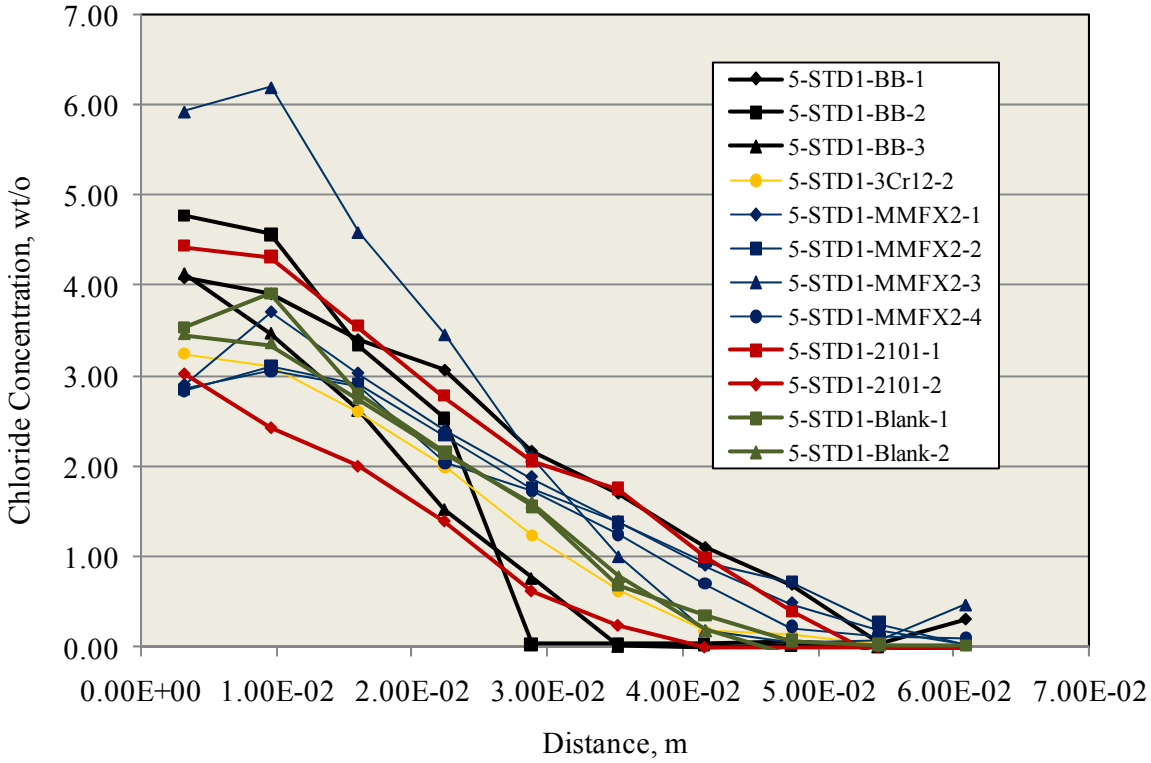

Figure 77. Graph. Chloride concentrations as a function of depth into concrete as determined from cores taken from the indicated specimens.

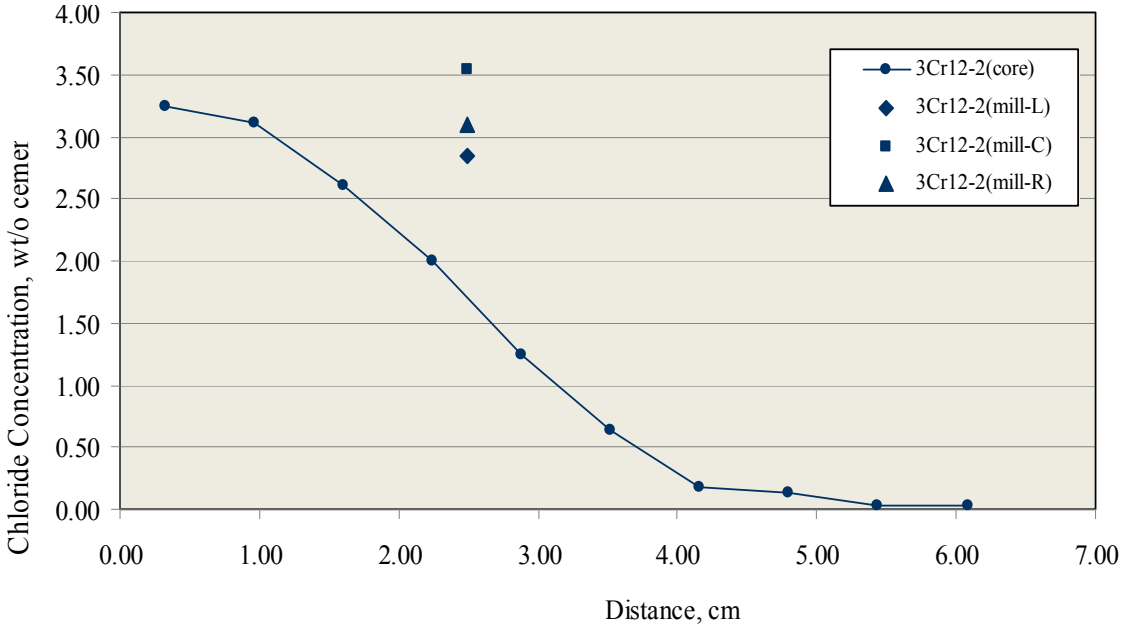

Figure 78. Graph. Chloride concentrations determined from a core and millings for specimen 5-STD-1-3Cr12-2.

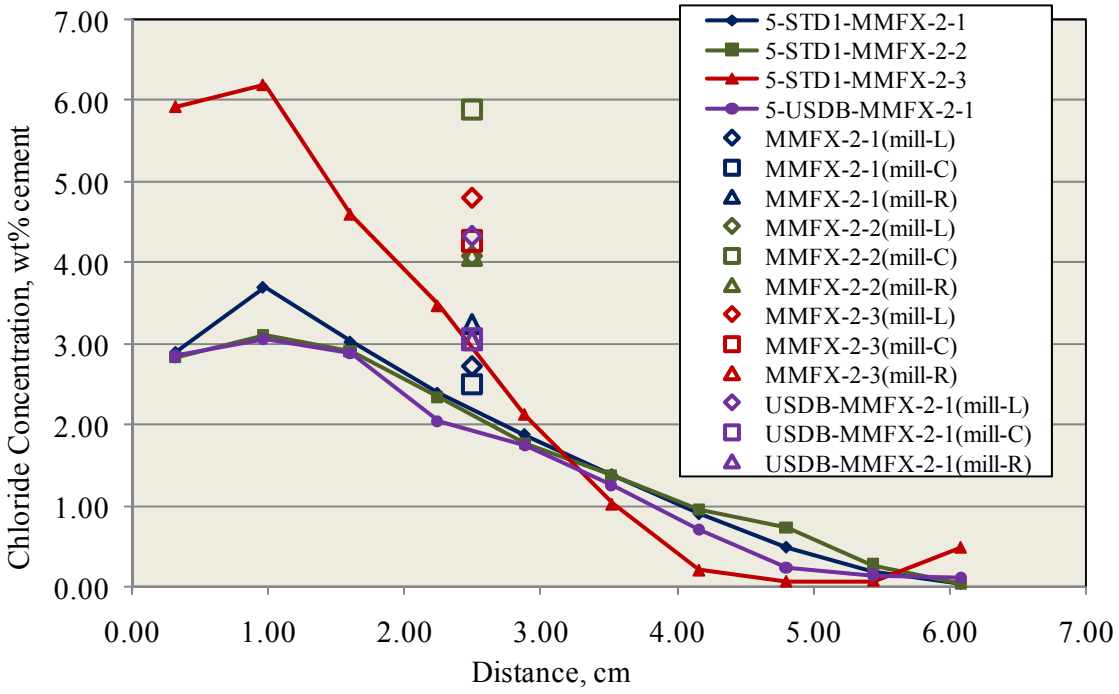

Figure 79. Graph. Chloride concentrations determined from a core and millings for MMFX-2 reinforced specimens.

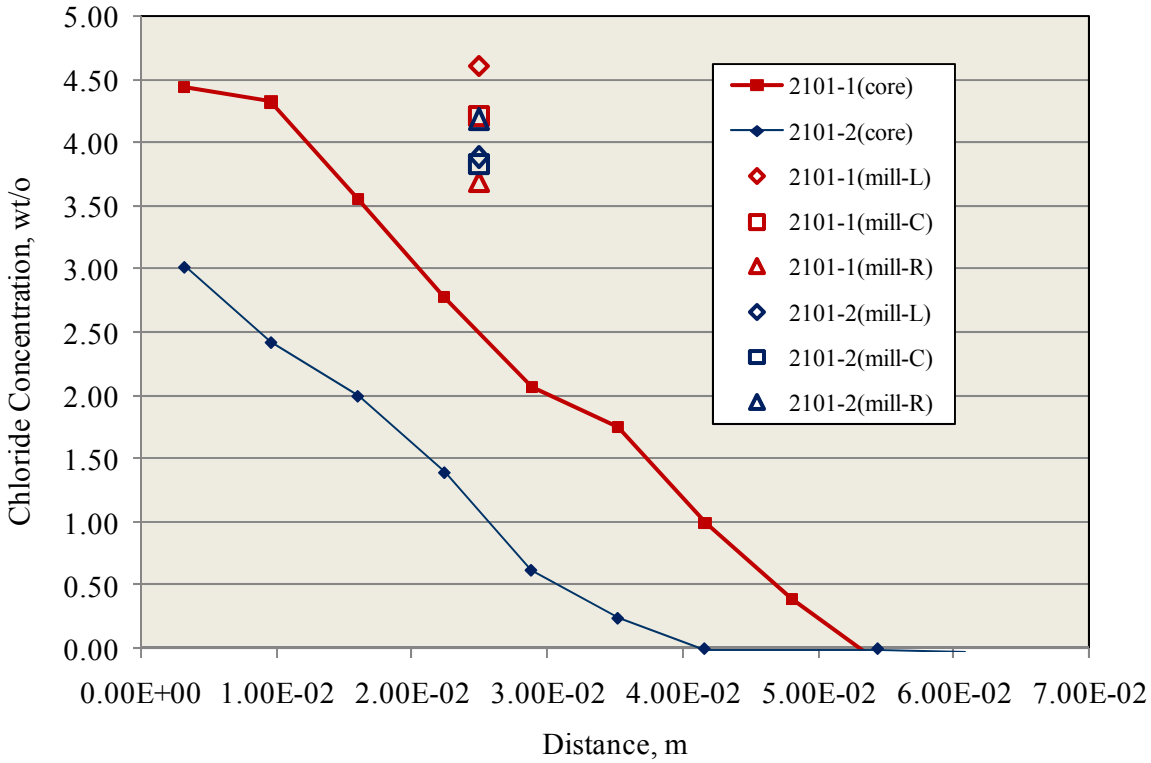

Figure 80. Graph. Chloride concentrations determined from a core and millings for 2101 reinforced specimens.

4.2.2 Diffusion Coefficient and Chloride Threshold

Based upon the [Cl^-] data from individual cores (table 50 to table 55), values for the effective diffusion coefficient, D_e, were calculated using a least squares fit to the one-dimensional solution to Fick's second law (equation 3). They are listed in table 58 below.

Table 58. D_e values calculated from core [Cl^-] data.

Specimen No	D_e (m^2/s)
BB-1	7.41E-11
BB-2	2.72E-11
BB-3	2.36E-11
3Cr12-1	2.60E-11
MMFX-2-1	1.56E-11
MMFX-2-2	1.93E-11
MMFX-2-3	1.78E-11
USDB-MMFX-2-1	1.60E-11
2101-1	1.95E-11
2101-2	2.03E-11
Average	**2.59E-11**

Using the average D_e ($2.59 \cdot 10^{-11}$ m^2/s), C_T was calculated for each top bar of all of the improved performance specimens using equation 3, which is based upon T_i for each individual top bar and assuming C_s = 18 kg/m^3 (7.22 cement wt percent basis). Figure 81 and figure 82 show Weibull CDF plots of C_T where for the former, C_T is in units of kg Cl^- per m^3 of concrete, and in the latter, it is wt percent Cl^- referenced to cement.

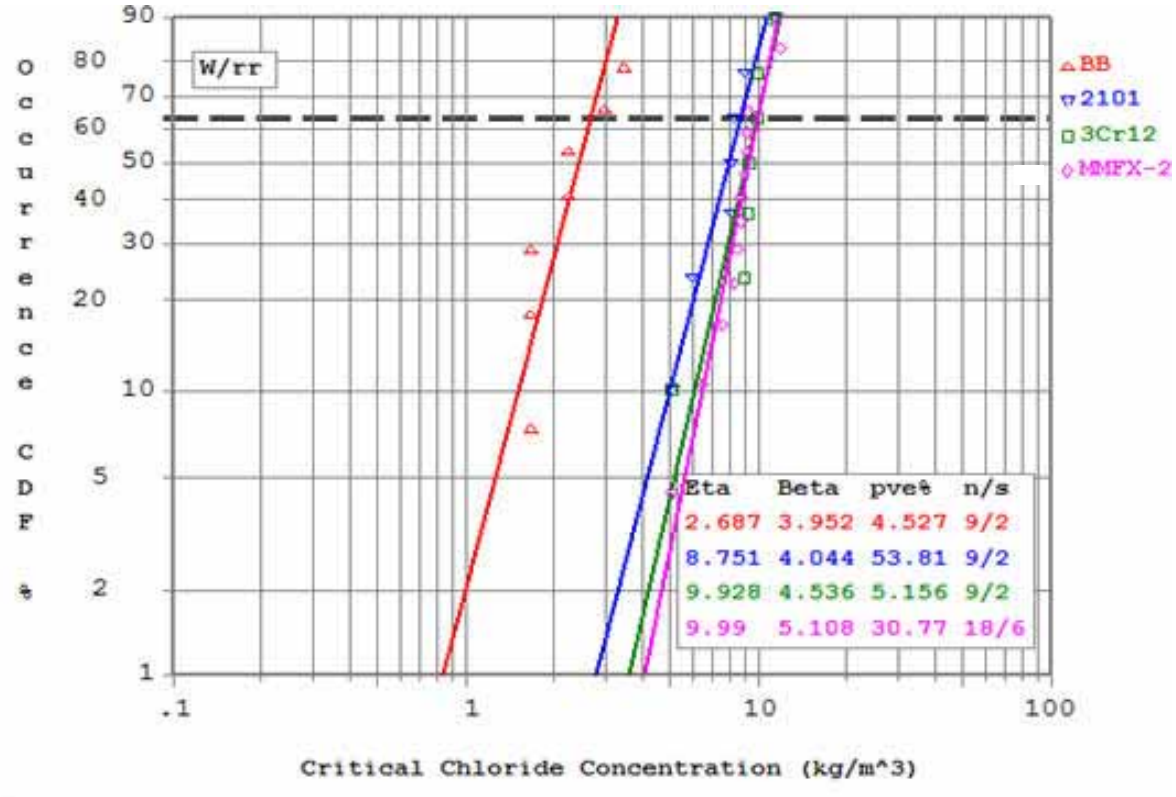

Figure 81. Graph. Weibull cumulative distribution of C_T in units of kg Cl^- per m^3 of concrete.

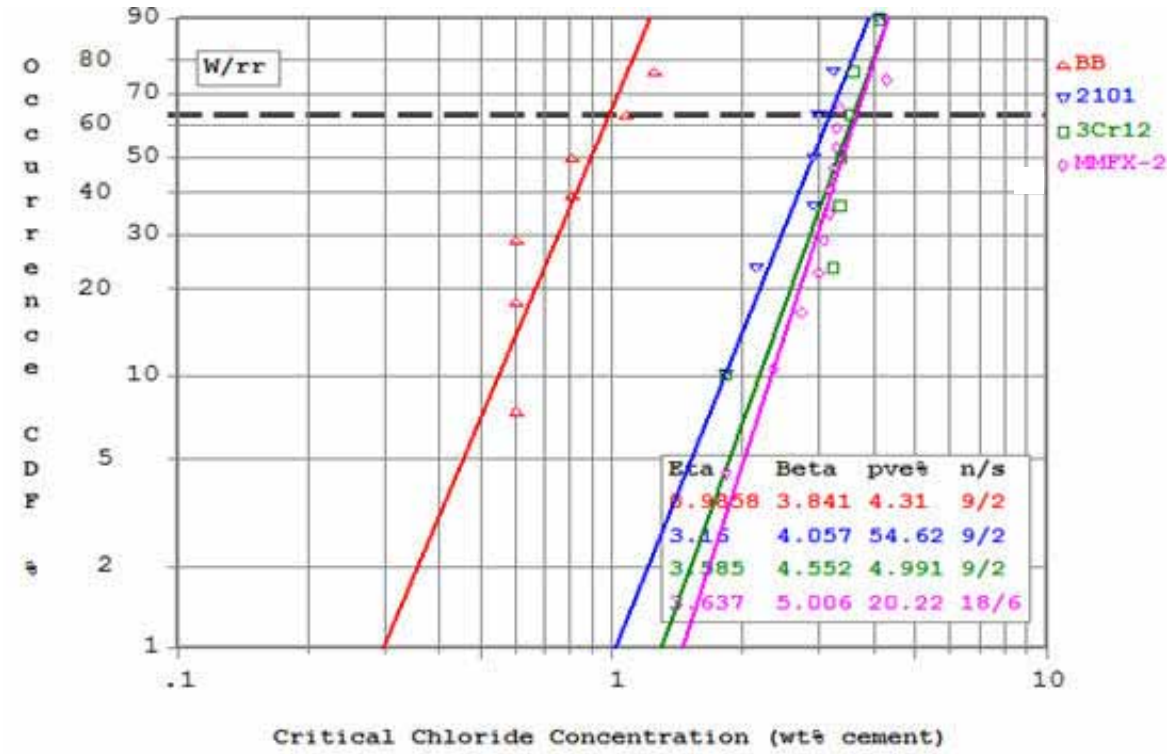

Figure 82. Graph. Weibull cumulative distribution of C_T in units of wt percent Cl^- referenced to cement.

Similar to what was done for the T_i data, table 59 lists C_T for each of the four steels at 2 percent, 10 percent, and 20 percent active. It also shows C_T(alloy)/C_T(BB) for 3Cr12, MMFX-2, and 2101. Values for the C_T ratio range from a low of 3.3 for 2101 at 20 percent active to a high of 4.8 for MMFX-2 at 2 percent active. These results are in general agreement with those of Clemeña and Virmani,[24] who reported values for C_T(alloy)/C_T(BB) as 4.7–6.0 for MMFX-2 and 2.6–3.4 for 2101 based upon slab experiments in 0.50 w/c concrete.

Table 59. Listing of C_T (kg/m^3) for the improved performance reinforcements and black bar and C_T(alloy)/C_T(BB).

Percent Active	Alloy				C_T(alloy)/C_T(BB)		
	BB	3Cr12	MMFX-2	2101	3Cr12	MMFX-2	2101
2	1.0	4.4	4.8	3.6	4.4	4.8	3.6
10	1.4	6.3	6.5	5.2	4.5	4.6	3.7
20	1.9	7.2	7.2	6.2	3.9	3.9	3.3

Minimal or no corrosion activity occurred for high alloy reinforcements except in conjunction with clad defects and perhaps crevices. Table 60 lists the five stainless steels in this category, the time each was exposed, and the corresponding [Cl^-] that is projected to be present at the bar depth based upon the diffusion analysis explained above (C_s = 18 kg/m^3 and $D_e = 2.59 \cdot 10^{-11}$ m^2/s). It is concluded that C_T for the individual bar types is greater than the indicated concentration.

Table 60. Projected [Cl^-] at the bar depth for the different reinforcement types after the indicated times.

Reinforcement Type	Exposure Time (days)	[Cl^-] (kg/m^3)
316	1,726	13.9
304	440	10.2
2304	929	12.5
Stelax	1,726	13.9
SMI	944	12.5

4.3 COMPARISON OF C_T FROM CONCRETE EXPOSURES AND ACCELERATED AQUEOUS SOLUTION EXPERIMENTS

In the initial interim report for this project, an attempt was made to correlate C_T results from an accelerated aqueous solution test method with T_i data from lots 1–3 reinforced concrete

exposures.[19] The former method involved potentiostatic polarization at +100 mV (SCE) of 10 identical specimens of each reinforcement in synthetic pore solution (0.05N NaOH and 0.30N KOH of pH ≈ 13.2–13.25), to which Cl^- was incrementally added. The results indicated a general correlation in the two data sets but with large scatter, which may have resulted from the absence of heat shrink on the reinforcement ends. The possibility of such a correlation was revisited based upon results from set 5 SDS and MS specimen data. Figure 83 reproduces the aqueous solution accelerated C_T results reported previously, and table 61 lists the mean and standard deviation of these data for each alloy.

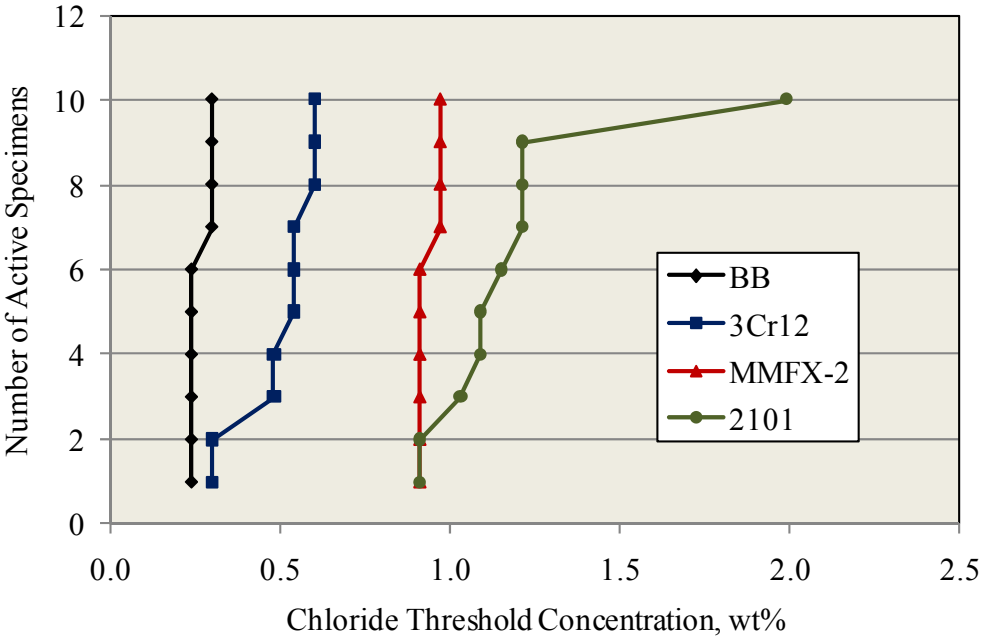

Figure 83. Graph. Previously reported chloride threshold concentrations as determined from aqueous solution potentiostatic tests.

Table 61. Listing of C_T data (wt percent) from accelerated aqueous solution testing.

Alloy	Mean	St Dev
BB	0.26	0.03
3Cr12	0.50	0.11
MMFX-2	0.94	0.03
2101	1.18	0.31

Figure 84 plots these data versus those from the SDS-STD1 slabs for 10 percent and 20 percent active and the mean. The accelerated test data indicate that 2101 had the highest C_T of the four reinforcements. The SDS data, on the other hand, indicates that MMFX-2 and 3Cr12 had the highest C_T, although the difference between these and 2101 was small and may have been within

experimental variability. However, the average accelerated test C_T data for 3Cr12 was about 60 percent below that for 2101 and MMFX-2. In the figure, the three successive data points with increasing threshold of each alloy correspond to 10 percent, 20 percent, and mean percent activation.

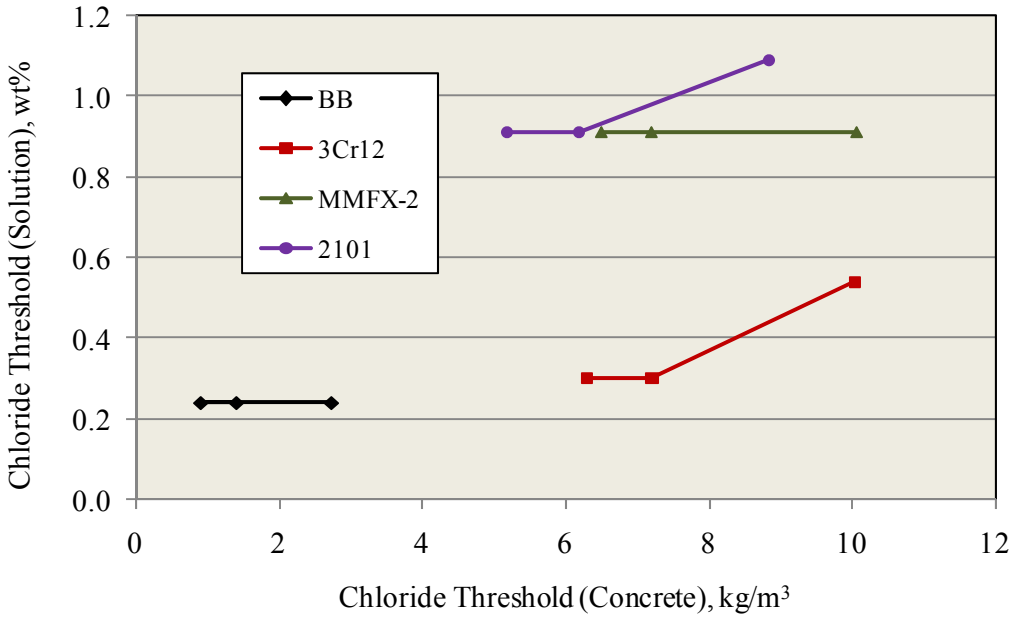

Figure 84. Graph. C_T determined from accelerated aqueous solution testing versus C_T from SDS concrete specimens.

Figure 85 provides a similar plot for STD-MS specimens where accelerated test C_T data at 20 percent and mean active are plotted versus T_i for the concrete specimens. The two successive data points with increasing T_i for BB, MMFX-2, and 2101 correspond to 20 percent active and mean C_T, whereas the three 3Cr12 are the actual T_i values. Arrows on the MMFX-2 and 2101 data connecting lines indicate that one or both of the two respective points are runouts. These results are similar to those for the SDS-STD1 specimens in figure 84 where the accelerated aqueous solution results indicate C_T for 3Cr12 specimens were only slightly greater than the BB results and well below those for MMFX-2 and 2101. However, T_i for 3Cr12 concrete specimens was among the highest vales recorded. It is concluded that the accelerated test method did not adequately project performance of 3CR12 reinforcement in concrete.

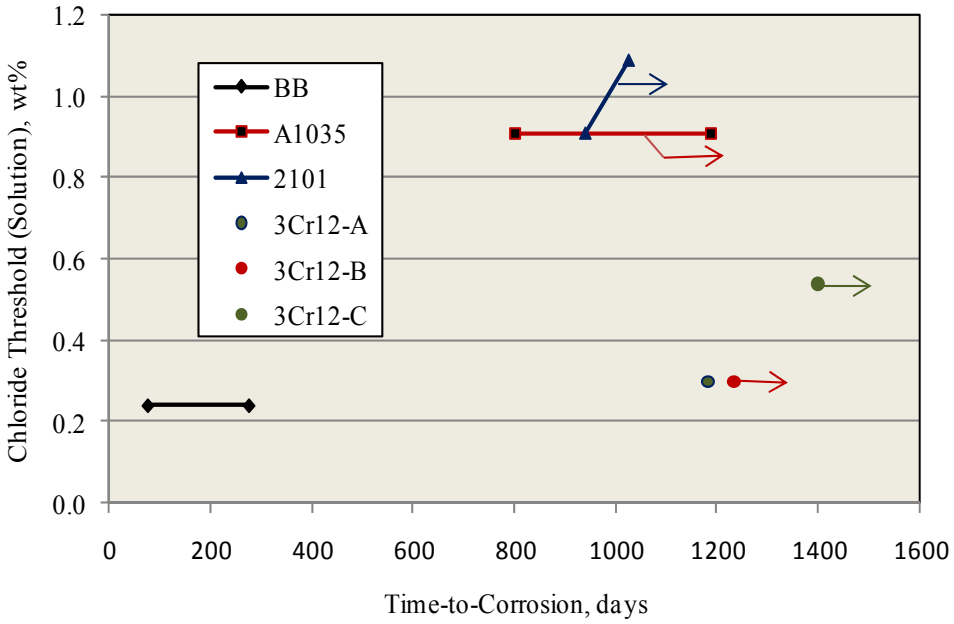

Figure 85. Graph. C_T determined from accelerated aqueous solution testing versus T_i for STD2-MS concrete specimens.

4.4 SPECIMEN DISSECTIONS

4.4.1 Dissection of SDS Specimens

Figure 86 is a photograph of a typical rebar trace upon the dissection of specimen 5-STD1-BB-1 2 weeks after detection of macrocell current. From the figure, a relatively small area of corrosion product is apparent. These observations are taken as confirmation of the experimental approach for defining T_i and C_T.

Figure 86. Photo. Upper R bar trace of dissected specimen 5-STD1-BB-1 showing localized corrosion products (circled).

Figure 87 shows an exceptional case where corrosion was more advanced prior to test termination.

Figure 87. Photo. Upper L bar trace of dissected specimen 5-STD1-BB-1 showing corrosion products.

In addition, dissections were performed on selected high performance reinforced specimens that either exhibited corrosion damage or were considered to potentially have corrosion. These specimens are listed in table 62 along with the exposure time at termination for each.

Table 62. Listing of high alloyed specimens that were autopsied.

Specimen Number	Exposure Time (days)
2-BCAT-316-1	1,669
2-CCNB-316-2	1,669
4-BCCD-SMI-1	944
6-BCAT-304-2	440
6-CCNB-304-1	440
6-CVNC-SMI-1	440

Figure 88 shows a side view photograph of specimen 2-BCAT-316-1 prior to dissection. Corrosion products are apparent extending from the BB on the lower left, and a thin concrete crack emanates from this and extends to the lower center bar.

Figure 88. Photo. Specimen 2-BCAT-316-1 prior to dissection (red markings identify specimen for removal).

No corrosion was apparent upon dissection on any of the three top bars (figure 89); however, corrosion was extensive on the bottom BB (figure 90). The fact that corrosion appears most advanced at the bar ends indicates that absence of end sleeves was a contributing factor.

Figure 89. Photo. Top R bar and bar trace of specimen 2-BCAT-316-1 subsequent to dissection.

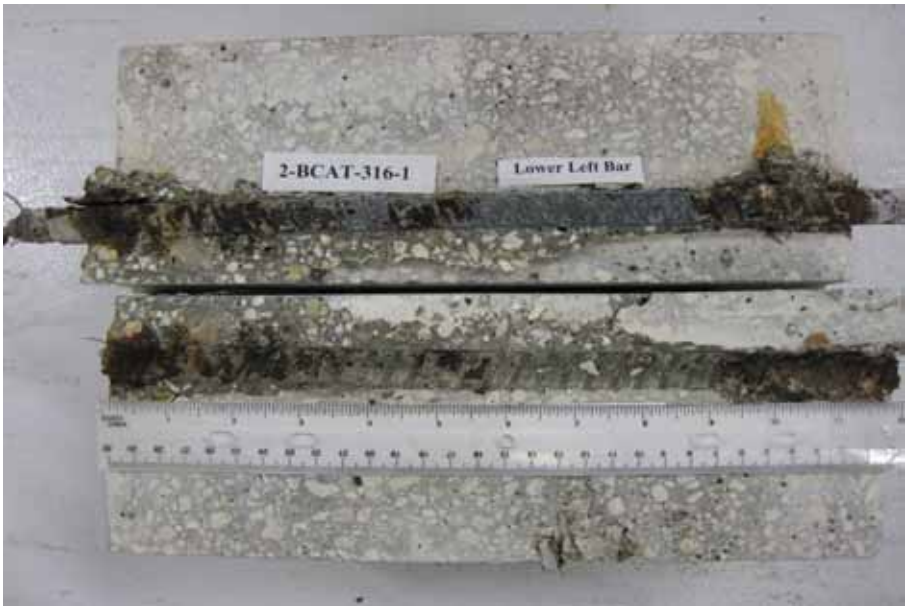

Figure 90. Photo. Lower L BB and bar trace of specimen 2-BCAT-316-1 subsequent to dissection.

Figure 91 shows a photograph of specimen 2-CCNB-316-2 prior to dissection. Although corrosion products are minimal, the concrete was delaminated along the plane of the bottom bars because of corrosion-induced cracking.

Figure 91. Photo. Specimen 2-CCNB-316-2 prior to dissection (red markings identify specimen for removal).

Minor staining was apparent on the top bars at locations beneath the simulated crack, as illustrated in figure 92. Concrete cracks that occurred during dissection are seen in the figure extending from the simulated crack.

Figure 92. Photo. Top C bar and bar trace of specimen 2-CCNB-316-2 subsequent to dissection.

Figure 93 shows the typical condition of the bottom bars, which were heavily corroded.

Figure 93. Photo. Lower R bar and bar trace of specimen 2-CCNB-316-2 subsequent to dissection.

Figure 94 and figure 95 show the typical appearance of top and bottom bars from specimen 4-BCCD-SMI-1. In the former case, corrosion has occurred locally at several of the 3-mm-diameter holes drilled through the cladding. Corrosion on the bottom BB was extensive, as seen in figure 95.

Figure 94. Photo. Top L bar and bar trace of specimen 4-BCCD-SMI-1 subsequent to dissection.

Figure 95. Photo. Lower R bar and bar trace of specimen 4-BCCD-SMI-1 subsequent to dissection.

Figure 96 to figure 98 show the appearance of the three top bars of specimen 4-CSDB-SMI-1 subsequent to dissection. Here, corrosion ranges from slight product staining (figure 98) to extensive staining at the crack base (figure 97). Corrosion at several of the 3-mm-diameter holes drilled through the cladding is also apparent away from the crack in figure 96 and figure 97.

Figure 96. Photo. Top C bar and bar trace of specimen 4-CSDB-SMI-1 subsequent to dissection.

Figure 97. Photo. Top R bar and bar trace of specimen 4-CSDB-SMI-1 subsequent to dissection.

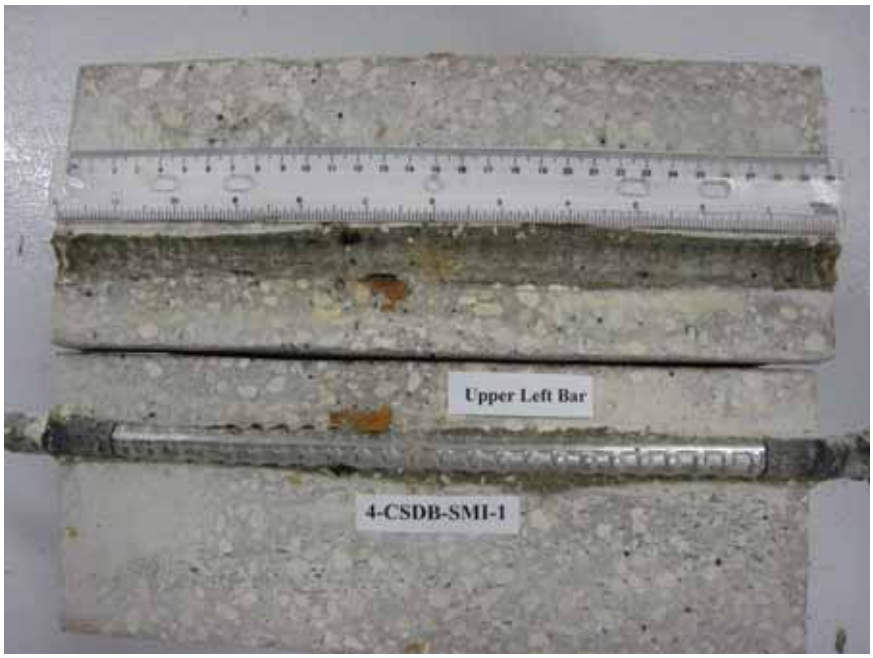

Figure 98. Photo. Top L bar and bar trace of specimen 4-CSDB-SMI-1 subsequent to dissection.

External appearance of specimen 6-BCAT-304-2 prior to dissection was characterized by corrosion product staining from each of the three bottom bars, as shown in figure 99. The red markings identify the specimen for removal.

Figure 99. Photo. Specimen 6-BCAT-304-2 prior to dissection.

No corrosion was apparent on any of the top bars (figure 100) and ranged from nil to extensive on the bottom BB (figure 101). Likewise, no top bar corrosion was apparent on any of the three top bars of specimen 6-CCNB-304-1 (figure 102), and only minor corrosion was evident on the bottom BB (figure 103).

Figure 100. Photo. Top C bar and bar trace of specimen 6-BCAT-304-2 subsequent to dissection.

Figure 101. Photo. Lower right BB and bar trace of specimen 6-BCAT-304-2 subsequent to dissection.

Figure 102. Photo. Top C bar and bar trace of specimen 6-CCNB-304-1 subsequent to dissection.

Figure 103. Photo. Lower left BB and bar trace of specimen 6-CCNB-304-1 subsequent to dissection.

Figure 104 shows a photograph of specimen 6-CVNC-SMI-1 after dissection where corrosion of the exposed carbon steel core is apparent (circled areas).

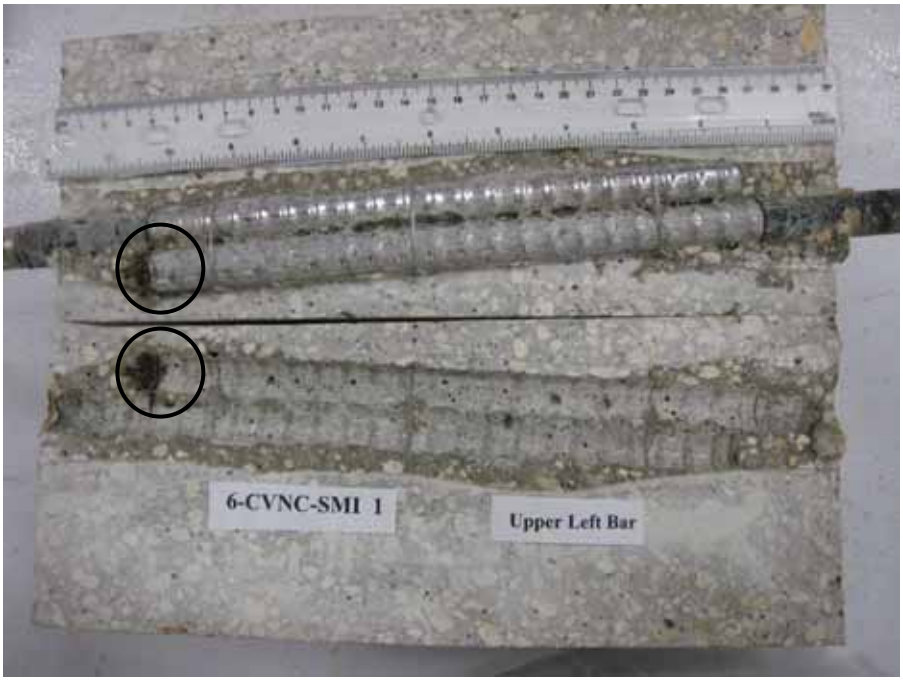

Figure 104. Photo. Top L bar pair and bar pair trace of specimen 6-CVNC-SMI-1 subsequent to dissection.

4.4.2 Dissection of MS Specimens

All but one of the improved performance MS specimens have been terminated and dissected. As indicated by figure 31 to figure 34, this was done well after corrosion had initiated. Table 63 reproduces T_i for these specimens from table 21 and also lists time at termination and time under test subsequent to T_i (propagation time, T_p).

Table 63. Listing of T_i, propagation time (T_p), and total time of testing for BB and improved performance bars in MS specimens.

Reinforcement Type	Time-to-Corrosion (days)			Time-at-Termination (days)			Propagation Time (days)		
	A	B	C	A	B	C	A	B	C
BB	97	147	182	474	474	474	377	327	292
3Cr12	121	212	488	474	474	505	353	262	17
MMFX-2	211	68	230	474	474	474	263	406	244
2101	295	215	144	474	474	474	179	259	330

In general, observations regarding the corrosion of bars from dissected MS specimens were in accord with those for SDS specimens. This is illustrated in figure 105 to figure 107, which show photographs of the three STD1-MMFX-2 specimens. For these and other specimens, the extent of corrosion tended to correspond to the length of T_p. Exceptions to this and examples of interest are discussed subsequently.

Figure 105. Photo. Top bar and bar trace for specimen MS-MMFX-2-A.

Figure 106. Photo. Top bar and bar trace for specimen MS-MMFX-2-B.

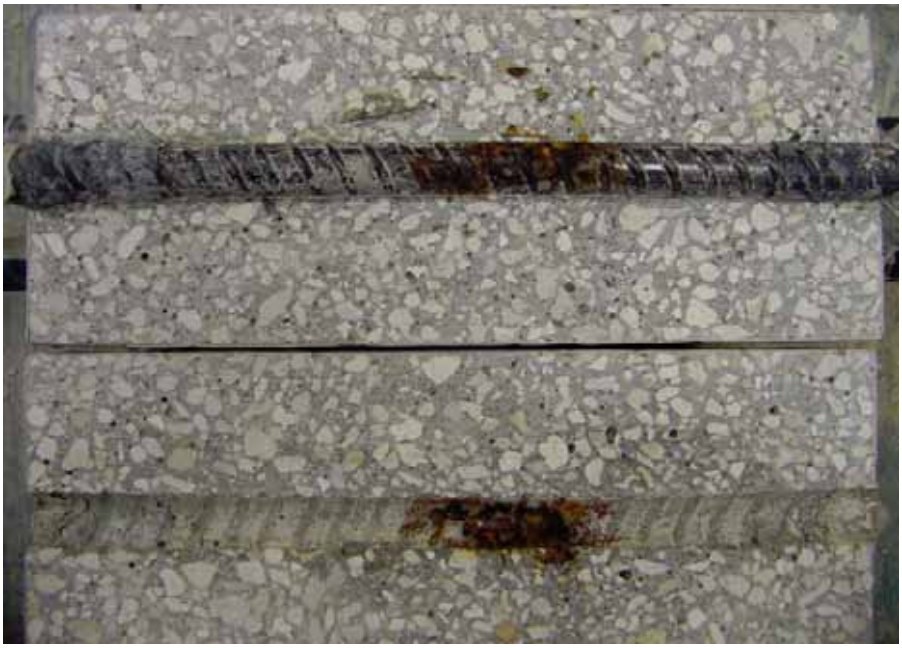

Figure 107. Photo. Top bar and bar trace for specimen MS-MMFX-2-C.

Figure 108 shows specimen MS-CBDB-MMFX-2-A after sectioning above the top bent bar. A small amount of corrosion product is apparent at what was the crack base and also near the bar ends.

Figure 108. Photo. Top bent bar trace in concrete for specimen MS-CBDB-MMFX-2-A.

Figure 109 shows the top bar from this specimen after its removal from the concrete.

Figure 109. Photo. Top bent bar from specimen MS-CBDB-MMFX-2-C after removal.

Corrosion was also disclosed on several of the high performance bars in MS specimens. Figure 110 provides one example where a small amount of corrosion products is apparent on the bar trace of specimen MS-CTNB-316-C (circled region) subsequent to dissection. The attack was beyond the footprint of the ponding bath and appeared to have resulted from crevice corrosion beneath the heat shrink sleeve.

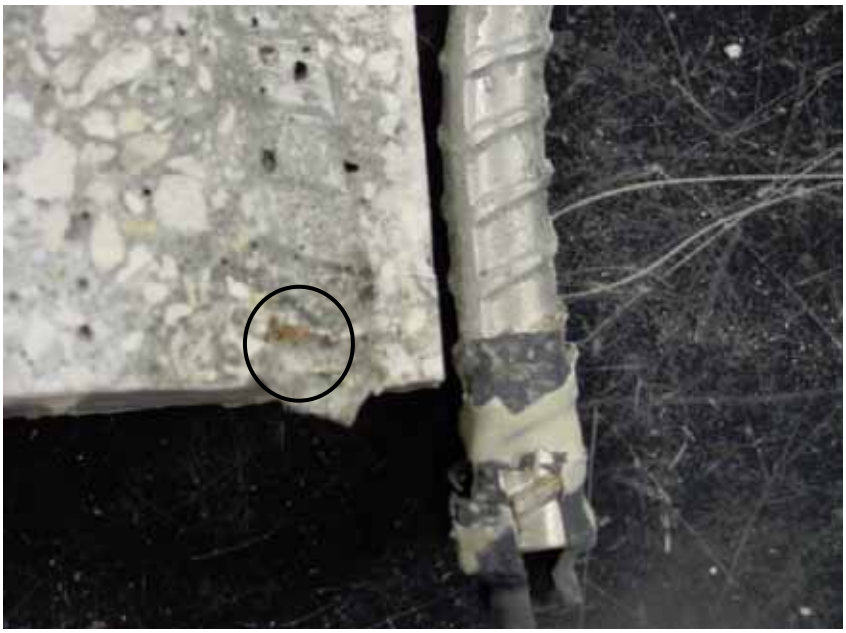

Figure 110. Photo. Top bent bar from specimen MS-BTNB-316-C after removal.

Figure 111 shows similar corrosion that occurred on the top bent bar of specimen MS-CBNB-316-B.

Figure 111. Photo. Localized corrosion on the top bent bar from specimen MS-CBNB-316-B.

Lastly, figure 112 and figure 113 show corrosion at intentional 3-mm-diameter cladding defects on the top bent bar of specimen MS-CBDB-SMI-B. The defect in the first case was

directly beneath the simulated crack, whereas the one in the second case was away from the crack in sound concrete.

Figure 112. Photo. Corrosion at an intentional clad defect on the top bent bar from specimen MS-CBDB-SMI-B.

Figure 113. Photo. Corrosion at a second intentional clad defect on the top bent bar from specimen MS-CBDB-SMI-B.

4.4.3 Dissection of 3BTC Specimens

Only two 3BTC specimens, 3BTC-STD2-BB-B and 3BTC-STD2-2101-C, were dissected. Photographs of these are shown in figure 114 and figure 115. In both cases, concrete surface cracks were present in line with the longer bars. Corrosion is apparent upon the exposed bars, and corrosion products are visible along the rebar trace beginning about 200 mm above the specimen base.

Figure 114. Photo. Specimen 3BTC-STD2-BB-B after sectioning and opening along the two longer bars.

Figure 115. Photo. Specimen 3BTC-STD2-2101-C after sectioning and opening along the two longer bars.

4.5 COMPARISON OF RESULTS FROM DIFFERENT SPECIMEN TYPES

Table 64 lists the mean T_i for BB, 3Cr12, MMFX-2, and 2101 reinforced STD1-SDS and -MS specimens and the percent difference. Although caution must be exercised in placing too much emphasis on the differences because results for the MS specimens are based only on data for three bars of each type, T_i was still shorter for MS specimens than for SDS in the case of three of the four rebar types. This is in spite of the fact that the former were ponded with 3.0 wt percent NaCl and the latter with 15.0 wt percent NaCl. Apparently, the rate controlling steps for corrosion initiation were more rapid with the MS specimen design. In addition, comparison of the T_i results shows that for the SDS specimens, T_i(alloy)/T_i(BB) was in the approximate range of 2–4 for 3Cr12, MMFX-2, and 2101 (figure 28 and table 13) at 2 percent to 20 percent active. For the MS (figure 35 and figure 36), this ratio was near unity (within the range of expected experimental scatter). Thus, there was a lack of agreement between the two specimen types for ranking these reinforcements.

Table 64. Comparison of T_i values for STD-SDS and -MS specimens.

	Mean Time-to-Corrosion (days)			
	BB	3Cr12	MMFX-2	2101
SDS	77	459	435	296
MS	142	274	170	218
Percent difference, MS to SDS	46	-68	-156	-36

The STD2 mix design was common to both MS and 3BTC specimens, for which T_i(alloy)/T_i(BB) for MS MMFX-2 specimens was 3.4 to > 5.7 and 2.7 to > 4.8 for 2101 (table 23). For 3BTC specimens, these same ratios were 3.7–5.2 and 2.1–2.9 (table 44), indicating general mutual agreement. Data scatter precluded, including results for 3Cr12 in this analysis. For 3BTC STD3 specimens, the ratios were 1.2–3.1 for 3Cr12 and 0.9–3.2 forMMFX-2 (table 45) at 2 percent, 10 percent, and 20 percent active. For this class of specimens, experimental scatter for 2101 rebar specimens was sufficiently large that an analysis could not be performed. These results indicate that the T_i enhancement realized by these improved performance reinforcements was greater the higher the concrete quality. This happened because the greatest T_i(alloy)/T_i(BB) occurred for the STD2 mix design and least T_i(alloy)/T_i(BB) occurred for STD1. The STD1-MS specimens apparently provided too severe an exposure to reveal differences between these reinforcements. As noted in the previous section, macrocell current subsequent to T_i was greater for MS than SDS specimens, suggesting that the relative severity of the MS type specimen applies to the propagation as well as initiation phases.

4.6 EXAMPLE ANALYSIS

An example projection was made for T_i for a concrete member reinforced both with black steel and an improved performance CRR with properties within the range reported previously. In doing this, the C_T data in table 59 at 2 percent, 10 percent, and 20 percent active for BB and the average for 3Cr12 and MMFX-2 were employed (figure 81). These data are based upon exposures in STD1 concrete; however, for high quality concrete, greater enhancement of C_T for CRR relative to that for BB should result. In which case, an analysis based upon the previously listed choices should be conservative.

An effective Cl^- diffusion coefficient of 10^{-12} m^2/s, a concrete cover of 63 mm, and a surface [Cl^-] of 18 kg/m^3 were assumed. The solution to Fick's second law (equation 3) was then employed to calculate T_i for each C_T. This yielded times-to-corrosion of 17 years and 43 years for BB and the CRR at 2 percent active and 24 years and 86 years at 20 percent active. Figure 116 provides a plot of these results.

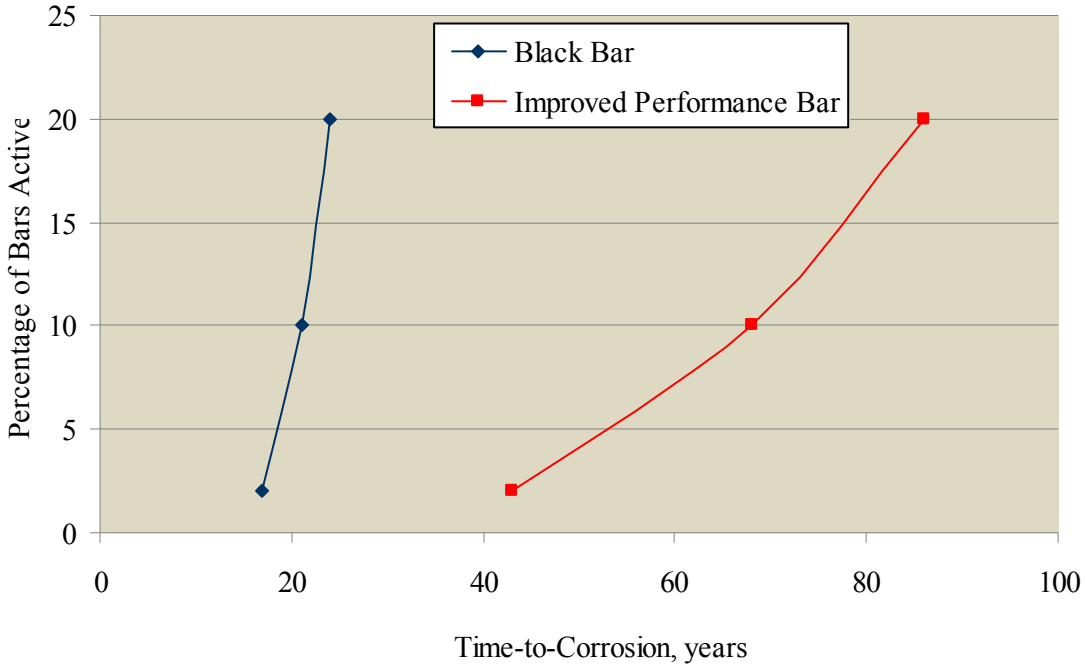

Figure 116. Graph. Comparison of T_i at 2 percent to 20 percent activation for BB and an improved performance bar under conditions relevant to actual structures.

A limitation of this analysis is that it is based on mean values for D_e, x, and C_s, whereas, if fact, each of these parameters conforms to a distribution. Consequently, corrosion initiation at locations where D_e or x (or both) are less than the mean values and/or C_s is greater than the mean must be anticipated at lesser times than projected by figure 116. The calculation is based on one-dimensional diffusion; however, a lesser T_i should occur for bars at concrete corners where diffusion is in two dimensions.[25] Also, it is assumed that enhanced Cl^- transport along any concrete cracks is not significant. This shorter T_i compared to what is projected in figure 116 should be offset to some extent by the conservative choice for C_T in high performance concrete.

Time-to-corrosion calculations were not possible for the high performance reinforcements since T_i and C_T for these exceeded the exposure times and chloride concentrations that occurred. Certainly, C_T for these was greater than for the improved performance reinforcements, such that maintenance-free service life should extend well beyond the values in figure 116. In addition, the high performance bars provide greater confidence and margin for error.

5.0 CONCLUSIONS

Two specimen types, SDS and MS, which were intended to represent a reinforced concrete bridge deck exposed to deicing salts, and two other specimen types, 3BTC and FC, which represented a marine substructure element, were exposed to chlorides. Reinforcements included stainless steels 316 (UNS-S31603), 304 (UNS-S30400), 2304 (UNS-S32304), 2101 (ASTM A955-98), and 3Cr12 (UNS-S41003); two types of 316 clad BB, AASHTO MP 13M/MP 13-04, and MMFX-2 (ASTM A1035); and BB (ASTM A615), the last being for baseline comparison purposes. Bars were cast into concrete specimens in the as-received condition, which was either as-rolled or pickled depending upon the source, after solvent cleaning. Specimen configurations included the following:

- Bent bars.
- Bars wire brushed.
- Simulated concrete crack or crevice between adjacent bars (or both).
- Corrosion-resistant rebar top layer and BB lower (SDS and MS specimens).
- Intentional defects in the case of clad bars.

These were in addition to a standard specimen for which all bars were straight, and none of the above conditions were present (standard condition for MS specimens was with bars wire brushed). Three concrete mix designs, termed STD1 (high permeability), STD2 (intermediate permeability), and STD3 (permeability between that of STD1 and STD2) were employed. All specimens were tested outdoors where the SDS and FC were fully exposed and the MS and 3BTC were sheltered. A second set of MS specimens was tested under controlled temperature and relative humidity (25 ^{o}C and 50 percent).

Based on the study, several conclusions were reached. The reinforcements, other than BB, were classified into two groups as either improved performance or high performance where alloys in the former category initiated corrosion during the project time frame, and ones in the latter did not, at least in cases for specimens of the standard configuration (STD—all straight bars in the as-received condition without crevices and no simulated concrete cracks). Improved performers were 3Cr12, MMFX-2, and 2101 (BB-reinforced specimens were included in this grouping also for reference purposes). The other alloys were high performers. These alloys ranked according to time for corrosion to initiate as BB < 2101 < 3Cr12, MMFX-2.

No SDS specimens with 304 and clad or solid 316 bar, besides those with BB lower layer, initiated corrosion, and no sustained macrocell currents were detected during the exposure period. Test times for the 304 reinforced specimens were as long as 440 days and 1,726 days for the 316 reinforced specimens. The MS and 3BTC specimens with these reinforcements exhibited both anodic and cathodic macrocell current "spikes" to as high as 16 μ A for 316 and 0.8 μ A for 304. However, net mass loss associated with these was calculated as 0 μ A. In general, macrocell current activity was less for 304 than for 316, which is in contrast to the normally

perceived better corrosion resistance of the latter alloy. Also, macrocell currents were less for specimens in the higher quality concrete (STD2) compared to the lower (STD1). Corrosion potentials remained relatively positive, and the macrocell current activity was not considered indicative of corrosion initiation.

For improved performance and BB reinforcements, T_i and C_T were distributed over a range rather than being a discrete value. Chloride threshold for corrosion initiation of 3Cr12 and MMFX-2 reinforced SDS specimens was about four times greater than for BB specimens and slightly less than four times greater in the case of 2101 specimens. Weibull analysis of the [Cl^-] data indicated that at 2 percent of bars being active, C_T for BB was 1.0 kg/m^3 or 0.36 wt percent cement and 4.0 kg/m^3 or 1.44 wt percent cement for 3Cr12 and MMFX. On the other hand, there was little difference in T_i between each of the three improved performance reinforcements compared to BB for STD1 MS specimens. For STD2 MS specimens, however, T_i for MMFX-2 and 2101 was from 3.4 to more than 5.7 times greater than for BB (limited data precluded this determination for 3Cr12). For 3BTC specimens, this ratio for these same two alloys (MMFX-2 and 2101) in STD2 concrete was from 2.1 to 5.2. The results imply that the enhanced corrosion resistance that is derived from these reinforcements relative to BB increases with increasing concrete quality.

Time-to-corrosion for STD1 MS specimens was shorter than for SDS specimens, and macrocell currents for the former were an order of magnitude or more greater than for the latter. Apparently, the MS type specimens and exposure conditions provided a more severe testing of the reinforcements than the SDS specimens. The finding that T_i for improved performance bars was about the same as for BB in STD1 MS specimens but about four times greater in SDS ones may have resulted because of this.

The MS specimens exposed outdoors exhibited shorter T_i and greater macrocell current activity than identical ones tested at constant temperature and relative humidity. The former condition is thought to have fostered a higher level of sorptive moisture and Cl^- transport, such that the corrosion threshold was reached in a shorter time.

The FC specimens, which were exposed in the tidal zone on the Intracoastal Waterway at Crescent Beach, FL, with improved performance and BB reinforcements, typically initiated corrosion within the first several days. This is thought to have resulted because of poor concrete quality and possible cracks that provided direct water access to the reinforcement. With one exception, the high performance reinforcements have remained passive. The exception was a 316 reinforced column that was damaged during installation.

A ranking of these CRR based on Cl^- threshold failed to correlate with results from previously performed short-term potentiostatic tests in synthetic pore solution to which chlorides were incrementally added. This calls into question the usefulness of this and perhaps other accelerated test methods for evaluating corrosion resistant alloys for service as reinforcements in concrete.

In specimens with lower layer BB, corrosion of the BB was often extensive and to the point that delaminations occurred along the plane of these bars. If a corrosion-resistant steel upper bar layer is to be combined with a BB lower one, the concrete should be of sufficient quality and with limited or no cracks such that Cl^- concentration at the lower bars remains below the black steel threshold for the design life of the structure.

Corrosion occurred at defects and unprotected embedded bar ends for stainless clad reinforcements. The likelihood that this attack or corrosion at clad defects will ultimately cause concrete cracking and spalling is uncertain, but it depends on corrosion morphology, geometry, and rate factors. Corrosion-induced concrete cracking and spalling probably result in time if the surface area of the exposed core carbon steel and extent of attack exceed a certain value. Further research is needed to define this threshold.

Life-cycle cost analyses for CRR should consider not only differences in C_T and macrocell current, but also the possibility that concrete cover can be reduced. This, in turn, could lower superstructure and, hence, substructure size, weight, and initial cost, accordingly. Also, lower cover may reduce the number and width of concrete cracks, leading to less corrosion of top bars and lower maintenance costs in the long term.

An example analysis was performed that calculated T_i of a concrete structure reinforced first with BB and second, with an improved performance rebar. The calculation was based on an effective Cl^- diffusion coefficient of 10^{-12} m^2/s, concrete cover 63 mm, surface [Cl^-] 18 kg/m^3, and C_T for the corrosion resistant alloy as four times greater than for BB. The analysis yielded T_i for BB as ranging from 17 years to 24 years and for the corrosion resistant alloy from 43 years to 86 years as the percentage of bars being active increased from 2 percent to 20 percent. Limitations of this analysis are that, first, the above input parameters for the calculation are mean values, whereas these are, in fact, distributed such that corrosion will initiate at some locations sooner than projected. Second, enhanced inward Cl^- migration along any concrete cracks was not considered. Further, corrosion should initiate sooner at concrete corners because inward Cl^- diffusion is from two directions here rather than just one. On the other hand, the above difference in C_T for black compared to the improved performance bar was based on data acquired from highly permeable concrete. However, this difference is expected to be greater for concrete with a Cl^- diffusion coefficient of 10^{-12} m^2/s.

The C_T and macrocell current data indicate that the intended service life of major reinforced concrete bridge structures (75–100 years) can confidently be achieved with the solid high performance reinforcements that were investigated. This may be the case also for the clad reinforcements, provided there is adequate control of surface defects and bar ends are protected. This same service life may also result with the improved performance bars, provided design and construction quality control are good, and concrete cracking is minimal but with a lesser degree of confidence and margin for error compared to the high performance reinforcement.

REFERENCES

1. Virmani, Y.P., Jones, W.R., and Jones, D.H. (1984). *Public Roads*, *84*(3), 96.

2. Koch, G.H., Brongers, P.H., Thompson, N.G., Virmani, Y.P., and Payer, J.H. (March 2002). *Corrosion Costs and Prevention Strategies in the United States.* Report No. FHWA-RD-01-156. Federal Highway Administration. Washington, DC.

3. Yunovich, M., Thompson, N.G., and Virmani, Y.P. (2003). "Life Cycle Cost Analysis for Reinforced Concrete Bridge Decks." Paper No. 03309. Presented at CORROSION/03, March 10–14. San Diego, CA.

4. Stratfull, R.F., Jurkovich, W.J., and Spellman, D.L. (1975). *Transportation Research Record*, *539*, 50.

5. (2002). "Frequency of Inspections." Code of Federal Regulations, Section 650.305. U.S. Government Printing Office. April 1, 2002 revision. Washington, DC.

6. Tutti, K. (1983). "Corrosion of Steel in Concrete." Report No. 4. Swedish Cement and Concrete Research Institute. Stockholm, Sweden.

7. Hausman, D.A. (1967). "Steel Corrosion in Concrete." *Materials Protection*, *6*(11), 19.

8. Glass, G.K. and Buenfeld, N.R. (1995). "Chloride Threshold Levels for Corrosion Induced Deterioration of Steel in Concrete." Paper No. 3 presented at RILEM International Workshop on Chloride Penetration into Concrete. October 15–18. Saint Rémy-les-Chevreuse, France.

9. Sagüés, A.A. (2003). "Modeling the Effects of Corrosion on the Lifetime of Extended Reinforced Concrete Structures." *Corrosion*, *59*, 854.

10. Torres-Acosta, A.A. and Sagüés, A.A. (2000). "Concrete Cover Cracking with Localized Corrosion of the Reinforcing Steel." Proc. 5th CANMET/ACI International Conference on Durability of Concrete, SP-192, Ed. v.M. Malhotra. American Concrete Institute. 591. Farmington Hills, MI.

11. Stafford, R.T. (1973). "Epoxy Coated Rebars." *Parking*, 39.

12. Clifton, J.R., Beehgly, H.F., and Mathey, R.G. (1974). *Non-Metallic Coatings for Concrete Reinforcing Bars*. Report No. FHWA-RD-74-18. Federal Highway Administration. Washington, DC.

13. Virmani, Y.P. and Clemena, G.G. (1998). *Corrosion Protection: Concrete Bridges*. Report No. FHWA-RD-98-088. Federal Highway Administration. Washington, DC.

14. Powers, R.G. and Kessler, R. (1987). *Corrosion Evaluation of Substructure, Long Key Bridge*. Corrosion Report No. 87-9A. Florida Department of Transportation. Gainesville, FL.

15. Powers, R.G. (1988). *Corrosion of Epoxy-Coated Rebar*. Keys Segmental Bridges Monroe County. Report No. 88-8A. Florida Department of Transportation. Gainesville, FL.

16. Zayed, A.M. and Sagüés, A.A. (1989). "Corrosion of Epoxy-Coated Reinforcing Steel in Concrete." Paper No. 386. Presented at CORROSION/89, April 21. New Orleans, LA.

17. Gustafson, D.P. (1988). "Epoxy Update." *Civil Engineering*, *58*(10), 38.

18. Hartt, W.H., Powers, R.G., Leroux, V., and Lysogorski, D.K. (2004). *A Critical Literature Review of High-Performance Reinforcements in Concrete Bridge Applications*. Report No. FHWA-HRT-04-093. Federal Highway Administration. Washington, DC.

19. Hartt, W.H., Powers, R.G., Lysogorski, D.K., Liroux, V., and Virmani, Y.P. (2007). *Corrosion Resistant Alloys for Reinforced Concrete*. Report No. FHWA-HRT-07-039. Federal Highway Administration. Washington, DC.

20. "Standard Practice for Making and Curing Concrete Specimens in the Laboratory." ASTM C192-04. American Society for Testing and Materials. *Annual Book of Standards*. West Conshohocken, PA.

21. Krane, S.C., Sagüés, A.A., and P-Moreno, F. (2002). "Decreased Corrosion Initiation Time of Steel in Concrete due to Reinforcing Bar Obstruction of Diffusional Flow." *ACI Materials Journal, 99*(1), 51.

22. Yu, H. and Hartt, W.H. (2007). "Effect of Reinforcement and Coarse Aggregates on Chloride Ingress into Concrete and Time-to-Corrosion: Part I—Spatial Chloride Distribution and Implications." *Corrosion*, *63*, 843.

23. Yu, H., Himiob, R.J., and Hartt, W.H. (2007). "Effect of Reinforcement and Coarse Aggregates on Chloride Ingress into Concrete and Time-to-Corrosion: Part II—Spatial Distribution of Aggregates." *Corrosion*, *63*, 924.

24. Clemena, G.G. and Virmani, Y.P. (2004). "Comparing the Chloride Resistances of Reinforcing Bars." *Concrete International,* 39.

25. Sagüés, A.A., Krane, S.C., Presuel-Moreno, F., Rey, D., Torres-Acosta, A., and Yao, L. (2001). "Corrosion Forecasting for 75-Year Durability Design of Reinforced Concrete." Report No. BA502, Submitted to Florida Department of Transportation by University of South Florida. December 31, 2001.

HRDI-10/04-09(600)E